MEASURING LATEX PROPERTIES USING ULTRASOUND

MEASURING THE PROPERTIES OF POLYMER LATICES USING HIGH FREQUENCY LONGITUDINAL STRESS WAVES

By

Eric B. Wasmund, B.Sc

A Thesis
Submitted to the School of Graduate Studies
in Partial Fulfillment of the Requirements
for the Degree
Master of Engineering

McMaster University
October 1991

MASTER OF ENGINEERING (1991) McMaster University
(Chemical Engineering) Hamilton, Ontario

TITLE:	Measuring the Properties of Polymer Latices Using High Frequency Longitudinal Stress Waves
AUTHOR:	Eric B. Wasmund, B. Sc (Queen's University)
SUPERVISOR:	Prof. J.F MacGregor
NUMBER OF PAGES:	xi, 129

ABSTRACT

There is a great need for sensors that can infer the properties of polymer latices. Measuring ultrasonic wave travel parameters through a latex and calibrating these against polymer properties is one potential technique for measuring the polymer properties of a latex without separating the polymer particles from water. Ultrasonic longitudinal waves can be characterized by three travel parameters: the velocity, the attenuation and the frequency. For colloidal systems the attenuation will depend on molecular properties of the system inside a frequency window where diffraction and scattering are negligible.

In this thesis the equipment for measuring ultrasonic waves is discussed and a measurement cell for measuring waves in liquids is designed and built. This equipment is used to measure the velocity and attenuation as functions of frequency for two sets of copolymer latices. These latices were measured separately using a combination of standard quality control analyses and polymer characterization techniques. It was discovered that the velocity of sound through latices does not differ significantly from the velocity for pure water while the ultrasonic attenuation of latices at solids concentrations of greater than 10 percent is much greater than the value for pure water.

For the copolymer latices produced from styrene and methyl-methacrylate the attenuation measurements were all too similar to distinguish between changes in the properties of the latex. For the copolymer latices produced from styrene and butadiene, the attenuation and composition were related by an approximately linear relationship between 30 and 80 mole percent styrene. In this region, the attenuation spectra were regressed onto the property space using a linear multivariate algorithm called projection to latent structures. It was found that the attenuation is only useful for predicting latex properties that are related to composition in this range. Future work should focus on the use of a non-linear regression technique to model the behaviour of attenuation over the entire composition range and the use of independent analyses to better characterize some of the polymer properties such as crosslinking.

ACKNOWLEDGEMENTS

I would like to thank all of the people who contributed their time and effort to various aspects of this project.

Dr. John MacGregor provided ideas and had many fruitful suggestions throughout. Gord Slater provided technical assistance, and Bill Warriner gave me some very good practical design advice in addition to building equipment.

Lisa Morine, Kris Kostanski and Doug Keller all provided invaluable assistance in the area of polymer characterization.

All of the other graduate students in Chemical Engineering helped me along in many ways. Jim Kresta, Paul Gossen and Paul Gloor shared many conceptual aspects of their respective fields of expertise which helped me to understand the observations I have recorded and attempted to convey in this thesis.

BASF Canada was extremely co-operative with supplying latices and analytical measurements. In particular, I would like to thank Orest Chick and Mike Taylor for their assistance.

Dr. N. Patel from the Department of Material Science designed and built the ceramic tranducers used in this study. Prof. G. Johari from the Department of Material Science provided a good theoretical background for understanding some of the observations that resulted from this work.

Finally I would like to thank the Department of Chemical Engineering for financial support and for all of the assistance that everybody has given me.

TABLE OF CONTENTS

	Page
Abstract	iii
Acknowledgements	iv
List of Tables	ix
List of Figures	x
1. Introduction to On-line Sensing	1
1.1 The Role of Sensors in Feedback Control	1
1.2 Performance Criteria for Sensors	3
1.3 Limitations of Traditional Sensors	5
1.3.1 Off-line Analyses of Product Quality	6
1.4 Improvements that Make Novel On-line Sensors Possible	9
1.4.1 Improvements in Computing Power	9
1.4.2 Improvements in Calibration Methods	9
1.4.2.1 Traditional Calibration Methods	10
1.4.2.2 Bilinear Calibration Methods	11
1.5 Techniques for Developing New Sensors	14
1.5.1 Selection of the Property Space	14
1.5.2 Transducer Selection	14
1.5.3 Design a Sensor System	15
1.5.4 Manufacture a Set of Test Objects	15
1.5.5 Calibrate Sensor Output	15
1.5.6 Develop Shortcuts in the Measurement Procedure	15
2. Important States in Latex Systems	17
2.1 What is A Latex?	17
2.2 Important Properties of a Latex	18

2.2.1 Polymer Properties 18
2.3 The Two Systems to Be Studied 22
2.3.1 A Styrene-methylmethacrylate Copolymer 22
2.3.2 A Styrene-butadiene Rubber Copolymer 23

3. Introduction to the Travel of Stress Waves 26
3.1 Propagation of Ultrasonic Waves 26
3.2 Stress/Strain Relationships 28
3.2.1 Shear Modulus 29
3.2.2 Longitudinal Modulus 29
3.3 Propagation of Waves through Solids and Fluids 32
3.3.1 Mechanical Q 33
3.3.2 Reflection and Transmission of Stress Waves 33
3.4 Ultrasonic Velocity and Attenuation 35
3.4.1 Ultrasonic Velocity 35
3.4.2 Ultrasonic Attenuation 36
3.4.2.1 Absorption Contribution in Homogeneous Systems 36
3.4.2.2 Dispersion Contribution 39
3.4.2.3 Scattering Contribution 40
3.4.2.4 Diffraction Contribution 40
3.5 Wave Travel in Suspensions 42
3.5.1 Wave Travel in Polymer Latices 43

4. The Experimental Set-up 46
4.1 Generators and Detectors of Stress Waves 46
4.1.1 the Piezoelectric Effect 46
4.1.2 Piezoelectric Materials as Electro-mechanical Transducers 46

4.1.3 Differences Between Crystal and Ceramic Transducers 49
4.1.4 Transducers Used in this Study 50
4.2 Description of the Equipment for Measuring Velocity and Attenuation 53
4.2.1 The Pulse Echo Method for Measuring Velocity and Absolute Attenuation 53
4.2.2 The Phase Detection Method 53
4.2.3 Sources of Error for Measurement Equipment 54
4.2.4 Transducer Configuration 55
4.3 The Measurement Cell Design 56
4.4 The Rigorous Measurement Method 59
4.5 The Shortcut Measurement Method 63
4.5.1 Calculating the Reflection Loss 63
4.5.2 Measuring the Attenuation Constant 64

5. Results 67
5.1 Some General Observations 67
5.2 Results for the Styrene-methylmethacrylate system 68
5.3 Results for the Styrene-butadiene system 69
5.3.1 An Explanation of the Non-linear Dependence of Attenuation on Composition 71
5.3.2 Building a Predictive Relationship Between Polymer Properties of the Latex and Attenuation Spectra 79
5.3.2.1 Assessing PLS Models and Data Sets 79
5.3.2.2 Case One 81

5.3.2.3 Case Two 88
5.3.3 Summary of the Results for the Styrenebutadiene System 90

6. Conclusions 92
6.1 The Sensor Problem for Latex Systems 92
6.2 Ultrasonic Wave Travel in Polymer Latices 92
6.3 The Measurement Problem 93
6.4 Ultrasonic Attenuation Measurements in a Polymer System 94
6.5 Ultrasound as an On-line Sensor For Emulsion Polymerization 94

References 96
Appendix 1: Attenuation Measurements from the Rigorous Method 100
Appendix 2: Velocity Measurements 114
Appendix 3: Measurements of the Reflection Loss 115
Appendix 4: Attenuation Measurements by the Shortcut Method 119
Appendix 5: Summarized Attenuation Information 122
Appendix 6: SIMCA Output for Calibration of SBR Data Set 126

LIST OF TABLES

Table		Page
1.1	A Partial List of Temperature Measuring Devices	6
2.1	A List of Emulsion and Polymer Properties of a Latex	19
2.2	Homopolymers Made from the Monomers Used in the Example Systems	21
2.3	Property Space of the Sty-MMA Copolymer System	22
2.4	Property Space of the Sty-But Rubber Copolymer System	24
4.1	Advantages and Disadvantages of Ceramic and Crystal Transducers	50
5.1	The values of each of the constants in the second attenuation spectra simulation	74
5.2	The values of each of the constants in the third attenuation spectra simulation	78
5.3	Percent Sum of Squares Explained in **Y** by Column for PLS Case One.	83
5.4	Cross Validated Percent Sum of Squares Explained in **Y** by Column for PLS Case One.	83
5.5	Percent Sum of Squares Explained in **Y** by Column for PLS Case Two.	88
5.6	Cross Validated Percent Sum of Squares Explained in **Y** by Column for PLS Case Two.	89

TABLE OF FIGURES

Figure		Page
1.1	An Hypothetical Feedback Control Loop	2
1.2	The Matrix Relationships for Ordinary Least Squares	11
1.3	The Matrix Relationships for a Bilinear Decomposition	12
2.1	Reciprocal Swells vs Gels for the Sty-But System	25
2.2	Composition vs Crosslinking for the Sty-But System	25
3.1	Three Types of Stress Waves	27
3.2	The Shear Modulus	30
3.3	The Longitudinal Modulus	30
3.4	A Longitudinal Wavefront in Encounters a Sphere	41
3.5	The Competing Effects of Scattering and Diffraction in a Colloidal System	44
4.1	How a Piezoelectric Works	47
4.2	Performance of a Crystal and Ceramic Transducer	51
4.3	The MBS 800 Measurement Hardware	52
4.4	Transceiver Mode and Sender/Receiver Mode	56
4.5	Cross-section of the Measurement Cell	57
4.6	Calibrating the Pitch of the Measurement Cell	59
4.7	Attenuation and Transit Time as Functions of Distance for SMB56	62
5.1	Attenuation Dependence on Composition of Sty-But Latices at 13% Solids	69
5.2	Attenuation Dependence on Composition of Sty-But Latices	70

at 26% Solids
5.3 Dependence of Glass Transition Temperature on Composition for Sty-But Polymer 72
5.4 Attenuation Spectra for Simulation Two. 73
5.5 Attenuation vs Relaxation Frequency for Simulation Two. 75
5.6 Attenuation Spectra for Simulation Three. 76
5.7 Attenuation vs Relaxation Frequency for Simulation Three. 77
5.8 The Inner Relation for the First and Third Latent Variables in PLS Case One Model 84
5.9 Fitted vs Observed Latex Properties for the Sty-But System Using PLS Case One Model 85
5.10 Fitted vs Observed Latex Properties for the Sty-But System Using PLS Case Two Model 89

CHAPTER ONE

INTRODUCTION TO ON-LINE SENSING

1.1 The Role of Sensors in Feedback Control

The strategy for a feedback control system is to be able to hold a key variable at a desired value by manipulating another variable that effects the key variable. In automatic process control, the key variable is called the process variable, its desired value is called the setpoint, and the variable that is used to influence the process variable by its own position is called the manipulated variable. Using feedback control, it is possible to maintain a process variable at its setpoint despite unpredicted disturbances in the process (regulatory control) or to bring the value of the process variable to a new physically realizable setpoint in a safe manner (servo-control).

In spite of all of the complexity that is possible in the real world, all feedback control loops are made up of three basic components as pointed out by Liptak (1967). The first component is a **sensing device** that measures and reports the value of the process variable. This device provides a signal which is proportional to the value of the process variable. The signal medium transports the signal with minimum corruption to the second component which is the **controller**. The controller takes the sensor input and compares it with a setpoint using a mathematical algorithm to decide whether corrective action should be taken. The decision of the controller is enforced with an output signal which is used to determine the position of the manipulated variable via the **final control element**. The value of the manipulated variable will effect the process variable by

bringing the process to a new set of equilibrium conditions in response to a disturbance or a new setpoint. In Figure 1.1, an hypothetical feedback control loop is shown to demonstrate the relationships between each component in the loop.

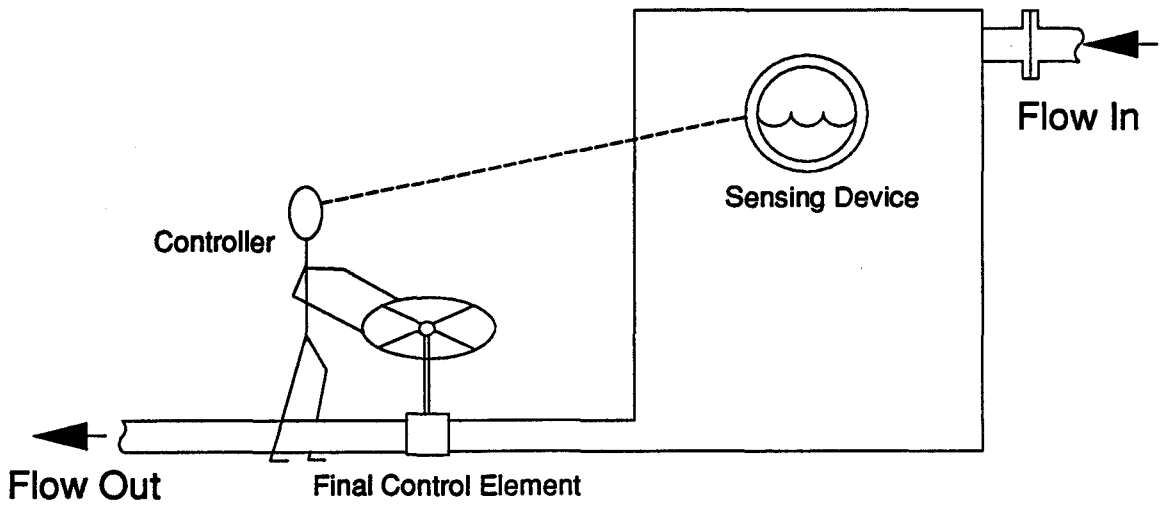

Figure 1.1 An hypothetical feedback control loop for controlling the level in a tank

In this case, an operator (the controller) is trying to control the level in a hold-up tank by opening or closing a valve on the outlet of the tank (the final control element). The sensing device that tells the operator about the level in the tank is the sight glass. In addition to these three components, most automatic control systems also have supervisory hardware so that the setpoints of process variables can be adjusted and data can be logged/displayed.

Although most process control research concentrates on the process modelling and the efficiency of the control algorithm, the success of any control scheme depends on the accuracy and dependability of the sensors that are used to monitor the process variables. Due to a lack of reliability, the sensors often represent a weak link in the

feedback control loop. Elaborate filtering calculations are sometimes necessary to condition the measurement signal when the precision of a measurement is poor or contaminated with noise. This thesis is concerned with the development of a sensing device which can be used to provide information about the polymer properties in latex systems.

All process sensors are a subset of a larger group of devices known as *transducers*. Ratzlaff (1987) uses the Instrument Society of America's description of a transducer as an introduction to the subject of sensors in his book. This body has defined a transducer as a physical device which can "provide a usable output in response to a specified measurand... a physical quantity, property, or condition which is measured." In this general sense, a transducer refers to a device which can convert a signal in one medium into a proportional signal in a second medium, for example, an electrical current signal into a proportional pressure signal. In the special case of a sensor, the level of the signal in the second medium is used to infer the position of the first medium.

Sensors are often considered to be made up of two separate devices, the sensing element and the transmitting element. Having made this distinction, only the sensing element is a transducer, while the transmitting element would be that part of the sensor that is used for transmitting the measurement signal along with any other devices required to amplify this signal. Sensors are also described as being active or passive. Active sensors are driven by their own power source which is separate from the system they are measuring while passive sensors are driven by taking energy out of the system which they are measuring.

1.2 Performance Criteria For Sensors

There are many different types of process sensors that have been developed since the birth of the process industry. A number of criteria such as those listed by Taylor (1989) have been defined to assess the quality of a particular sensor. It is important to

define some of these in this section. It is helpful when discussing these criteria to describe a graph, often called a calibration curve, which defines the true value of some variable as a function of the signal of a sensor that is used to measure it.

1.2.1 Linearity of the Sensor Output

The mathematical relation that describes how the true value of the measured variable fits the sensor signal data is important for determining how much effort is required to extract an inference of the measurand from the sensor signal. If this relation is a straight line, then the behavior of the sensor output is linear. Linearity is important because it allows the sensor to be simply calibrated and it requires the minimum amount of signal processing to yield the measurand. If the sensor output is non-linear over its entire range, the range is often broken down into smaller regions over which the sensor output is approximately linear.

1.2.2 Span of the Sensor

The range of values of the measured variable over which the sensor output can be used to infer this variable is called the span of the sensor. For obvious reasons, it is necessary that a useful sensor have a span that includes the whole range of values that would be expected for a process.

1.2.3 Sensitivity of the Sensor

The steepness of the slope of the calibration curve is called the sensitivity of a sensor. The steeper the slope the more sensitive the sensor signal is to changes in the measured variable.

1.2.4 Accuracy and Precision

The accuracy of a sensor describes how closely the true value of the measured variable is to the value that is predicted from the sensor. This will be dependent on the limitations imposed by the calibration of the sensor, for example, the range of the calibration and the standard used to calibrate the sensor.

The precision is the error variance associated with replicate measurements while the true value of the measured variable is held constant. The precision can be influenced by factors such as measurement and transmission noise, or aging of the internal parts of the sensor.

1.3 Limitations of Traditional Sensors

In modern industry there are two main types of process measurements. On-line measurements are taken from sensors that are built into the process, and report the value of some measurand with an output signal. Off-line measurements are remote measurements that are made on a small sample of the process fluid after it has been collected and removed from the process. These latter measurements are usually labour intensive and introduce substantial deadtime into a feedback loop.

Most on-line process sensors have been developed to measure state variables such as temperature or pressure in a batch system or state variables and flowrates in a continuous system. As an example, Table 1.1 gives a partial list of the many different techniques that have been developed for on-line temperature sensing. Unfortunately, variables that can be measured by standard sensors are usually inappropriate for monitoring or controlling complicated systems as pointed out by Chien and Penlidis (1990). This is due to the complex physical and molecular nature of the product, especially in the polymer industry.

When it was discovered that changes in the molecular properties of a polymer such as molecular weight or chain branching would yield a product with different performance properties, it became necessary to measure these predictors of product quality off-line using analytical techniques and standard test methods. Predictors of product quality are called **quality variables** because their values will influence the

Table 1.1 A partial list of temperature measuring devices

Device	Operating Principle	Range (C)
resistance thermometer (RTD)	resistance sensitive to temperature	-250 to 1000
thermistor	resistance sensitive to temperature	-100 to 300
quartz crystal thermometer	resonant frequency sensitive to temperature	-40 to 230
thermocouple	voltage of bimetallic junction sensitive to temperature	-260 to 2800
radiation pyrometry	thermal radiation sensitive to fourth power of temperature	0 to 7000
infrared pyrometry	thermal radiation sensitive to fourth power of temperature	0 to 4000
ultrasonic velocity	sound velocity of a sealed fluid sensitive to temperature	-260 to 760
someone's finger	human's central nervous system can estimate temperature	0 to 70
fluid filled devices	thermal expansion of a fluid sensitive to temperature	-260 to 760

quality or value of the final product. The chemical industry has universally acknowledged the absence of capable sensors by developing the quality control lab, where off-line measurements are used to measure product quality variables.

1.3.1 Off-line Analyses of Product Quality

One advantage of a central location for off-line analyses is that the cost of analytical resources and expertise can be shared by more than one plant operation. The major disadvantage is that the time required to analyze a sample off-line can be too long to provide feedback to the process. This is especially true for heterogeneous chemical reactions such as emulsion polymerization, where the product has to be separated from the dispersion medium before it can be analyzed. Another problem is that many chemical reactions such as crosslinking are irreversible with kinetics that are very fast relative to an

off-line analysis. Because off-line sampling is so difficult to implement, quality variables are often only examined at the end for many industrial batch processes or infrequently for continuous processes.

Some attempts have been made to include intermittent off-line measurements in a feedback policy for polymer reactors. An example of the direct use of laboratory measurements for the control of quality in an industrial polymerization process is given by Roffel et al (1990). Another method is to use an observer or state estimator such as a Kalman filter, which is a stochastic observer. This family of techniques uses a continuous or discretized state space model of the process along with a set of variables measured on-line to track the process states, even though not all of the states are measured on a regular basis. The designer is able to weight either the model's estimate or the measurement's estimate of all the states in the tracking calculation by specifying the covariance matrix of the measurement error and the covariance matrix of the model lack-of-fit error. Gagnon and MacGregor (1991) demonstrated that unmeasured disturbances could be compensated by including additional stochastic states in the process model. Other recursive estimation strategies have also been used to estimate the level of an infrequently measured process variable between measurement intervals. One application has been the on-line estimation of melt flow index and density in a continuous fluidized bed polyethylene reactor by MacAuley and MacGregor (1991). Although these methods are sometimes used in industry, the problem with all model based state estimators is that a complex mechanistic process model must be developed.

A less mathematical but more widely accepted practise is to let the plant operators develop their own intuitive methods for adjusting the manipulated variables based on the results from lab analyses. Although this practise is highly successful, the problem is that the operator is a knowledge-based system, and will not usually be able to respond optimally to a situation that has not been previously encountered.

All methods that attempt to incorporate off-line analyses into a control strategy are generally suboptimal because of the deadtime introduced into the feedback loop or impractical because of the amount of detailed information that is required to develop a process model. Even in the cases where one of these strategies is being effectively used,

an off-line analysis is expensive to perform and additional variation is introduced by the sampling method, sample handling and analysis which are not always carried out by the same group of people. A less expensive and more efficient strategy would be to develop on-line sensors that respond to changes in the important molecular properties or quality variables of a process. An example of this strategy is a conductivity meter, which can be used to infer the composition of a binary liquid mixture in a distillation column.

A stumbling block that has impeded the development of novel sensors is the philosophy that a sensor's measurement signal should relate directly to only one measurand. Before the widespread use of digital microelectronics in the process industries, numerical processing of the measurement signal was not possible so that sensors had to correspond to the measurand by simple univariate relationships. The implicit assumption that still exists today is that one sensor can only give information about one process or quality variable. This approach generally fails to recognize that most process variables are inter-related to varying extents. In addition, some sensors such as spectroscopic devices are able to generate multiple measurements simultaneously. These spectra can depend on many different properties of a polymer system. Some examples of spectroscopic devices are NIR sensors which can measure the absorbance or transmittance of near infra-red light over a frequency range or ultrasonic measurement equipment which can measure attenuation and velocity of sound waves over a frequency range.

The use of a multivariate relation can be used to combine sensor measurements to infer the level of unmeasured variables. For example, a conductivity measurement can be used alone to infer the composition of a binary mixture or it can be used to infer the composition in a ternary mixture if it is combined with a temperature measurement. Two improvements in technology have made it possible to make great strides in the field of on-line sensors; computing power and multivariate calibration methods. These improvements are discussed briefly in the next section and in greater detail by Callis et al (1987).

1.4 Improvements that Make Novel On-line Sensors Possible

1.4.1 Improvements in Computing Power (circa 1975)

Because of tradition, most measurement signals are transmitted as pneumatic or analog voltage signals. By the mid-1970's, integrated circuits had become so versatile and powerful as computing engines, that microprocessors such as the Intel 8080 (introduced in 1974) were being used by manufacturers in many consumer applications to control devices such as the microwave oven and the VCR. This chip can perform 200,000 operations per second and currently costs about $2 today. Hardware that could be used to interface analog measurement signals with digital processors such as analog to digital converters and digital to analog converters was soon developed to take advantage of the computational power of digital microelectronics. This power allows microprocessor based controllers to execute very numerically intensive control algorithms very quickly. On-line computing power also makes it possible to perform many calculations to transform a measurement signal that is non-linear or to consider process sensors with outputs that require extensive mathematical conditioning. The result is that a whole new selection of instruments and analyzers can be considered for process applications as on-line sensors.

1.4.2 Improvements in Calibration Methods

Before the on-line computing power discussed in the previous paragraph can be utilized, mathematical models have to be developed that can transform raw measurements into predictions of important unmeasured process variables. The procedure of finding a relationship between a sensor measurement and the true value of the measurand is called a calibration. Almost all process sensors need to be calibrated because the measurand is inferred indirectly from its effect on a related property. For example, a thermocouple measures the voltage generated at a bimetallic junction and uses this value to infer a point temperature. Most traditional sensors can be calibrated by univariate functions; one dependent variable (the measurand) is defined as a function of one independent variable (the measurement signal) based on one or more calibration points. In matrix notation, the

column vector containing the true values of the measured variable is called **Y** and the column vector which contains the corresponding measurement signals is called **X** for where each row (object) is a calibration point.

1.4.2.1 Traditional Calibration Methods

One popular statistical method for describing how the independent variable (x) is a function of a dependent variable (y) is ordinary least squares regression. This algorithm calculates a matrix of linear coefficients (**b**) that are multiplied by x to give an estimate of y ($\hat{y}$ using the nomenclature for statistics). The linear coefficients are calculated so that the sum of the squares of the residuals between the curve and the actual data points is minimized. A graphical description of OLS regression is shown in Figure 1.2. The columns that are included in **X** are chosen to fit the type of relationship that is expected between x and y. When a proportional relationship between the measurement signal and the measurand is expected, **X** is just a column vector of the measurement signals. If an intercept is expected ($\hat{y} = b_o + b_1 x$) then a column of ones is inserted in **X**. OLS regression can also be extended to model the effect of more than one independent variable on y (the multivariate case) by including extra columns in **X**.

Unfortunately, OLS is not a very practical algorithm when there is extreme correlation in the block of independent variables. This is because the calculation of the matrix of linear coefficients requires an inversion of $\mathbf{X}^T\mathbf{X}$ which is not possible if $\mathbf{X}^T\mathbf{X}$ is singular or nearly so. There are two cases when we would like to use multiple sensor measurements to predict one or more variables that cannot be readily measured on-line. The first case involves combining a group of different sensor measurements (as in the conductivity meter example). The second case is when one sensor gives many measurements simultaneously (such as a spectroscopic device). In both cases, there is usually some correlation in the independent variables for all of the calibration points so that the true basis of **X** has a lower dimension than **X**. Because very little is known

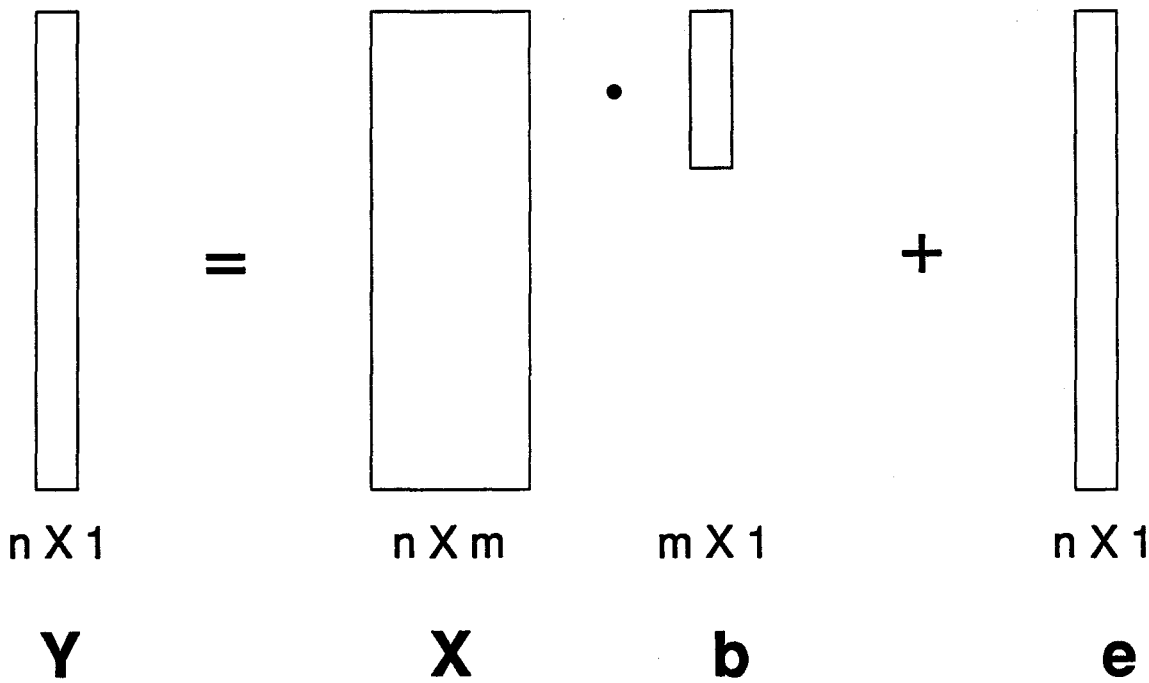

Figure 1.2 The matrix relationships for Ordinary Least Squares Regression

about the causal relationship between the dependent and independent variables, it might be very difficult to initially throw out the redundant variables in **X** that are causing the collinearity in order to obtain good estimates of the regression coefficients.

1.4.2.2 Calibration Methods that are Insensitive to Collinearity (circa 1980)

Kresta et al (1990) stated a threefold challenge for multivariate statistical algorithms:

(1) • they must be able to deal with collinear data of high dimension in independent (**X**) and dependent variables (**Y**)

(2) • they must reduce the dimension of the problem

(3) • they must be able to give good predictions of **Y** from **X** (the calibration)

One group of techniques that seems to meet these requirements is the family of bilinear methods that have been refined by a number of workers and described in articles by Kowalski (1983), Geladi and Kowalski (1986) and others. A bilinear method is an iterative technique for decomposing a matrix of observations (**X** or **Y**) into two separate matrices **T** and **P**. An example of the bilinear decomposition of **X** is shown in Figure 1.3. Each column vector in **T** is called a score (denoted t_i) and each column vector in $\mathbf{P}^T$ is called a loading (denoted p_i). The product of each score and loading pair (t_i,p_i, where i=1 to r) is a singular n by m matrix of rank one which accounts for some of the variation in **X**. The algorithm for calculating the scores and loadings is iterative so that the first pair (t_1, p_1) accounts for the maximum covariance between **X** and **Y**. Subsequent iterations will decompose the residual matrix **e** until there seems to be no remaining structure. The main assumption used in developing these methods is that the variation that is observed in all of the m independent variables is really the result of movement along a few (r) underlying **latent variables** where r<m.

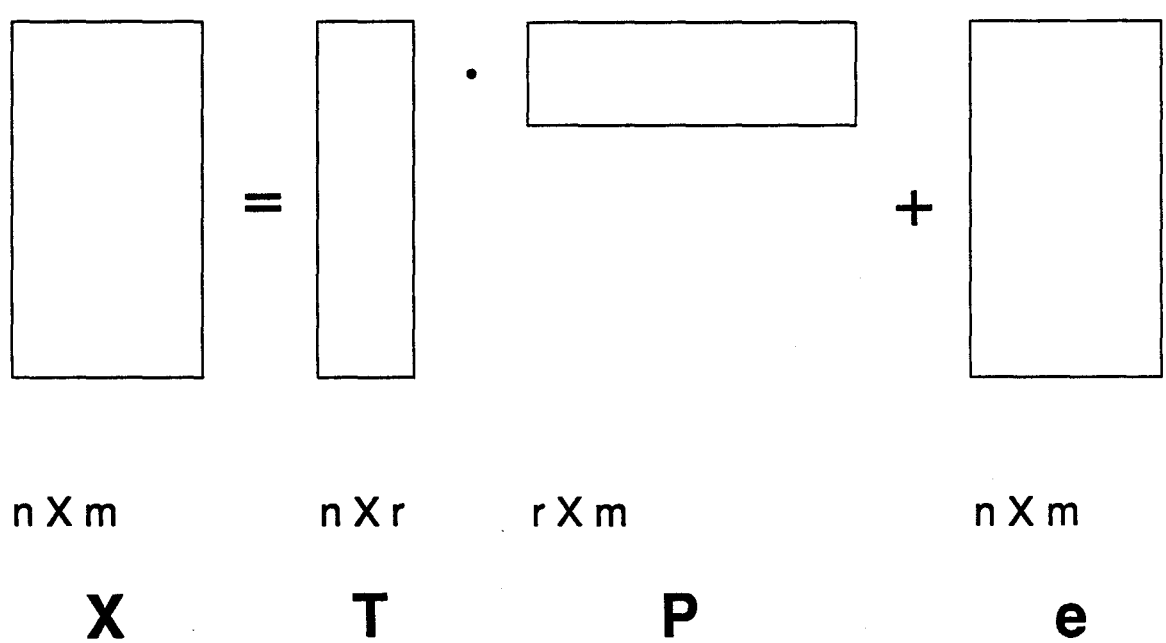

Figure 1.3. **X** is decomposed into the score matrix **T** and the loading matrix $\mathbf{P}^T$

Geometrically, the loading vectors (p_i's) define the direction of each principal component with respect to the columns of **X** so that they represent a rotation of the basis vectors of **X**. The score vectors (t_i's) are least squares projections of **X** down onto each of the new basis vectors of **X** (the p_i's). For example, p_1 is a linear combination of all of the columns of **X** in the direction of greatest variation. The bilinear decomposition allows us to remove the (m-r) dimensions that only account for a small amount of independent variation. When only one matrix is decomposed, the bilinear method is very similar to a canonical transformation or singular value decomposition of **X** by eigenvalue/eigenvector methods. In this case, the scores **T** are equivalent to the eigenvectors of $\mathbf{XX}^T$ and the loadings **P** are equivalent to the eigenvectors of $\mathbf{X}^T\mathbf{X}$ (p_1 is the eigenvector corresponding to the largest eigenvalue).

A bilinear decomposition method has also been developed to simultaneously decompose **X** and **Y** to find the linear latent structures in **X** and **Y** that are the most highly correlated with each other. This method is called **PLS** (Projection onto Latent Structures). It can be shown that the loading vectors used by the PLS algorithm are the eigenvectors of $\mathbf{X}^T\mathbf{YY}^T\mathbf{X}$. PLS turns out to be an excellent improvement over OLS for multivariate calibration problems because of its ability to handle correlated data when developing predictive relationships between dependent and independent variables. The use of PLS methods for multivariate calibration are treated by Marten and Naes (1989).

1.5 Techniques for Developing New Sensors

Now it is time to put together some of the ideas discussed in this chapter. The first section of this chapter emphasized that a sensing device is an essential component in a feedback loop. In the third section, it was stated that there is a lack of sensors that are able to measure important variables in the process industries. In the fourth section, two important technological advances were discussed that would allow a new generation of instruments to be considered as candidates for novel sensors, increased available computing power and multivariate calibration algorithms that are insensitive to collinearity. In this section, a general method for assessing new on-line sensors is presented. This outline should also serve to steer the reader through the remainder of this thesis, as we design and calibrate a sensor for measuring the molecular properties of a copolymer latex system.

1.5.1 Selection of the Property Space

Sensor development can only begin after one decides what set of variables one would like to have available on-line during a process operation. These could be molecular or physical properties such as molecular weight, crosslink density, particle size or quality variables such as Mooney viscosity, melt flow index, colour. These variables are the **property space** of the system and **Y** in a multivariate calibration. A discussion of the important polymer properties in emulsion polymerization systems is given in chapter two.

1.5.2 Transducer Selection

The next step is to choose a sensing element which is sensitive to changes in the property space. The sensing element should be able to measure changes in a common property that varies as variables in the property space change. For example, if variables in the property space depend on the elastic modulus, then a useful sensor might indirectly measure the elasticity. In chapter three, there is a discussion of the scientific principles governing the travel of ultrasonic waves and how they can be related to the elastic

properties of the material that they travel through.

1.5.3 Design a Sensor System

A prototype of the sensor system will help to determine whether on-line measurements are practical and it is necessary for calibrating the sensor in the next step. The system for measuring the velocity and attenuation of stress waves through a latex sample is discussed in chapter four.

1.5.4 Manufacture a Set of Test Objects for Calibrating Sensor

An experimental design should be used to obtain a set of calibration objects that contain independent variations in the variables of the property space. The variation in the property space of the calibration objects should reflect different levels that are realistic for the process under investigation. If the properties in Y are correlated with each other, it will not be possible to infer a definitive causal relationship between the individual properties of Y and the measurements of X.

1.5.5 Calibrate Sensor Output with Test Objects Using a Bilinear Method

The first questions that need to be answered are common for the calibration of any sensor. Does the sensor output span the property space? Is the sensor output sufficiently sensitive to measure significant changes in the property space? Does a linear model fit the data better if the measurement output is transformed? This step should also show which variables in the property space can be predicted by the sensor and which cannot. The results of a multivariate calibration for the two systems studied in this thesis are discussed in chapter five and some conclusions are made in chapter six.

1.5.6 Develop Shortcuts in the Measurement Procedure

Often, simplifying assumptions can be made that make the sampling method more routine. The purpose of this last step is to make the procedure easier to implement

on-line. One simplification that makes the measurement of wave attenuation much quicker is discussed in chapter four.

Notation

b	column vector of OLS regression coefficients
e	matrix of model lack of fit residuals
m	number of independent terms in an OLS or bilinear model
n	number of objects or samples on which model is based
p	individual loading vector
P	matrix of loading vectors
r	number of latent variables in a bilinear decomposition
t	individual score vector
T	matrix of score vectors
x	an independent variable
X	matrix of independent variables
y	a dependant variable
Y	matrix of dependent variables

CHAPTER TWO

IMPORTANT STATES IN LATEX SYSTEMS

Some of the physics and chemistry of polymer colloids or **latices** will be discussed in this chapter. This summary will focus on the polymer properties of latices. In the final section, the two example latex systems under investigation in this thesis will be described.

2.1 What is a latex?

A good description of polymer latices is given by Ottewill (1982). A polymer latex is a colloidal dispersion of polymer particles suspended in some continuous liquid phase. The particles range in size from 10 to 10^3 nm and are suspended by Brownian motion. In all of the examples considered in this thesis the continuous phase is water and the particles are stabilized by mutual electrostatic repulsion. The particles can consist of a homopolymer or a copolymer.

The net charge on a latex particle is the result of ionic groups that have been built into the polymer or amphiphillic molecules that have adsorbed onto the surface. These stabilizing molecules (sometimes called the surfactant or emulsifier) have a hydrophobic tail such as a long alkane which is non-polar and sticks preferentially to the polymer surface and a hydrophillic head such as the salt of an acid or base which orients itself on the aqueous side of the interface. The hydrophillic head can be cationic, anionic or non-ionic. The surface charge of the polymer particles is balanced by a cloud of aqueous

counterions. These are held in place by the competing forces of electrostatic attraction to the polymer surface and diffusion into the bulk solution. This double layer of charge covering the polymer colloid is called the electrical double layer (Popiel (1978)).

Although a latex can be manufactured by milling a polymer down to colloidal dimensions and dispersing it in water with a surfactant, this is not the normal mode of production. Almost all latices are produced by emulsion polymerization. By this technique, polymer particles are nucleated in the aqueous phase and grow in a huge number of separate locations (for example 10^{15} to 10^{19} per liter) that are partitioned in the water by a surfactant. Manufacturing latices by emulsion polymerization is reviewed by Duck (1966) and modelling and control of latex reactors have been addressed by many authors including Kirillov and Ray (1978) and Hamielec and MacGregor (1982).

2.2 Important Properties of a Latex

The properties of a latex system are usually divided into two categories; emulsion properties and polymer properties. Emulsion properties are measured because they can be used to assess the stability of the polymer particles in the water and the performance of the latex in its end use application. Polymer properties are only concerned with what is inside the polymer particles themselves and are measured because they strongly affect the behavior of the latex in its end use application. A list of some of the important properties in each category that are measured in latex systems is provided in Table 2.1.

Although properties from both categories should be measured for the purposes of providing feedback to the process, this work is concerned with developing a sensor that responds most sensitively to the polymer properties of a latex. For this reason, some of the properties listed in Table 2.1 will be discussed in the remainder of this chapter.

2.2.1 Polymer Properties

The properties of polymers and their effects on rheology is a topic that has been

Table 2.1 A list of emulsion and polymer properties of a latex.

Emulsion Properties	Polymer Properties
particle size	copolymer composition
percent solids	molecular weight
pH	branching frequency
surface tension	crosslink density
viscosity	chain regularity
mechanical (shearing) stability	structure (percent crystallinity)
total surfactant	glass transition temperature
dissolved electrolyte (conductivity)	melt flow index

researched extensively. Only the specific properties that pertain to this work will be discussed here. Two good introductory texts are by Hiemenz (1984) and Ferry (1980). Polymer properties can be divided into two categories; intramolecular properties that measure the structure of the polymer chain and intermolecular properties that measure how polymer chains interact with each other. Some of the intramolecular properties define attributes of the polymer chain such as molecular weight, branching frequency and crosslink density. In the case where more than one monomer is incorporated into the chain, additional properties such as composition and distribution of monomer repeat units in the chain also have to be measured. Some examples of intermolecular properties are the percent crystallinity and the glass transition temperature.

Propagation reactions result in chains that are made up of many monomer repeating units. The length of repeating units in a chain is described by its **molecular weight.** Most polymer reactions yield polymer chains with a distribution of molecular

weights. The number average molecular weight M_n is defined as the average of the molecular weights of every polymer chain in a population. Higher average molecular weights are also defined to characterize the shape of the molecular weight distribution. The weight average molecular weight M_w weights each chain in the average according to its molecular weight. The ratio of these two averages is used to give an indication of the breadth of the molecular weight distribution or polydispersity.

Polymer chains are also characterized by **chain branching** and **chain crosslinking**. Branches are chains that extend off the main backbone of a polymer. Short chains can be incorporated into a polymer produced by free radical polymerization by using a monomer that has a short chain such as an alkyl group attached to the vinyl carbon. Long chain branches and crosslinks are introduced by polymerizing a monomer that can be attacked by a radical at more than one position such as a divinyl monomer. A crosslink is a bridge that connects two polymer chains. A high degree of crosslinking reduces the mobility of individual chains and creates a polymer with a 3 dimensional structure that is insoluble in all solvents.

Many intermolecular properties such as tensile strength, glass transition temperature and hardness are known to vary linearly with the **copolymer composition** if two monomers are polymerized. This is because these properties are dependent on chemical factors such as chain stiffness and stereoregularity which depend on the type of repeating unit in the chain. One method for producing a polymer with unique "tailor-made" bulk properties is to adjust the composition of the monomer used to produce a polymer.

Another important property that can be used to measure the intermolecular structure of the polymer is the **glass transition temperature** (T_g). This is the approximate temperature below which the bulk properties of a polymer correspond to a glassy solid and above which the bulk properties correspond to a viscous liquid. The value of the T_g is interpolated from the change in the slope of properties such as specific volume, heat capacity, or shear modulus as a function of temperature. Below the T_g the polymer chains have no translational or rotational motion. In this condition an amorphous polymer possesses physical properties more similar to a crystalline solid, even

though there is no structural symmetry and its nearest neighbor structure is more like a liquid. This type of material is called a glass. Above the T_g but below the melting temperature, the polymer can behave like a viscous liquid or an elastic solid or something in between. The different types of behavior that can be expected for a polymer between T_g and the melting point are discussed in section 3.3. The T_g is affected by the mobility of the polymer chains. Properties that decrease the freedom of the polymer chains such as crosslinking and increased molecular weight generally raise the T_g. Of course, polymer mobility is largely determined by the structural flexibility of the polymer backbone which is a strong function of composition. The glass transition temperature for some homopolymers is shown in Table 2.2 (Hiemenz (1984)).

Table 2.2. Homopolymers made from some of the monomers used in the example copolymer systems.

Homopolymer	Monomer formula	T_g (deg C)
poly(styrene)	C=C—C$_6$	100
poly(1,4 butadiene)	C=C—C=C	-101
poly(methylmethacrylate)	C=C(C)—C(=O)—O—C	115
poly(acrylic acid)	C=C—COOH	106

2.3 The Two Latex Systems to be Studied

2.3.1 A Styrene-methylmethacrylate Copolymer

The first example is a set of five styrene-methylmethacrylate latices produced at McMaster University in a one gallon reactor and described by Gossen (1992). All batches were taken to complete conversion so that there was no residual monomer in droplets or dissolved in the polymer. Copolymer composition and percent solids were inferred from the initial charge, and particle size and density were measured off-line using a NICOMP light scattering particle sizer and a vibrating U tube densitometer respectively. The weight average molecular weight was assessed using low angle light scattering. The property space for this set of latices is shown in Table 2.3.

Table 2.3 Property Space of the Sty-MMA Copolymer System.

Object	% Solids	% Sty	% MMA	Density	Wgt Av Mol Wgt ($\times 10^6$)	P.S (nm) (Std)
SMB52	31.5	60.0	40.0	1.0405	N/A	34.9 (23.7)
SMB53	31.5	66.6	33.4	1.0366	2.22	56.9 (13.3)
SMB54	31.5	60.0	40.0	1.0393	2.50	67.3 (11.5)
SMB55	31.1	60.0	40.0	1.0383	4.00	76.8 (10.0)
SMB56	31.1	66.6	33.4	1.0359	3.57	75.0 (15.2)

2.3.2 A Styrene-butadiene rubber copolymer

The second example is a set of eleven styrene-butadiene copolymer latices produced in an industrial scale batch reactor. These latices represent different grades of a copolymer rubber that is sold commercially as an adhesive. All of the samples that were analyzed had been steam stripped to remove residual styrene. The following properties have been measured as part of an off-line batch analysis; percent solids, particle size, pH, monomer composition, gels and swells. Gels and swells are quality variables that are obtained by making a film with the latex and drying it. A known weight is placed in toluene. The mass percent that does not dissolve in toluene is the percent gel. The additional weight of toluene that has swollen into the undissolved fraction of the film is the percent swells. There is some correlation between gels and swells. A plot of reciprocal swells and gels is shown in Figure 2.1. The reciprocal of percent swells is used empirically as a predictor of crosslink density. In addition to these measurements, the glass transition temperature was analyzed by differential scanning calorimetry. The property space for this set of latices is shown in Table 2.4.

Some of the characteristics of the copolymer system and this data set in particular will now be discussed. In addition to styrene and butadiene, a small amount (3.3 mole percent maximum) of acrylic acid is added to the reactor after the polymer particles have formed. Acrylic acid has a hydrophobic vinyl bond and a hydrophillic carboxylic acid (see Table 2.2). It is thought that some of this acid migrates to the surface of the polymer particles and is grafted with the carboxylic acid facing out into the water. This yields a surface modified polymer particle with most of the properties of a styrene-butadiene copolymer along with improved adhesive properties that are the result of the surface carboxylic acid. A good review article on this technique is by Dunn (1988).

There are two significant features of this data set. The first is that all of the samples have some degree of crosslinking so that they should behave differently from linear polymers above the glass transition temperature. The second feature is that there is a good amount of independent variation in the variables of the property space, especially composition and reciprocal swells. A plot of reciprocal swells as a function of composition is shown in Figure 2.2. Although this set of objects was not obtained from an experimental design, composition

and inverse swells are relatively uncorrelated so that it should be possible to determine if these two properties have an independent effect on the measurement space of an hypothetical sensor.

Table 2.4 Property Space of the Sty-But Rubber Copolymer System.

Code	Object	T_g (°C)	% Solids	% Sty	% But	% Acr	Gels (%)	Swells (%)	P.S (nm)
1	P1017	-4.4	54.5	53	44	3.3	92.7	7.9	231
2	P1163	-49.3	51.4	25	77	3.2	57.5	16.9	172
3	P1376	47.3	52.2	77	21	2.4	72.2	23.7	148
4	P1377	34.8	54.9	68	29	3.2	90.1	4.1	151
5	P1380	12.6	53.8	61	37	2.2	83.5	9.1	174
6	P1382	-31.8	54.7	42	55	2.2	42.1	23.5	156
7	P1406	-22.1	53.6	50	49	1.5	75.0	15.1	209
8	P1006	-29.1	52.7	42	56	2.2	74.8	12.9	185
9	P1123	-62.0	50.8	15	85	0	88.8	26.5	N/A
10	P1764	47.2	54.0	77	21	2.4	63.0	16.2	N/A
11	P9999	51.0	54.0	85	15	0	53.3	19.5	N/A

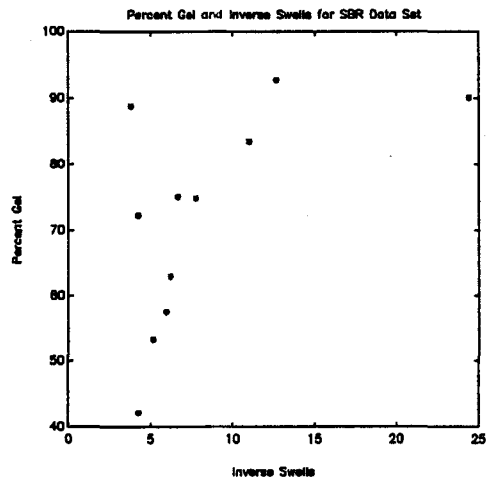

Figure 2.1 Reciprocal swells and gels for the styrene-butadiene data set.

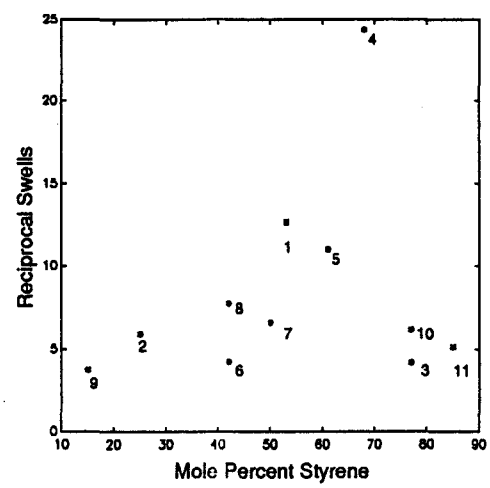

Figure 2.2 Composition and Crosslinking are varied independently. Numbers are coded objects from Table 2.4.

CHAPTER THREE

AN INTRODUCTION TO THE TRAVEL OF HIGH FREQUENCY STRESS WAVES

The purpose of this chapter is to show how travelling longitudinal pressure waves can be used to provide information about some of the properties in a latex polymer system. Some of the theoretical relationships between the wave travel parameters and the physical properties of the system will be described. The point of this thesis however is to develop empirical models between these wave travel parameters and the physical properties of the system so that most of the theory will not be developed rigorously.

3.1 Propagation Of Ultrasonic Waves

High frequency stress waves propagate through a material by one of three modes shown in Figure 3.1 and discussed in extreme detail in texts such as Meyer and Neumann (1972) and Morse and Ingard (1968). The two important types of waves for this study are shear (A) and longitudinal (B).

For a longitudinal wave, particles move in the same direction as the wave. Zones of compression and rarefaction are created as particles are pushed together and pulled apart by the proceeding wave. With a shear wave, particles travel in a direction that is perpendicular to the direction of propagation. In the case of solids that propagate both compressional and shear waves simultaneously, the transverse waves are always slower.

The simplest type of wave to examine theoretically is a longitudinal wave. It is usually assumed that stress waves radiate with a uniform wavefront that moves forward as

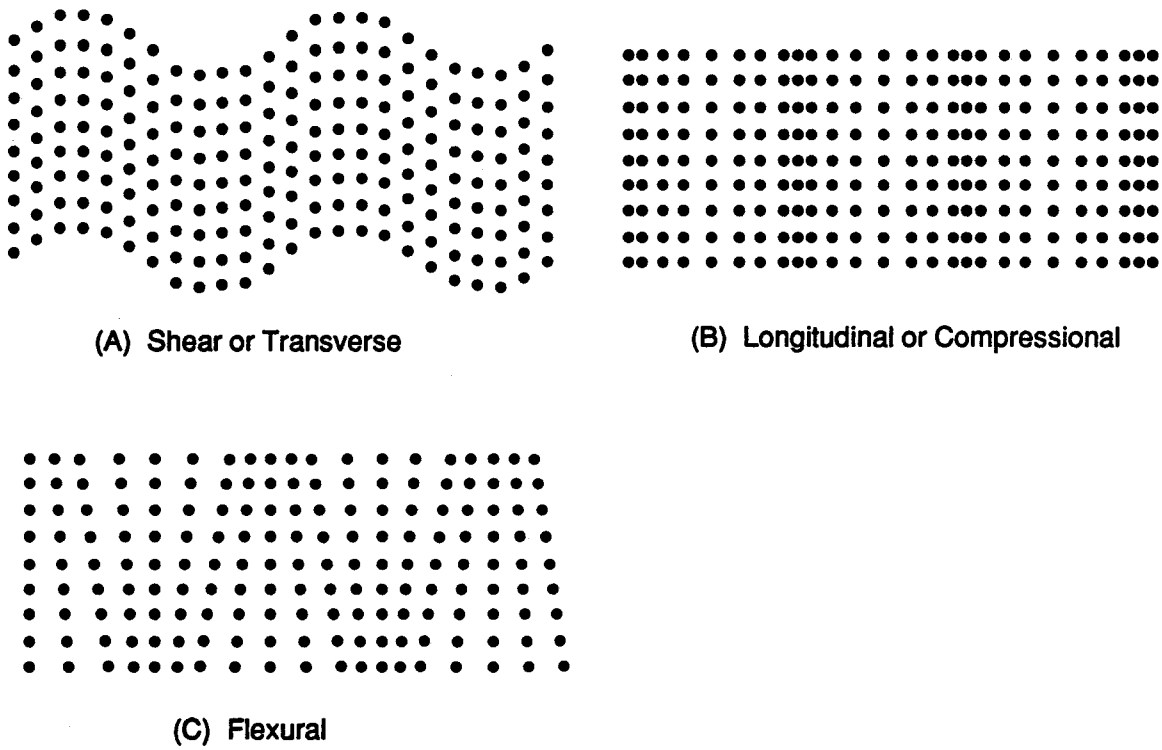

Figure 3.1 Three Types of Stress Waves

a plane. All points on the plane normal to the direction of the travelling wave will experience a common force distributed over the area of the beam of the field. The excess pressure caused by an oscillating longitudinal stress field is decribed by equation 3.1.

$$p = p_o e^{j\omega t - \Gamma x} \tag{3.1}$$

In this expression, x is the distance in the direction of wave travel, t is the time that the wave has been travelling with respect to x, p_o is the excess pressure when x=0 and t=0, ω is the angular velocity of the stress field and Γ is the complex propagation constant. The propagation constant is defined by equation 3.2.

$$\Gamma = \alpha + j\beta \tag{3.2}$$

In equation 3.2, α is the attenuation constant in nepers/m and β is the propagation constant (ω/v) in m^{-1}. By substituting equation 3.2 into 3.1, it can be shown that a travelling longitudinal stress field is damped by the product of the distance (x) and the attenuation constant (α) which is a characteristic of the material through which the wave is travelling (equation 3.3).

$$p = p_o e^{-\alpha x}[\cos(\omega t - \beta x) + j\sin(\omega t - \beta x)] \tag{3.3}$$

This equation confirms that all stress waves will eventually damp out in materials with α greater than zero. The excess pressure will be a real quantity when the wave is in phase with a reference.

3.2 Stress/Strain Relationships

How a material responds to the force that is applied by a travelling wave depends on its chemical constitution. Continuum mechanics is the study of how a small element of a material will deform or strain when forces are applied in different directions. The extent to which a material will deform when a force is exerted against it is described by its elastic modulus which is equal to the ratio of the applied stress to the resulting strain. The elastic modulus is a characteristic of the material and is defined in equation 3.4.

$$\text{Elastic Modulus} = \frac{\text{Stress (force/area)}}{\text{Strain (dimensionless)}} \tag{3.4}$$

The stress is measured in units of force over the affected area. The strain is defined as the forced displacement divided by the unstressed length or size. The elastic modulus is a complex quantity, to include the possibility that an oscillating strain is not in phase with the originating oscillating stress field. The real component of the complex elastic modulus is called the storage modulus and represents the amount of wave energy that is recovered after each wave cycle. The imaginary component is called the loss modulus and represents the amount of wave energy that is lost through amplitude attenuation.

All materials being considered here are isotropic, meaning that they do not have any regular molecular orientation. For an isotropic material the elastic moduli is independent of the direction in which it is measured in a sample. This is almost always true for fluids

but not for crystalline solids which are anisotropic. Anisotropic solids are described by a matrix of elastic moduli. Each entry describes the elastic modulus for a strain in a co-ordinate axis by a force from one of the co-ordinate axes. The elastic behaviour of crystalline solids is described in Mason (1950) and Truell, Elbaum and Chick (1969).

There are two important type of elastic behaviour that play a role in the damping of longitudinal waves travelling in isotropic materials. These are described in the next two sections.

3.2.1 Shear Modulus

The shear modulus measures the shear stress that is required to overcome the internal friction which prevents two layers inside of a material from sliding over one another. This internal friction comes into play when one layer of the material is subjected to a shear stress which tends to pull other adjacent layers along with it. The shear modulus is defined by equation 3.5 and Figure 3.2.

$$\text{Shear Modulus} = \frac{\text{Shear Stress}}{\text{Shear Strain}} = G^{*} = \frac{F_t/A}{\Delta x/h} = G' + jG'' \qquad (3.5)$$

One important observation about shear deformations is that the change in shape caused by a shear stress does not involve a volume deformation. For materials that flow freely (Newtonian fluids), the shear stress will not have a restoring force and the shear modulus has only an imaginary component (G' =0).

3.2.2 Longitudinal Modulus

The longitudinal modulus is a measure of how compressible an element of material is in the direction of an imposed stress. The longitudinal modulus is defined in equation 3.6 and Figure 3.3.

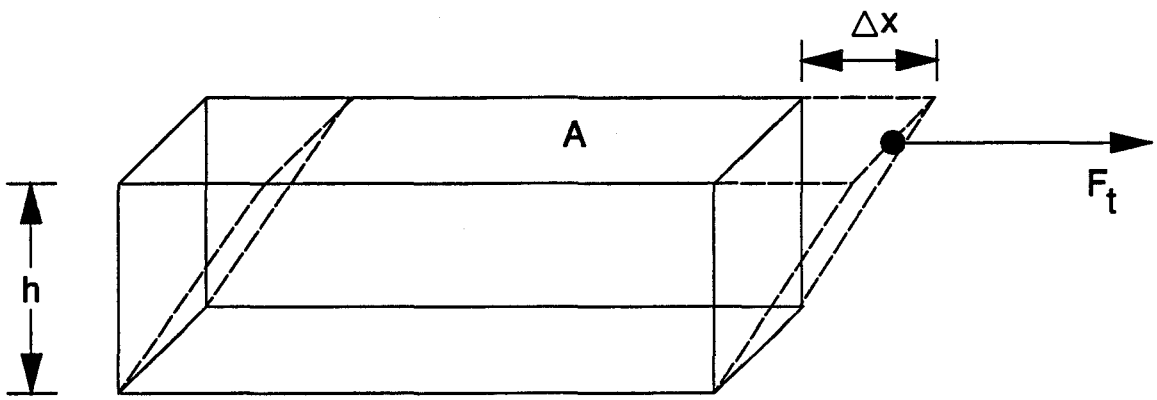

Figure 3.2. The Shear modulus. The top plane of this rectangle with area **A** is subjected to a shear stress $\mathbf{F_t}$ which moves it a distance Δx while the bottom plane at a distance Δh perpendicular to the stress remains at rest.

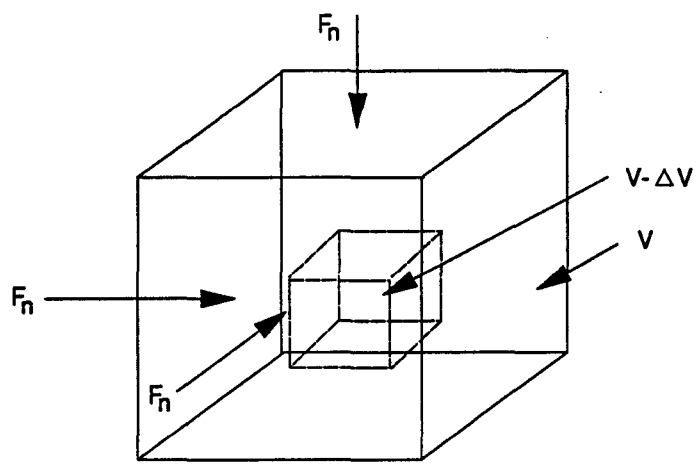

Figure 3.3. The longitudinal modulus measures a volume deformation of an element of material that is subjected to a normal stress.

$$\text{Longitudinal Modulus} \quad (K^*) = \frac{\text{Normal Stress}}{\text{Volume Decrease}} = \frac{F_n/A}{-\Delta V/V} = K' + jK'' \quad (3.6)$$

A material with a very high value of the longitudinal modulus such as a solid will deform grudgingly in response to a normal stress while a material with a low longitudinal modulus such as an ideal gas will more readily deform.

It is important to remember that the shear modulus measures the behaviour of a non-compressional shape deformation in response to a shear wave and the compressional modulus measures a volume deformation due to a longitudinal wave. In many materials, the travel of longitudinal stress waves is determined by an elastic modulus which is a combination of compressional and non-compressional (shear) moduli. This will be described in section 3.3.

3.3 Propagation of Waves through Solids and Fluids

Elastic solids and Newtonian fluids are two model systems most often used when developing theory about the transmission of high frequency stress waves. The difference between these two systems is the way in which they each respond to shear waves.

In elastic solids, it is assumed that very small strains induced by an external stress will be opposed by a restoring force that is proportional to the displacement at any point. This is an application of Hooke's law. It can only be applied to real solids when the strain is small enough that higher order terms in the restoring force can be neglected. In an elastic solid, a restoring force will exist for transverse and normal stresses. Longitudinal waves radiating into an elastic solid will be refracted into separate longitudinal and shear waves if the sample dimensions are large enough and the incident wave is not normal to the surface. This situation will be discussed in more detail in the next section.

For Newtonian fluids, the shear stress is proportional to the rate of shear strain and is independent of the actual strain. If the stress is considered to oscillate sinusoidally, this means that the strain will be 90 degrees out of phase with a shear stress ($d \sin\theta / d\theta = \cos\theta = \sin(\theta + 90^o)$). This means that the shear modulus for a Newtonian fluid will only have an imaginary non-zero component using the notation of equation 3.3. There is no restoring force for a shear stress and the stress is dissipated through viscous losses. Because Newtonian fluids are unable to support shear waves, only longitudinal waves will travel through them.

The stress/ strain relationships of many useful materials are intermediate between Newtonian fluids and elastic solids. They are called *viscoelastic*, denoting that for shear stresses, there is a simultaneous viscous loss and elastic restoring force; some of the energy associated with a shear wave is recovered for the next cycle and some is lost. The phase angle between stress and strain for an oscillating stress is somewhere between 0 and 90 degrees. There is a long list of industrially significant materials that have viscoelastic properties. Most of these are polymers.

When a longitudinal wave is radiated into a sample where the direction normal

to the stress is much larger than the wavelength, the effective elastic modulus is a combination of the shear and compressional moduli where M^* is the bulk longitudinal modulus as described by Ferry (1980) and Philippoff (1965).

$$M^* = K^* + \frac{4}{3}G^* = M' + jM'' \tag{3.7}$$

3.3.1 Mechanical Q

For planar waves, the mechanical Q (or internal friction 1/Q) is defined to describe how plane waves are damped. Q is equal to 2π times the maximum energy stored over one period in a small elemental volume divided by the energy dissipated in the volume per period[10]. For a material with an elastic modulus defined in equation 3.7, Q is equal to equation 3.8.

$$Q = \frac{M'}{M''} \tag{3.8}$$

3.3.2 Reflection and Transmission of Stress Waves at Surfaces

So far, all of the discussion has concentrated on waves travelling through homogeneous materials. Another situation to consider is the case where a travelling stress wave meets a discontinuous surface. In this situation, part of the wave will be reflected back into the first medium and part of the wave will be transmitted into the second medium. When a longitudinal wave contacts a surface at an incident angle not equal to 90°, it will be split up into a reflected longitudinal and transverse wave and a transmitted longitudinal and transverse wave. The angles of refraction and reflection are determined by a law that is analagous to Snell's law for optics.

A special case in the wave equations exist where a longitudinal wave travels through a discontinuity perpendicular to the surface. One longitudinal wave is reflected at the interface and one longitudinal wave is transmitted. The amplitudes of each of these waves can be calculated based on a knowledge of the acoustic impedance of each medium. The acoustic

impedance (Z) is equal to the product of its density (ρ) and its ultrasonic velocity (v). The equations are

$$\text{Reflection Factor} = \frac{A_2}{A_1} = \frac{Z_2 - Z_1}{Z_1 + Z_2} \tag{3.9}$$

$$\text{Transmission Factor} = \frac{A_3}{A_1} = \frac{2Z_2}{Z_1 + Z_2} \tag{3.10}$$

where Z_1 and Z_2 are the acoustic impedances of the first and second materials and A_1, A_2, A_3 are the amplitudes of the incident, reflected and transmitted longitudinal waves (Mason (1958)).

3.4 Ultrasonic Velocity and Attenuation

The travel of a longitudinal ultrasonic wave is most easily measured by its velocity (v) and the attenuation of its intensity or amplitude over some distance (α). The velocity is an indication of the compressability of the material and the attenuation is an indication of how quickly the wave energy is being lost. Many empirical and semi-empirical relationships have been developed to describe how the velocity and attenuation depend on physical properties of the material that they are travelling through. Zacharias (1970a, 1970b) has found many empirical relationships between the ultrasonic velocity and the composition in liquid mixtures and suspensions. The attenuation has been related to chemical structure in homogeneous systems by many researchers. One detailed review paper on this subject that pertains specifically to wave attenuation in polymer solutions is by Pethrick (1983).

3.4.1 Ultrasonic Velocity

For the situation described in section 3.3 where the effective elastic modulus is the bulk longitudinal modulus M^*, the real and imaginary parts of the modulus can be calculated from equations 3.11 and 3.12

$$M' = \frac{\rho v^2(1-r^2)}{(1+r^2)^2} \tag{3.11}$$

$$M'' = \frac{2\rho v^2 r}{(1+r^2)^2} \tag{3.12}$$

where $r = \alpha/\beta$ which are defined in equation 3.2. For most high frequency waves the attenuation is small relative to the wavelength ($\alpha \ll \beta$), so that equation 3.11 can often be simplified to yield equation 3.13 according to Ferry (1980) and McSkimin (1964).

$$v \approx \left(\frac{M'}{\rho}\right)^{\frac{1}{2}} \tag{3.13}$$

Even when the attenuation constant (α) is very large, r only enters equation 3.11 as a minor correction. This means that the ultrasonic velocity depends on two bulk properties of the

transmission medium, the real part of the elastic modulus (or storage modulus) and the density.

3.4.2 Ultrasonic Attenuation

The attenuation constant is defined in equation 3.14.

$$\alpha = \frac{\ln(A_1/A_2)}{x_2 - x_1} \tag{3.14}$$

A_1 and A_2 are the amplitudes at two points of a travelling wave that are in phase and x_1 and x_2 are distances along the axis of travel where the amplitudes were measured. The attenuation constant can be evaluated in neper/m or dB/m (1 neper = 8.68 dB). The measured attenuation (α_{meas})will be the sum of a number of separate contributions. The individual effects are absorption, dispersion, diffraction and scattering.

$$\alpha_{meas} = \alpha_{abs} + \alpha_{disp} + \alpha_{scat} + \alpha_{diff} \tag{3.15}$$

Absorption and dispersion can give information about the sample medium. Diffraction and scattering effects depend on the frequency and the measurement set-up. To obtain reproducible results, most researchers have tried to examine systems in which all but one of these effects could be neglected.

3.4.2.1 Absorption Contribution of Attenuation in Homogeneous Systems

Absorption is also the sum of a number of separate effects that contribute to diminish the amplitude of a travelling wave. These can be broken down into the classical absorption and the excess absorption. Classical absorption is the dissipation of wave energy through viscous losses (shear waves) and heat conduction (longitudinal waves). Heat conduction results if the compression/expansion phases of a travelling wave are not perfectly adiabatic. Some heat energy will be driven out of the crests of a longitudinal wave by temperature differences caused by the travelling wave (thermal relaxation). This is more significant at lower frequencies and in materials with higher heat conduction coefficients such as liquid metals. Viscous losses occur when molecules are required to slide over one

another. The equation for classical absorption (α_{class}) is described in equation 3.16 by Herzfeld and Litovitz (1959) and Pinkerton (1947).

$$\frac{\alpha_{class}}{f^2} = \frac{8\pi}{3v^3\rho}\left[\eta_S + \frac{3}{4}(\gamma - 1)\frac{k}{C_p}\right] \tag{3.16}$$

In this equation f is the wave frequency, v is the wave velocity, and ρ, C_p, k, and γ are the density, heat capacity, thermal conductivity, and ratio of C_p/C_v for the propagating medium. For a sinusoidal wave the shear viscosity (η_S) is equal to the shear loss modulus divided by the angular frequency ($\eta_S = G''/\omega$) (Ferry (1980)). The first part of the right hand side of Equation 3.16 describes the wave absorption from viscous losses which were first considered by Stokes (1845)) and the second part describes absorption from heat conduction first considered by Kirchoff (1868). For most typical liquids, Lamb and Pinkerton (1949) have observed that the classical absorption is predominantly due to the shear viscosity (η_S).

By the late 1940's it had been observed by workers such as Pinkerton (1947) that fluids consisting of molecules with permanent dipoles had observed wave absorptions (α_{meas}) that were much larger than the value predicted by the classical absorption given in equation 3.16. The difference between the measured absorption and the calculated classical absorption is called the excess absorption. The excess absorption is related to a structural relaxation of the molecules in a sample following the volume deformation from an ultrasonic stress wave. When a stress is imposed on a sample, the molecules inside will adjust themselves with respect to one another to attain new equilibrium orientations. After the stress, they will return to their former orientations at a finite rate. The time required for the strain to disappear after the stress has been removed is equal to the relaxation time. For example, acetic acid will exist as single molecules and as a two molecule complex in equilibrium.

$$(CH_3COOH)_2 \leftrightarrow 2CH_3COOH \tag{3.17}$$

During the passage of a normal stress wave, the molecules will readjust themselves to reach a new equilibrium corresponding to the pressure of the stressed point. When the wave passes, the molecules will relax to their original equilibrium (Pinkerton and Lamb (1949)).

For monatomic fluids or diatomic fluids with no permanent dipoles (such as N_2 or O_2) there is no preferred intermolecular orientation that can minimize the free energy of an element after that element has been perturbed by a stress wave. This means that the excess absorption is approximately zero. In fluids composed of more structurally complicated molecules, there is a significant excess absorption. Litovitz and Davis (1965) have observed that the ratio of the actual absorption to the classical absorption ($\alpha_{meas}/\alpha_{class}$) is very nearly constant for a particular medium. This means that α_{meas}/f^2 should be independent of frequency for a particular material until $1/2\pi f$ approaches the relaxation time of the material. As the frequency in this region is approached, α_{meas}/f^2 should decrease to the classical value. For simple molecules like water, the relaxation time is very short and will not be observed below 1000 MHz while for liquids with large molecules such as polymers, the relaxation can be observed in the low megahertz range (Mason (1948). One convenient relationship that can be used to fit absorption and frequency data is Equation 3.18.

$$\frac{\alpha_{meas}}{f^2} = B + \frac{A}{1+(f/f_c)^2} \tag{3.18}$$

In this equation, f_c is equal to $1/2\pi\tau_c$ where τ_c is the characteristic time constant for the relaxation. A is an equal to the excess absorption and B is equal to the classical absorption from equation 3.16. For an intermolecular relaxation such as translation or whole molecule rotation, the observed relaxation time in a material belongs to a distribution, reflecting the fact that individual molecules in an element of liquid do not all have identical positions with respect to one another at a given time. For an intramolecular relaxation such as segmental rotation, the energy exchange will occur at a single discrete time (Pethrick (1983)).

Herzfeld and Litovitz (1959) have divided all liquids into three groups according to their excess absorption. Group One includes fluids that do not exhibit large excess absorption ($\alpha_{meas}/\alpha_{class} \approx 1$). This includes liquids such as Hg, N_2 and O_2. Group Two are mostly organic liquids where $\alpha_{meas}/\alpha_{class}$ varies between 3 and 400 and $\partial\alpha_{meas}/\partial T$ is greater than zero. In this case, the excess absorption is due to an exchange between intramolecular and intermolecular energy. Group Three are liquids that associate strongly such as acetic acid and water. The ratio $\alpha_{meas}/\alpha_{class}$ lies between unity and 3 and the excess absorption is

thought to be due to a structural relaxation although this can only be proven for water. The partial derivative $\partial\alpha_{meas}/\partial T$ is less than zero.

The excess absorption due to structural relaxation that has been observed experimentally can be accounted for by incorporating a volume viscosity (η_V) into equation 3.16 to give equation 3.19.

$$\frac{\alpha_{meas}}{f^2} = \frac{8\pi}{3v^3\rho}\left[\eta_S + \frac{3}{4}(\gamma-1)\frac{k}{C_p} + \frac{3}{4}\eta_V\right] \tag{3.19}$$

The excess absorption due to a volume viscosity will only be observed when the relaxation time is much shorter than the period of the ultrasonic stress wave. For a sinusoidal wave the sum of the volume viscosity and heat conduction losses can be related to the longitudinal loss modulus by the angular velocity ($\eta_V + (\gamma-1)k/C_p = K''/\omega$). Making all of the substitutions to eliminate all of the loss terms on the right hand side of equation 3.19, the attenuation constant can be rewritten as a function of the bulk longitudinal loss modulus.

$$\alpha_{meas} = \frac{4f}{3v^3\rho}[M''] \tag{3.20}$$

This equation predicts that the attenuation constant will be a linear function of the frequency in the case where the loss modulus is not a function of frequency. The measurement of the attenuation constant as a function of wave frequency is sometimes called ultrasonic spectroscopy.

3.4.2.2 Dispersion Contribution to Attenuation

Examples of dispersion have been discussed by Papadakis (1976), Lamb and Pinkerton (1949) and Redwood (1957). Ultrasonic waves travelling through a dispersive material will have a velocity that is dependent on the frequency. This is because the bulk storage modulus of a dispersive material is a function of the length of time that the stress has been imposed. For waves travelling at lower frequencies, the time period in which the sample medium has been subjected to an imposed stress will be longer than for stress waves with higher frequencies. If a train of ultrasonic waves has more than one frequency component, the stress

envelope will spread out in a dispersive material. Even if the wave is carefully generated at one frequency, dispersion can result by low frequency aliasing if the pulse length is small relative to the wavelength of the stress wave. As the different frequency components of a pulse separate, each wave retains less of its original intensity, and the measured attenuation appears to increase.

3.4.2.3 Scattering Contribution to Attenuation

The scattering effect is observed in materials that contain inhomogeneities that are much larger than the wavelength of the oscillating stress field. When a longitudinal wave travels through a fluid with suspended particles that are large compared to the wavelength, it will interact with them in two ways (Mason (1958)). Some of the incident wave will be transmitted through the suspended particle as longitudinal and shear waves (refraction). When each of these waves reaches the other side, they will produce more longitudinal and shear waves. Only the longitudinal wave will be propagated if the surrounding medium is a Newtonian fluid. The rest of the incident wave will be phase shifted and reflected as longitudinal and shear waves. This is shown in Figure 3.4. The reflected and refracted waves from many suspended particles will cause interference patterns that will add noise to ultrasonic measurements and make the attenuation look larger than it really is due to absorption. If the suspended particles are gas bubbles with a low acoustic impedance relative to the continuous phase, almost all of the incident wave will be reflected at the interface and the scattering will be too high to make any measurement (Monkr (1990)).

3.4.3.4 Diffraction Contribution to Attenuation

Diffraction or *beam spreading* is usually significant when the wavelength of the stress wave is about the same size or larger than the particles in the material. A spreading wave in a bounded sample cell will be reflected from the cell wall back into the beam of the wave. Bass (1958) and Truell, Elbaum and Chick (1969) have reported spurious attenuation results from sidewall reflections that cause interference patterns. Pinkerton (1949) has shown that for an ideal piston source, the diffraction will be negligible in the first half of the near field or Fresnel diffraction zone. The length of the Fresnel diffraction zone can be calculated from equation 3.21.

$$x < \frac{a^2}{\lambda} \tag{3.21}$$

In equation 3.21 x is the axial distance from the piston source, a is the radius of the piston and λ is the wavelength. Mathematical corrections have been developed for handling measurements made outside of the Fresnel zone (the Fraunhofer zone). For real transducers, Bass (1958) has reported that the attenuation loss over the Fresnel zone for a semi-infinite cell (no sidewalls) is less than 1 dB.

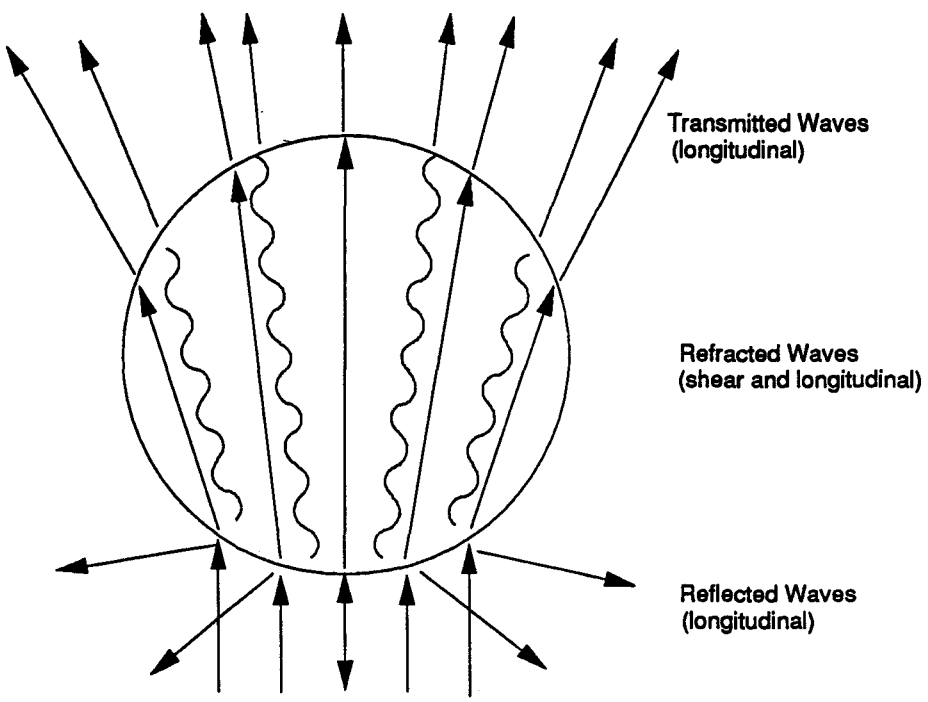

Figure 3.4. A longitudinal wavefront in a Newtonian fluid encounters an elastic sphere. Snell's Law determines the angle of refraction at the surface.

3.5 Wave Travel in Suspensions

Most of the initial work done to measure the velocity and attenuation constant in liquids concentrated on homogeneous materials as the wave propagating medium. Consequently, most of the theory for the transmission of waves has been developed for homogeneous materials. Within the last thirty years, some researchers have begun to apply ultrasonic measurement techniques to waves travelling through colloidal dispersions. Some of the original theoretical work was pondered by Herzfeld (1930a, 1930b). Carhart and Epstein (1953) have studied the problem of waves travelling through liquid aerosols and Chow (1964) has extended some of the theoretical results to examine liquid/ liquid suspensions as the propagating medium. Hawley (1967) and his first graduate student (Allegra (1970)) both studied the problem of measuring ultrasonic waves in suspensions and related those measurements to theoretical calculations of the attenuation constants. The theoretical calculations were derived from a first principles approach to the constitutive equations that govern a liquid with suspended spheres of a second material. The calculated attenuation could be broken down into separate contributions due to scattering, viscous losses and heat conduction. Polystyrene latices and aqueous polyvinyl acetate were studied by Allegra although no attempt was made to relate the attenuation to the polymer's molecular properties. Allegra observed that the attenuation constant for polystyrene latices was proportional to the solids concentration at intermediate concentrations and constant frequency.

Wada (1958) has reported that for particles that are comparable in size to the wavelength of the stress field, scattering losses will be the predominant mechanism of wave attenuation. As the particles become smaller compared to the wavelength, scattering will become less important. Wada's criterion for determining the importance of scattering is given as equation 3.22.

$$ka > .5 \quad \text{Scattering is predominant} \tag{3.22a}$$

$$ka < .5 \quad \text{Scattering is less than classical losses} \tag{3.22b}$$

In equation 3.22, k is equal to $1/2\pi f$ and a is the mean particle radius. For particles that are much smaller than the wavelength of sound, the effect of scattering on attenuation can be neglected. This situation is summarized by Urick (1949).

> "... as far as the sound is concerned, the discontinuities are non-existent, and the medium is simply a homogeneous mixture of the component substances."

Urick (1947) proposed that this fact could be used to infer the elastic moduli of solids. The solids could be milled down to colloidal dimensions so that $ka \ll 1$ and suspended in a non-swelling medium. By measuring the wave attenuation of the suspension and assuming that the composite attenuation could be calculated by treating the suspension as an ideal mixture, the elastic modulus of the solid was calculated.

3.5.1 Wave Travel in Polymer Latices

Because diffraction and scattering are both possible in suspensions, there is a window for measuring the effects of pure absorption on ultrasonic wave attenuation. Below a certain frequency, diffraction will play a prominent role in wave attenuation (equation 3.21). Above a certain frequency, scattering will be the main mechanism for wave attenuation (equation 3.22). This situation is depicted in Figure 3.5. Fortunately the significance of scattering and diffraction can both be assessed with the wavelength (λ) which is easily calculated from the frequency and the velocity. A number of workers have measured the velocity of sound in polymer latices (Povey and Scanlo (1983), Barrett-Gultepe et al (1983)) and reported that there is not much difference between the velocity of pure water so that an initial estimate of the wavelength for a latex can easily be calculated. The average size of polymer particles used in this study varied between 35 to 200 nm (chapter 2). This corresponds to a wavelength to particle size ratio that would vary between 800 to 23000 between 2 and 10 MHz. In this range the effects due to scattering are negligible. Ultrasonic measurements between 2 and 12 MHz are within the measurement window for the measurement cell (described in section 4.3) and latex samples (described in section 2.5) used in this study. Because the wave attenuation in water is much smaller than in viscoelastic polymer particles (Pinkerton, (1947)) the wave attenuation in latices is almost entirely due to the character of the polymer particles.

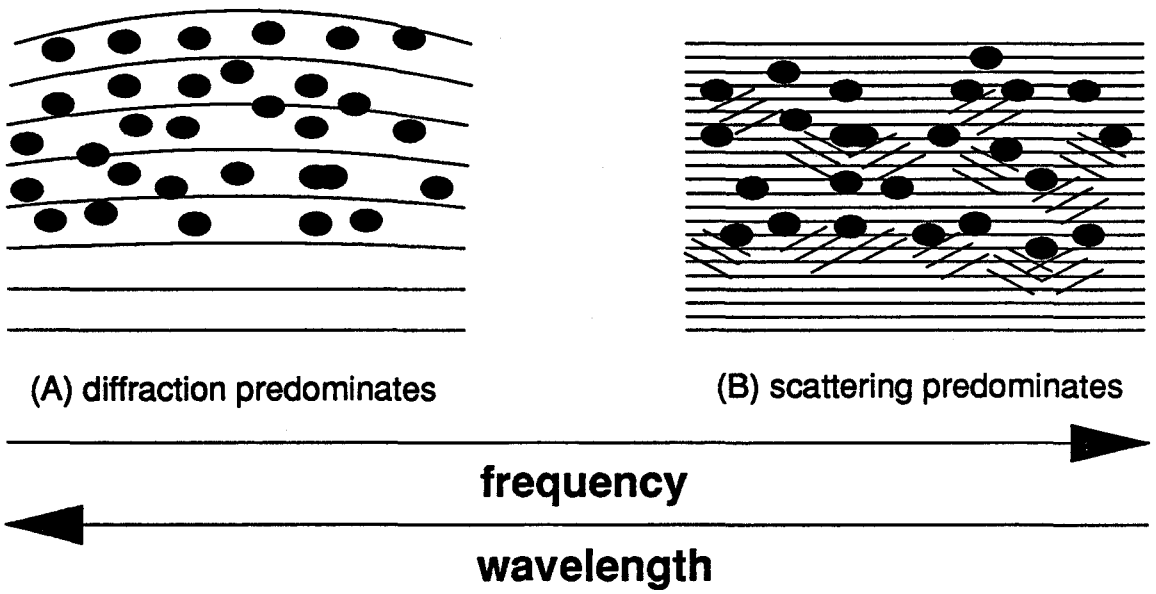

Figure 3.5. The competing effects of diffraction and scattering in a colloidal system. At low frequencies, attenuation due to diffraction is appreciable. At higher frequencies relative to the particle size, attenuation due to scattering is appreciable.

Notation

α	attenuation constant
β	propagation constant
η_S	shear viscosity
η_V	volume viscosity
Γ	complex propagation constant
γ	ratio of C_p to C_v
λ	wavelength of sound wave
ω	angular velocity
ρ	density
a	radius of ideal transducer, mean particle radius in suspension
A	area over which an area is applied
A_1	original amplitude of a stress wave
A_2	amplitude of reflected wave, returning wave
A_3	amplitude of wave transmitted at interface
C_p	heat capacity
f	frequency
f_c	characteristic frequency of a structural relaxation
F_n	normal force
F_t	transverse force
G	shear modulus
h	normal distance through which shear force is exerted
j	imaginary operator
k	thermal conductivity or reciprocal wavelength
K	longitudinal modulus
M	bulk longitudinal modulus
p	pressure along a plane
p_o	reference pressure
v	velocity of sound
V	volume of small compressed sample
x	distance parallel to direction of travelling longitudinal wave

CHAPTER FOUR

THE EXPERIMENTAL SET-UP

The experimental set-up that is used to measure the attenuation constant and velocity of sound waves through latex samples is discussed in this chapter.

4.1 Generators and Detectors of Stress Waves

4.1.1 The Piezoelectric Effect

Piezoelectric materials are essential for measuring the travel of stress waves because they are the physical medium through which a stress is converted into a voltage signal. The piezoelectric effect is observed in materials that are able to convert an excess of surface electrical charge into a proportional strain in one or more directions. The opposite effect is also observed so that a mechanical stress resulting in a strain to a piezoelectrically active axis of such a material will cause a net charge to form on the surface of the material. This is caused by a coupling of the dielectric and elastic properties of the material. All piezoelectric materials lack a center of symmetry and are therefore intrinsically anisotropic. The piezoelectric effect was first observed in single crystals, but can also be created in anisotropic (poled) ceramics.

4.1.2 Piezoelectric Materials as Electro-Mechanical Transducers

Piezoelectric materials are ideal for use as generators and detectors of high frequency stress waves. All piezoelectric materials consist of some oriented dipolar molecules that

are lined up to face in the same direction. In piezoelectric crystals, the dipoles are lined up because of the regular positioning of atoms in a lattice. In piezoelectric ceramics, the material has been poled to give it a remanent polarization. The permanent dipoles in a piezoelectric material are depicted as bar magnets in Figure 4.1. For the measurement system used in this study, only longitudinal waves are used so that all of the piezoelectric elements will be designed for longitudinal excitation.

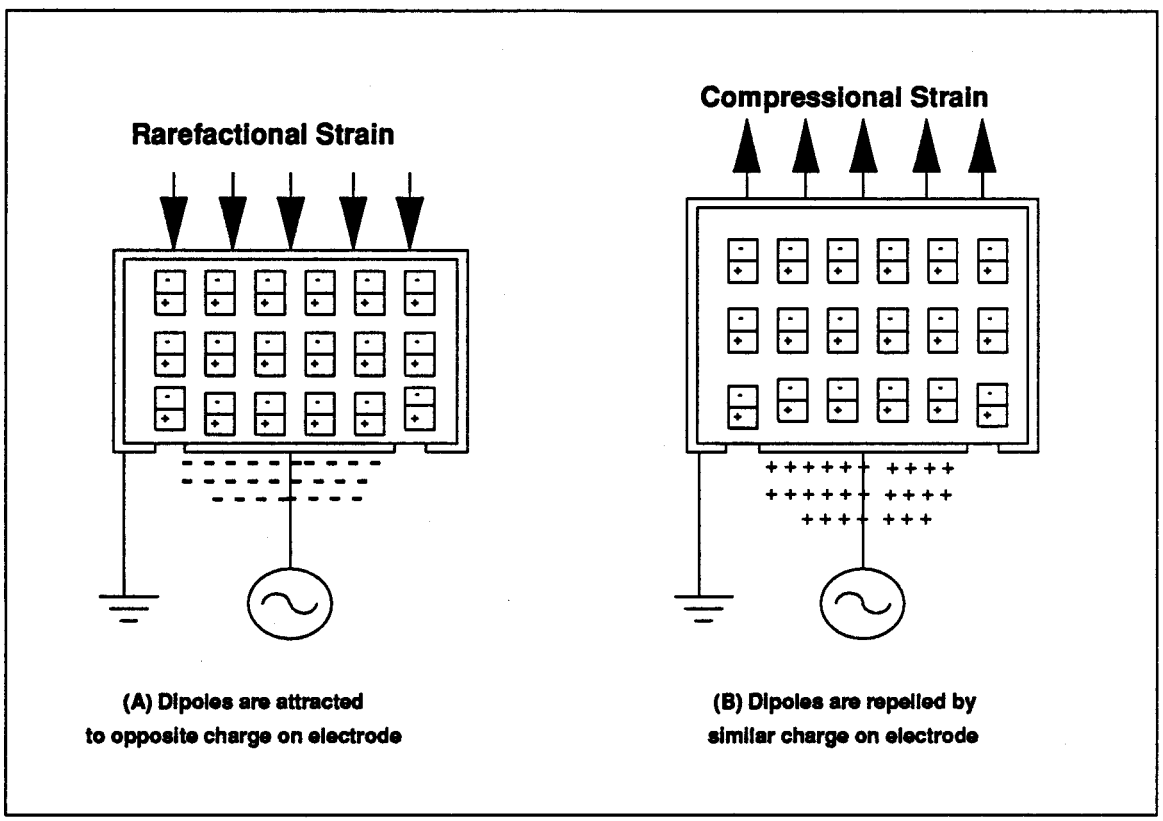

Figure 4.1 An alternating electrical potential is converted into a stress field by a piezoelectric transducer.

To prepare a piezoelectric transducer, the element is pressed (in the case of a ceramic) or cut (in the case of a crystal) into the shape of a disc and an electrode is plated on either face. One face is connected to a voltage supply and the other face is connected to a ground. When a voltage is applied across the electrodes, a charge (q) will accumulate on

one face of the transducer. The ratio of the accumulated charge to the accumulated charge when the electrodes are separated by a vacuum is the *dielectric constant* of the transducer material. The accumulated charge will cause a compression or expansion in the thickness of the disc which in turn causes a stress as the opposite face of the disc pulls (or pushes) against whatever is next to it. An alternating voltage wave can be converted to an alternating stress wave by the expansion and contraction of the transducer as shown in Figure 4.1. This stress is going to depend on the elastic modulus of the transducer material. The property that relates the dielectric and elastic characteristics is piezoelectricity. This is measured by the piezoelectric charge constant (D) which is described in equation 4.1 for a longitudinal mode transducer.

$$D = \frac{q/A}{F_n/A} \tag{4.1}$$

In this equation F_n/A is the induced normal stress that corresponds to a charge density *of* q/A. For an oscillating voltage, the accumulation of charge will not all be in phase with the voltage. A parameter analogous to the "Mechanical Q" defined in equation 3.8 is used to describe how much of the induced charge is out of phase with the voltage. Mason (1950) defines the electrical Q for a piezoelectric transducer by equation 4.2

$$\text{Electrical Q} = \frac{\text{Im(electrical impedance)}}{\text{Re(electrical impedance)}} = \frac{\text{reactance}}{\text{resistance}} \tag{4.2}$$

In general, ceramic transducers will have a lower Q than crystal transducers which makes them more useful for sending or receiving ultrasonic waves. A high Q transducer can sometimes be compensated for with an impedance matching circuit. These are described in the Matec Application Note AN-102. The value of Q is a characteristic of the transducer material.

The magnitude of the applied voltage that is required to excite a transducer will depend on how the transducer is damped or prevented from oscillating. Any inertial element that is physically coupled to the freely vibrating transducer will cause damping. Damping comes from three sources; the backing of the transducer, the way in which the transducer

is clamped into its holder and the adjacent medium to which the transducer is coupled. The energy input required to produce a stress wave will be minimal when the transducer and the adjacent medium have the same acoustical impedance as described in section 3.3.2. In this case, all of the wave energy from the transducer will be transmitted into the sample. For this reason, it is advantageous to have transducers with an acoustic impedance that is similar to the acoustic impedance of the sample medium. The transducer backing is a design parameter that will be discussed in the next section.

4.1.3 Differences Between Crystal and Ceramic Transducers

A good discussion of the manufacture, design and applications of piezoelectric transducers can be found for crystals in Mason (1950) and for ceramics in Jaffe, Cook and Jaffe (1971) or Randeraat (1968). Only ten of the thirty two crystal classes can be cut to make longitudinal mode transducers while most of the ceramic transducers are specifically manufactured for longitudinal excitation. There are three major differences between ceramic and crystal transducers which should be considered before deciding which type of transducer should be used to send and receive longitudinal ultrasonic waves. One of them is the electrical Q discussed in the previous section. The other two will be discussed now.

The thickness of the piezoelectric transducer element determines its *fundamental* or *natural frequency*. This can be calculated by dividing the speed at which sound travels through the material by its thickness. One difference between ceramic and crystal systems is the way in which they convert signals that have frequencies that are different from the natural frequency. Most crystals have a narrow passband which means that the transducer can only convert voltage signals to stress waves (or vice versa) when the frequency is very close to the natural frequency, higher or lower frequency signals are attenuated. Ceramic transducers have a relatively wider passband so that they can pass signals with frequencies that are farther away from the natural frequency of the transducer.

Another difference between ceramic and crystal transducers is that unbacked or slightly backed crystal transducers can be excited at odd harmonics of their natural frequency, for example a crystal transducer with a natural frequency of 1 MHz can also be driven at 3 MHz, 5 MHz, and so on up to some finite frequency. Producing ceramic transducers that

can be excited at odd harmonics with a stable output is not as common. To prevent an unstable output, the vibrations of a ceramic transducer are usually damped with a backing. A summary of the strengths and weakeners of each type of transducer is shown in Table 4.1.

Table 4.1 Advantages and Disadvantages of Ceramic and Crystal Piezoelectric transducers

Material of Construction	Advantages	Disadvantages
Ceramic	• low Q • wide passband	• cannot convert odd overtones
Crystal	• can convert odd overtones	• high Q • narrow passband

4.1.4 Transducers Used For this Study

Three types of transducers were initially screened as possible candidates for this study. Two sets of crystal transducers were purchased by Valpey Fisher (quartz and lithium niobate) and one set of ceramic transducers was manufactured at McMaster University (lead metaniobate). Each of the crystal transducers was unbacked and cut for longitudinal excitation. A layer of chrome and gold had been sputtered onto each face as an electrode. The transducer was set into a bored out brass cylinder with an electrically conducting silver epoxy. The quartz crystal had a diameter of 1/4 of an inch and the lithium niobate transducer had a diameter of 1/2 of an inch. The ceramic transducers were backed with a separate unpoled ceramic and set into a brass cylinder. One surface was sputtered with gold and the other surface was coated with silver epoxy to serve as electrodes. Originally 1/4 inch diameter ceramic transducers were used.

Figure 4.2 shows the performance of the quartz transducer (A) and the ceramic transducer (B), both at their natural frequencies in the low megahertz range. The upper trace for each transducer is the amplitude of each pulse echo and the lower trace is the

corresponding phase angle. It can be observed that the output from the ceramic transducer gives a more stable waveform which is essential for the subsequent measurements described in section 4.2. This is probably because of the lower Q and the fact that an impedance matching network was not used.

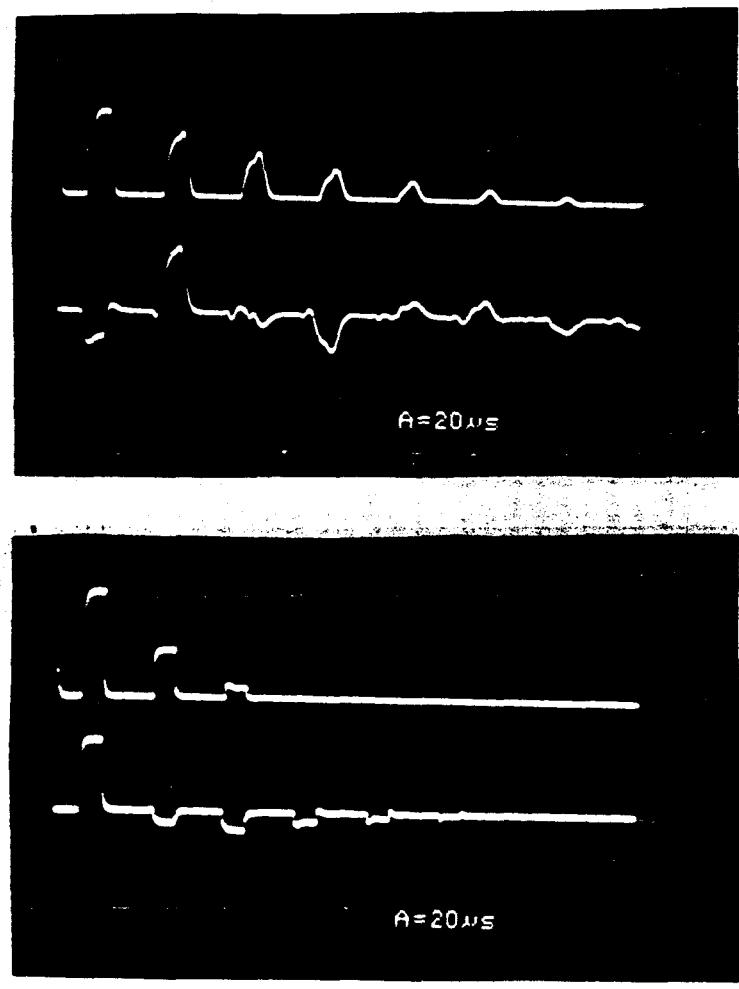

Figure 4.2. The performance of an unbacked quartz transducer (above) and a ceramic transducer (below) both without impedance matching.

Because the ceramic transducers appeared to function better for this application, it was decided to conduct all of the subsequent experiments with lead metaniobate ceramic transducers. Three more sets of transducers were built. The transducer size was increased to a 1/2 inch diameter to eliminate any diffraction contribution to the attenuation. The first set had a fundamental frequency at 10 MHz but could make measurements between 7 MHz and 12 Hz. The second set had a fundamental frequency of 7 MHz but could make measurements between 4 MHz and 10 MHz. The third set had a fundamental frequency of 3 MHz and could make measurements between 2 MHz and 4 MHz.

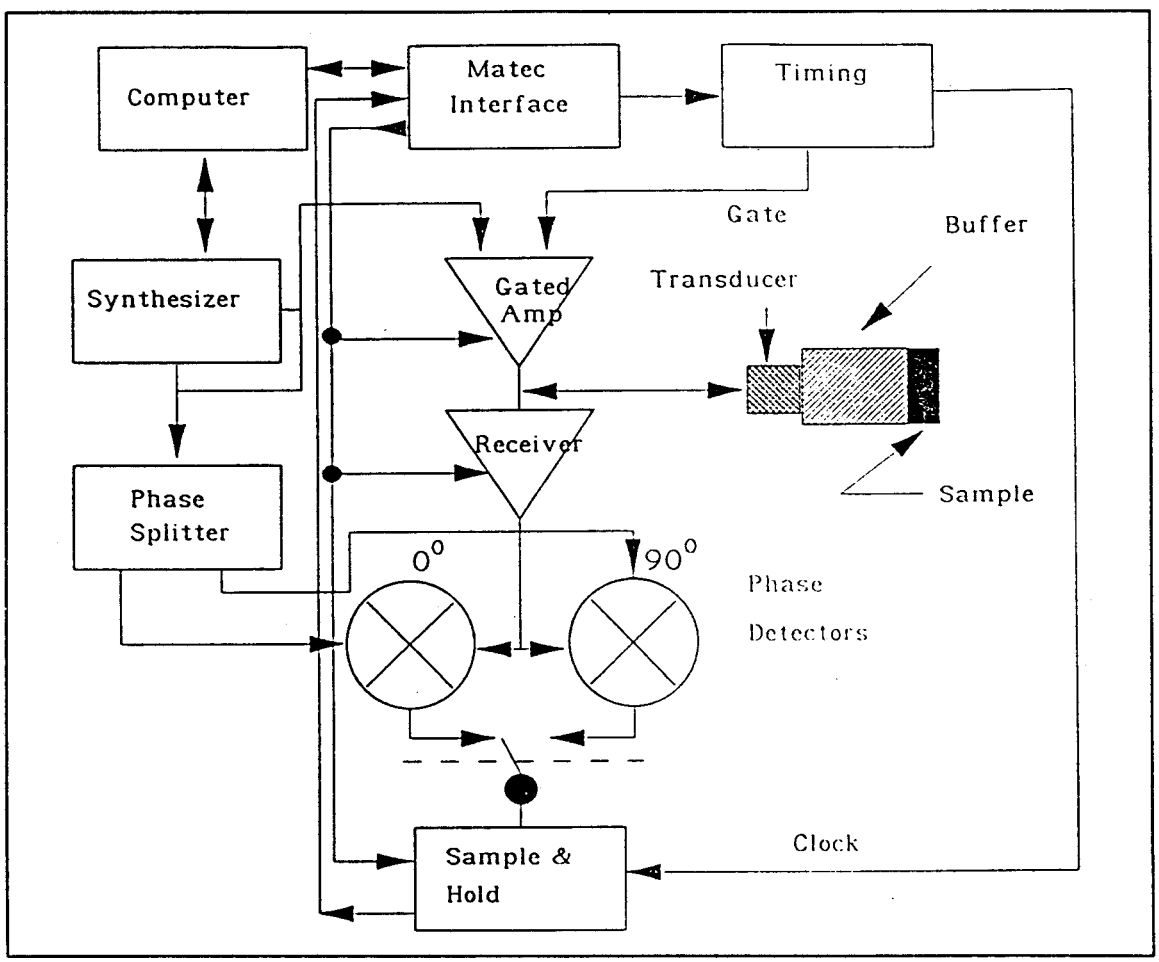

Figure 4.3 The MATEC MBS 8000 Measurement Hardware

4.2 A Description of the Equipment for Measuring Velocity and Attenuation

4.2.1 The Pulse Echo Method for Measuring Velocity and Relative Attenuation

The pulse echo method is one way to measure the ultrasonic velocity and attenuation through a sample. This method became popular because of radar techniques developed during the Second World War. Two of the original papers on this subject are by Pinkerton (1949) and Pellam and Galt (1946). A train of high frequency low voltage waves is generated at a set frequency and sent to a gated amplifier where it becomes a modulated pulse. This signal is sent to a piezoelectric transducer where the pulse is converted into a pulse of high frequency stress waves which travels through a prepared sample that has been acoustically coupled to the transducer. After travelling the length of the sample, the waves will reflect at an interface and return to the transducer where they are partially converted into a voltage signal and partially reflected back into the sample. The pulse makes a number of return trips between the transducer and the end of the sample before the amplifier lets another toneburst through the sample. The transit time is measured by the length of time between each successive echo. If the thickness of the sample is known, a transit velocity can be calculated. The logarithmic ratio of successive echo amplitudes along with the sample thickness can be used to calculate the absolute attenuation. There are many different methods for measuring the transit time and attenuation between echoes. The phase detection method is one of the most recent and is able to accurately measure pulse echoes with amplitude ratios of greater than 30 dB. This is the method that is used by the Matec MBS 8000 which was used in this study.

4.2.2 The Phase Detection Method

This method uses phase detection circuitry and the pulse echo method to measure the ultrasonic travel parameters. All of the circuitry and peripheral equipment is controlled by a personal computer via the IEEE 488 control bus using software written by MATEC using the ASYST programming language. A flowsheet of the MBS 8000 set-up, which has been used for this study is shown as Figure 4.3. The high frequency signal from the signal generator is divided into two identical signals. One signal is the input to a gated amplifier. The second part of the signal is split with a phase splitter to act

as 0 and 90° phase references for the alternating voltage from the signal generator. The sample and hold gate is positioned over the first pulse echo. The voltage pulse from the receiving transducer is amplified and filtered with an analog prefilter and sent to two phase detectors with the phase references from the signal generator. The output from each of the phase detectors is equal to $A\sin\delta$ and $A\cos\delta$ where A is the amplitude of the signal and δ is the relative phase angle of the pulse echo with respect to the input signal. The amplitude and phase angle for the first pulse are calculated from the outputs of each of the phase detectors using equations 4.3 and 4.4.

$$A = \sqrt{(A\sin\delta)^2 + (A\cos\delta)^2} \tag{4.3}$$

$$\delta = \tan^{-1}\left(\frac{A\sin\delta}{A\cos\delta}\right) \tag{4.4}$$

Because δ is not the absolute phase angle but a relative angle that can only vary between -90° and 90°, the input frequency is incremented slightly to adjust the phase angle by a small amount (less than 180°) and the measurement of the phase detectors is repeated to find a second phase angle from equation 4.4. The increment in the frequency and the phase angle are used to calculate the time required for a stress wave to traverse the sample (the transit time) using equation 4.5.

$$\text{transit time} = \frac{(\Delta\ \text{phase angle})}{(\Delta\ \text{angular velocity})} = \Delta t = \frac{\Delta\delta}{2\pi\Delta f} \tag{4.5}$$

This procedure is repeated to measure the transit time and amplitude of the second pulse. The transit time for one trip through the sample is calculated from a least squares regression of the transit time of each pulse against the number of trips for each pulse. The absolute attenuation is calculated from equation 4.6 using the amplitudes for each pulse.

$$\text{Absolute Attenuation} = -20\times\log_{10}\left(\frac{A_2}{A_1}\right) \tag{4.6}$$

4.2.3 Sources of Error For Measurement Equipment

The phase detection method is a phase adjustment technique. The likely errors for this

type of technique have been discussed by Papadakis (1976). These errors stem from the assumption (which is not always justifiable) that physical properties of the system are independent of frequency. When a longitudinal wave is reflected from a surface, the wave will be phase shifted. Because a relative measurement of $\Delta\delta$ is used in equation 4.4, the effect of the phase shift on the transit time should cancel out, provided that the phase shift is independent of frequency. This is not always the case at low frequencies. Another possible cause of error is dispersion. Fortunately, the change in frequency to adjust the phase angle can be made very small, so that $\partial\delta/\partial f$ and $\partial v/\partial f$ are insignificant. This isn't a problem since highly dispersive materials cannot be measured anyway and the phase shift for reflections at a liquid/solid interface is usually negligible as reported by McSkimin (1959). Errors due to the MBS 8000 circuitry have been discussed by Petersen (1989).

4.2.4 Transducer Configuration

If more than one transducer is available, the sample can be coupled between two transducers. In this case, one transducer acts as the sender of the pulse of stress waves and one transducer at the other end of the sample acts as the receiver. The *sending transducer* generally can have a very narrow passband while the *receiving transducer* is more broadband to allow for dispersion through the sample. An alternate configuration is the transceiver mode where only one transducer is used to make the measurements. In this case the transducer sends the pulse of stress waves which travel through the sample and bounce off a smooth flat surface back to the original transducer where they are received. Figure 4.4 shows how a pulse travels through the sample for each configuration. Velocity and absolute attenuation measurements can be made with the MBS 8000 set-up using either configuration. The major advantage of the transceiver mode is that only one transducer is required. The major advantage of the sender/receiver mode is that measurements can be made on samples with larger attenuation constants because it requires one less trip through the sample than measurements made in the transceiver mode.

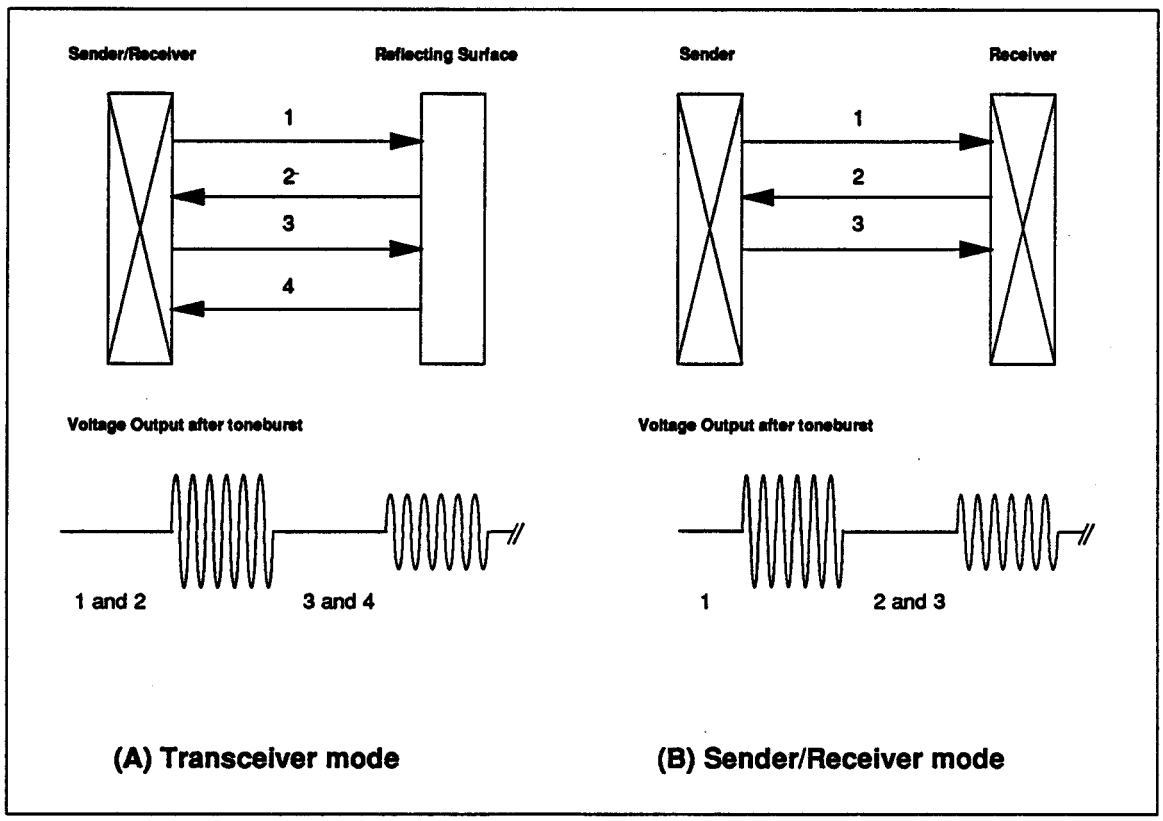

Figure 4.4. Transceiver mode and Sender/Receiver mode

4.3 The Measurement Cell Design

The ultrasonic wave travel parameters that can be measured with the MBS 8000 are the absolute attenuation between each pulse echo and the transit time. Unfortunately, these two measurements do not yield the velocity and the attenuation constant directly so a measurement scheme must be devised that can extract these two variables. Referring to Figure 4.4, it is apparent that the absolute wave attenuation between successive pulses is the result of two trips through the sample and one partial reflection at an interface. In section 3.3.2, it was stated that there will be some loss of amplitude when a wave is reflected at an interface unless the acoustic impedance of each zone is equal which is

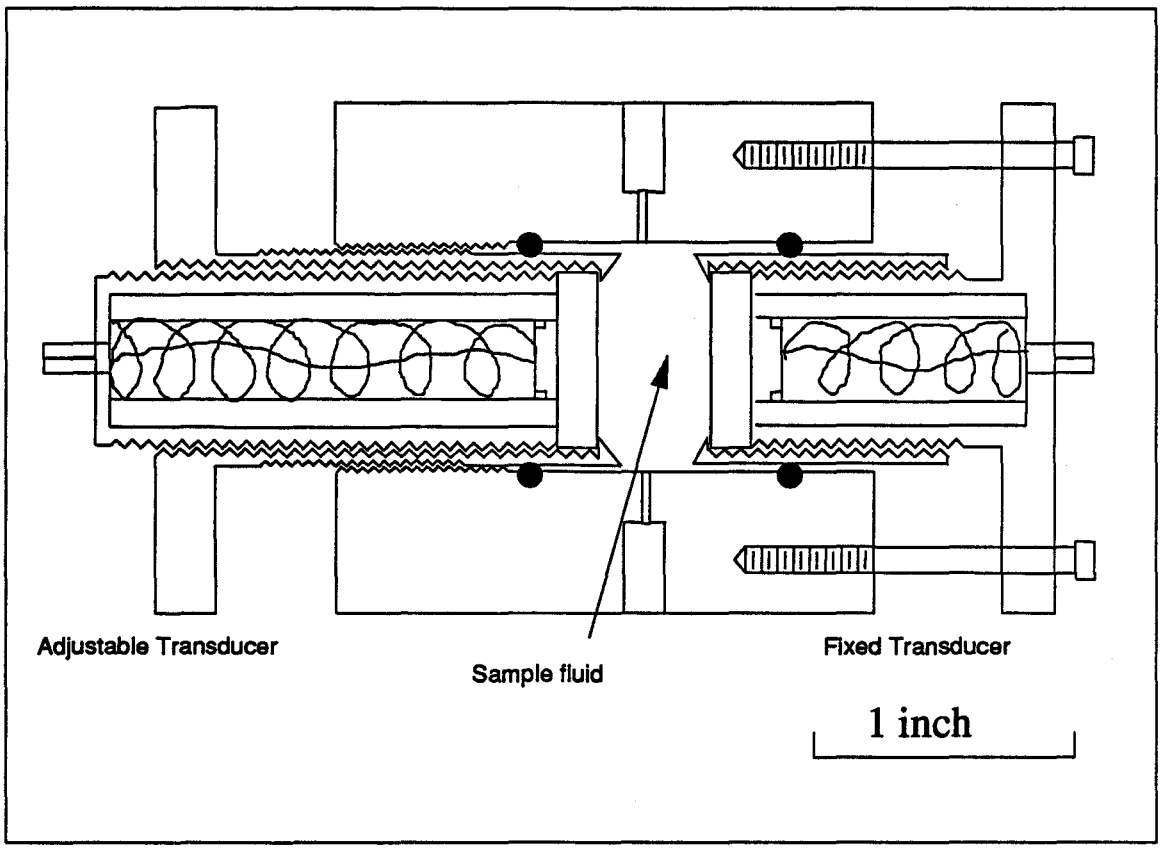

Figure 4.5. Cross-section of the measurement Cell.

generally not the case. The attenuation constant in equation 3.14 is a measure of the diminishing intensity of a wave as it travels through a sample only as a function of the distance. In order to obtain the attenuation constant from the absolute attenuation, it is necessary to subtract out the attenuation due to transmission through the reflecting interface. If the absolute attenuation was measured as a function of distance, there should be an offset that corresponds to the wave energy that is lost by transmission through the reflecting surface. In addition, the transit time must be also measured as a function of distance to be able to infer the velocity. This is not as critical because the distance between transducers can be inferred by measuring the transit time though a sample with a

known velocity. The dilemma is that it is not possible to only make one set of measurements to directly yield the velocity and the attenuation constant through a sample.

The approach taken in this work was to design a measurement cell for measuring liquid samples in which the distance between the transducers can be manually adjusted. A diagram of the cross-section of the measurement cell used in this work is shown in Figure 4.5. Each of the transducer discs described in section 4.1.4 is clamped tightly into a brass house. Each brass house can travel backwards and forwards along the inside of a polycarbonate cylinder which holds the sample fluid. Leakage from the cell is prevented with two O rings that seal each of the annular spaces between the transducer house and the inside surface of the cell. An RTD is used to monitor the cell temperature which is controlled manually using heating tape and a variable transformer.

The house on the right has three screws which can be adjusted to make both transducers perfectly parallel. A set of back nuts can be used to hold the house in place once a parallel configuration has been achieved. The house on the left in the diagram contains the adjustable transducer. The outside surface of the house has been threaded for 32 treads per inch to mate with the inside surface of the measurement cell. Every 360° turn of this house brings the transducers together by 1/32 of an inch. This was confirmed by measuring the change in transit time for water as the adjustable transducer was rotated by one full turn between each measurement. The transit time vs the number of rotations is shown in Figure 4.6. The reciprocal of the slope of this plot is within two percent of the reported value for the velocity of water at 21°C as reported by Greenspan and Tsiegg (1959) (1460.7 vs 1485.7 m/sec).

Some additional requirements were imposed on the design of the measurement cell to insure that the wave does not behave as a guided wave and that the measured attenuation was not caused by any diffraction or interference from reflected waves. These constraints are summarized in Appendix II of Hawley's thesis. The first constraint is that the acoustic path that is travelled to make a measurement must be within the near

diffraction field (equation 3.21). The second constraint is that the inside diameter of the cell wall is twice the diameter of the transducer. A third requirement is that the radius of the transducer is at least 25 times larger than the wavelength of the sound wave.

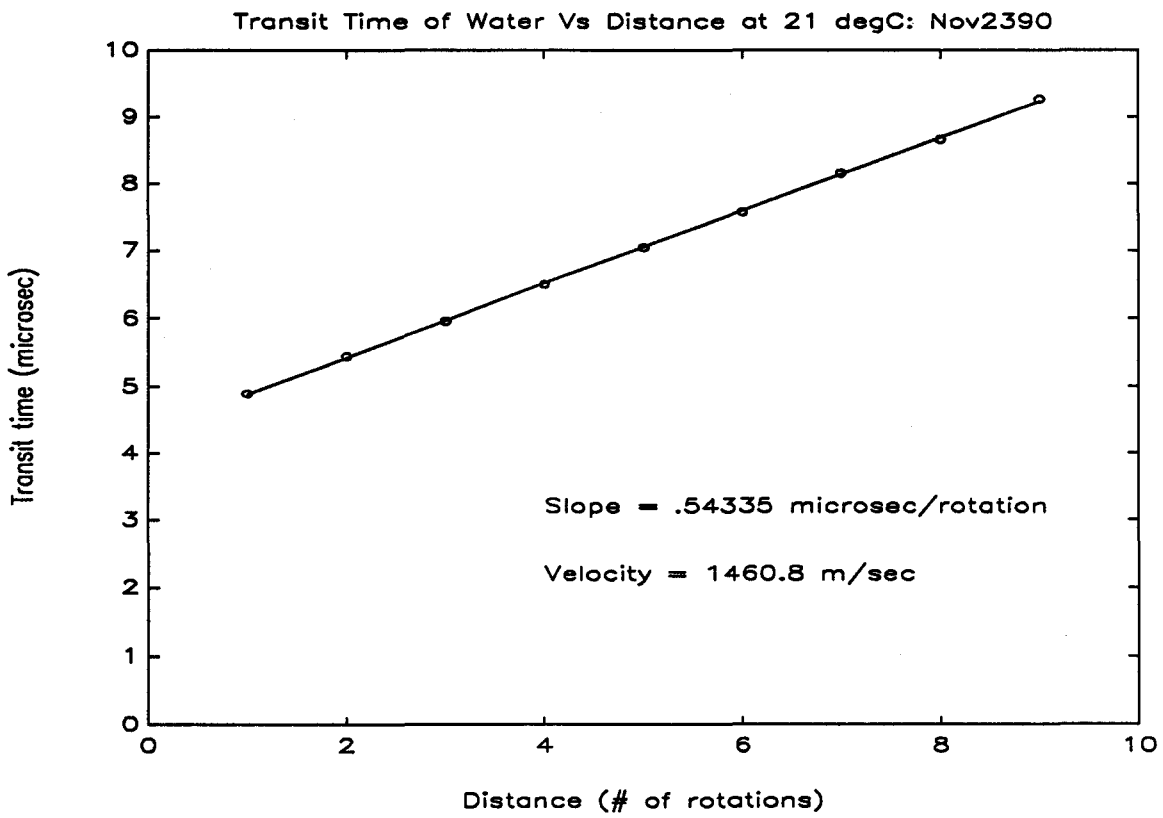

Figure 4.6. Confirming the change in distance with each rotation of the adjustable transducer by calibrating with water.

4.4 The Rigorous Measurement Method

The rigorous measurement method was developed to measure the velocity and attenuation constant when no prior information about the sample liquid is known. Once some information is known about the attenuation due to the incomplete reflection of waves at the sample/transducer interface, the shortcut method can be used which saves considerable time and makes on-line measurements possible. The idea behind the

rigorous method is that the attenuation due to incomplete reflection can be subtracted from the absolute attenuation by measuring the absolute attenuation at different distances between the transducers. The absolute attenuation and transit time are recorded as the distance is changed and then they are each regressed against the distance (which is the independent variable) using a first order least squares regression. The slope of the first model is equal to the attenuation constant and the slope of the second model is equal to the reciprocal of the velocity. Figure 4.7 shows how this method was used to measure the velocity and attenuation constant for the styrene-methylmethacrylate latex sample "SMB56" at frequencies between 5 and 10 MHz. Initially one measurement was made for each full rotation of the adjustable transducer. This was to confirm that the absolute attenuation and transit time were linear functions of the separation distance. One of the advantages of this technique is that it provides a way to estimate the confidence interval on each measurement of the velocity and attenuation constant. The confidence limits for the slope of a first order least squares model can be estimated by equation 4.7 and 4.8 from Box and Draper (1981).

$$s^2 = \frac{SS_{res}}{(n-2)} \tag{4.7}$$

$$b_1 = \hat{b}_1 \pm \frac{t_{n-2,1-1/2\alpha} \times s}{\sqrt{\{\Sigma(x_i - \bar{x})^2\}}} \tag{4.8}$$

After it had been established that the attenuation and reciprocal velocity were linear functions of the distance between the transducers, a more efficient method for measuring individual data points was utilized. By reviewing equation 4.8 it can be seen that the confidence interval on a parameter estimate can be decreased by increasing the number of measurements so that t goes down or by increasing the distance between the measurements and the centroid of the independent variable. To take advantage of this fact, all subsequent experiments took clusters of measurements around a low and high level. The low level was about 6 mm and corresponded to the distance between the transducers when their houses were touching. The high level was a separation distance of about 15mm. The rigorous measurements for the styrene methylmethacrylate system are given in Appendix 1A for the attenuation constants and Appendix 2 for the velocity. There did not seem to be any difference between the velocities of each of the styrene

methylmethacrylate latices. They were all very close to the velocity of water which is about 1500 m/sec at 25°C and so it was assumed that the polymer portion of the latex did not appreciably affect the speed of sound. Similar results were observed for the styrene butadiene system but are not reported here.

All of the styrene methylmethacrylate latex samples were measured with the transducers in the sender/receiver mode so that a separate set of measurements was required to measure the high and low frequency attenuation of each sample. In order to obtain a better range of frequencies, all of the styrene butadiene rubber latex samples were measured in transceiver mode with the 3 MHz transducer in one house and the 7 MHz transducer in the other house. In this configuration, the measurement signal from the 3 MHz transducer was reflected off of the 7 MHz transducer for measurements form 2 to 4 MHz and then the measurement signal from the 7 MHz transducer was reflected off of the 3 MHz transducer for measurements between 4 and 10 MHz. This allowed the attenuation constants to be measured between 2 and 10 MHz with one replicate at 4 MHz to evaluate any measurement bias between the transducers.

In general, the attenuation constants of the styrene butadiene latices are considerably higher than those of the styrene methylmethacrylate system. One problem with measuring samples with a high attenuation by the rigorous method is that the distance between the transducers should be varied between 6 and about 15 mm in order to obtain a measurement with an acceptable set of confidence limits. At these distances, the absolute attenuation measurements for the undiluted styrene butadiene latices would be much greater than the range of the measurement equipment which is about 30 to 40 dB. As a result, it was necessary to dilute all of the samples with deionized water.

Initially, all of the samples were diluted by 1/8 (one part of latex in eight). One problem with this dilution is that some of the resolution of the measurement equipment is lost since the polymer particles have a much larger contribution to the attenuation than water. At a higher dilution, the attenuation of the different latex samples tends to become more alike. In order to be able to measure the latex sample set with maximum resolution between samples , it is important to find the dilution ratio at which the latex sample with the highest attenuation constant registers measurements at the upper end of the sensor's

range. The dilution ratio that best fit this criterion was 1/4. The attenuation constants calculated from the rigorous method for each of the styrene butadiene latices at 1/4 dilution are given in Appendix 1B.

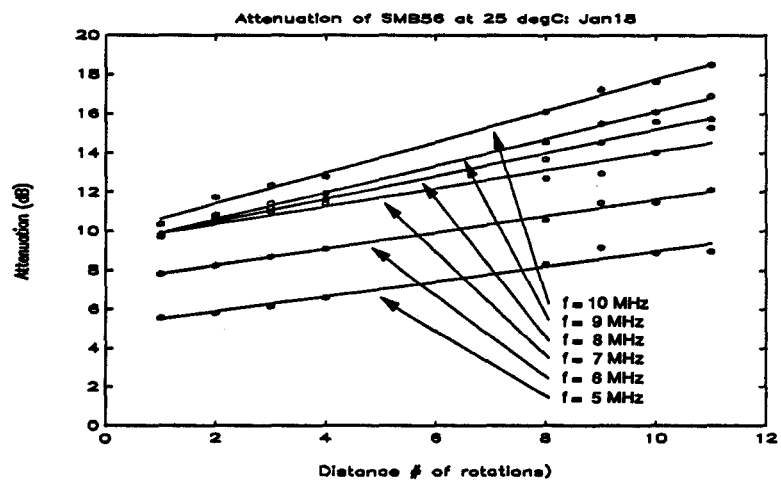

Figure 4.7A. Attenuation vs distance
is used to calculate the attenuation constant for SMB56 for $f = 5$ to 10 MHz.

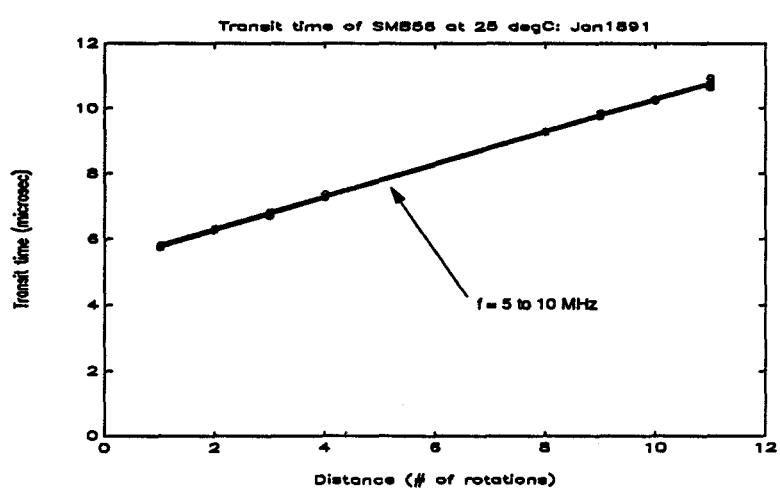

Figure 4.7B. Transit time vs distance is used to calculate the velocity for SMB56 for $f = 5$ to 10 MHz.

4.5 The Shortcut Method

The major problem with the rigorous method for measuring the attenuation constant and velocity is that it is a lengthy and laborious process. This procedure would have very limited practical use as a laboratory instrument and would be completely inappropriate as an on-line sensor. Once some information is known about the measurement set however, we are in a better position to make some assumptions that could simplify the measurement procedure.

4.5.1 Calculating The Reflection Loss

The whole point of the rigorous measurement method is to measure the absolute attenuation as a function of the transducer separation distance so that the attenuation loss due to an imperfect reflection can be subtracted from the absolute attenuation to give the attenuation constant. At least theoretically, this reflection loss is a function of the acoustic impedances of the latex and the reflecting surface. If the density and velocity do not change too much within a sample set, then the reflection loss will be constant for all of the latices. Using the transit time and attenuation sets that were used to calculate the attenuation constant and velocity from the rigorous method, the attenuation can be regressed against the transit time to yield a model like equation 4.9 where T.T is the transit time and Atten is the absolute attenuation.

$$\text{Atten} = \text{Atten}\,|_{T.T=0} + \text{Slope} \times \text{T.T} \tag{4.9}$$

The intercept term in this model (Atten $|_{T.T=0}$) is equal to the extrapolated attenuation when the transit time is equal to zero. This is the same as an estimate of the reflection loss. Using all of that data from the rigorous measurements, estimates of the reflection loss can be found by this method for the styrene methylmethacrylate system in Table A3.1 and for the styrene butadiene system in Tables A3.2, A3.3 and A3.4. The last column in each of these tables represents the average of all of the reflection losses at a particular frequency. Numbers that were not included in the average are in brackets.

Another way to estimate the reflection loss is to calculate the transmission loss between the liquid sample and the reflecting surface from equation 3.10. The loss in decibels can be calculated by substituting this expression into equation 4.6.

$$\text{Reflection Loss (dB)} = 20 \times \log_{10}\left(\frac{2Z_2}{Z_1 + Z_2}\right) \tag{4.10}$$

This calculation can be made if the acoustic impedances of the reflecting surface and the sample liquid are known. The theoretical reflection loss from equation 4.10 has been calculated for the latices in the styrene methylmethacrylate system to compare this value with the empirically estimated reflection loss. The acoustic impedance for the lead metaniobate transducer was reported as 261 g/cm^{2}sec by Patel (1990) and the acoustic impedance for the latices was calculated from the densities in Table 2.2 and the velocities in Appendix 2. These results are included as the "theoretical" values in Table A3.1.

4.5.2 Measuring the Attenuation constant

With an estimate of the reflection loss in hand (Atten $|_{T.T=0}$), it is possible to obtain the attenuation constant with only one measurement of the absolute attenuation. This is important because it makes the measurement of the attenuation constant and velocity for liquid samples simple and automatic. The following set-up procedure was used. The transducers are positioned between 8 and 15 mm apart. The exact distance depends on whether the liquid sample has a high or low attenuation constant (samples with a higher attenuation constant will have to be measured at shorter distances). The screws on the fixed transducer house are adjusted for parallelness and the nuts are tightened to prevent the houses from falling out of alignment. The exact distance between the transducers is inferred by measuring the transit time in deionized water. The distance (dist) is estimated using a value for the speed of sound from Greenspan and Tsiegg (1959). The sample cell is filled with a liquid sample and estimates of the attenuation constant and the velocity ($\hat{\alpha}, \hat{v}$) are calculated from the transit time (T.T) and the absolute attenuation (Atten) by equations 4.11 and 4.12.

$$\hat{\alpha} = \frac{\text{Atten} - \text{Atten}\,|_{T.T=0}}{\text{dist}} \tag{4.11}$$

$$\hat{v} = \frac{\text{dist}}{T.T} \tag{4.12}$$

This method was used to remeasure the attenuation constants for the styrene butadiene latices at 1/4 dilution using the average estimates of the reflection loss recorded in Table A3.2. The purpose of this is to compare the results of the rigorous method and the shortcut method. It is expected that the rigorous method will be more accurate. These results are given in Table A4.1. The styrene butadiene latices were also measured by the shortcut method at 1/2 dilution. In this case the reflection losses were approximated by an average of the average reflection losses at 1/4 dilution (from Table A3.2) and undiluted (from Table A3.4). These results are given in Table A4.2.

Notation

$\hat{\alpha}$	estimated attenuation constant
δ	relative phase angle
A	area of electrode, wave amplitude
Atten	total attenuation between echoes from all contributions
$\text{Atten}\,\vert_{T.T.=0}$	extrapolated attenuation due to reflection losses
$\hat{b}_1$	estimate of first order regression coefficient
b_1	true value of first order regression coefficient
dist	distance between transducers
n	number of measurements
$t_{n-2,1-1/2\alpha}$	Student's T statistic with n-2 degrees of freedom at 1-α significance
SS_{res}	sum of squares of the residuals between some data and a straight line fitted by least squares
s	the estimated standard deviation from a data set
T.T	transit time between transducers
$\hat{v}$	estimate of sound velocity
x	perpendicular distance between transducers
Z	acoustic impedance

CHAPTER FIVE

RESULTS

In this chapter, some of the properties of the latex systems described in chapter two are compared with the measured attenuation spectra from chapter four. The purpose is to determine whether a predictive empirical relationship can be derived to infer latex properties from the measured attenuation constants. Each of the two sample systems will be discussed separately. For the styrene-butadiene system, some of the latex properties are regressed onto the attenuation spectra using PLS.

5.1 Some General Observations

All of the attenuation spectra for both systems were roughly related to frequency by a linear relationship. This can be seen by plotting any of the spectra from Appendix 1 or 4 against frequency. This behavior was also observed for liquid polyisobutylene by Mason et al (1948) in the frequency region between 2 and 10 MHz. In Tables A5.1 and A5.2, the attenuation spectra for both systems have been summarized by a slope and intercept taken from a least squares regression of the attenuation constant onto frequency like that shown in equation 5.1.

$$\alpha(f) \;=\; \alpha\,|_{f=5\mathrm{MHz}} \;+\; \frac{\Delta\alpha}{\Delta f}\times(f-5\mathrm{MHz}) \qquad (5.1)$$

The sum of squares of the residuals and the associated degrees of freedom are also

included to indicate how closely each spectra conforms to a straight line.

5.2 Results for the Styrene-methylmethacrylate system

The individual attenuation spectra were measured by the rigorous method and are listed in Appendix 1A. These attenuation constants are all very similar, for example, the attenuation constant at 10 MHz for each of the samples is 103.9, 105.1, 106.4, 112.8, and 116.6 neper/m. The resemblance of these spectra is also apparent from the summarized attenuation data in Table A5.1. For this data set, the attenuation spectra are too similar to find a predictive relationship between the attenuation constants and any of the polymer properties. There are two possible reasons for this. The first is that the property space, and especially the composition have not been varied by sufficiently large amounts in the experimental design to be able to see an effect on the attenuation constant in the latex. The second reason is that the attenuation constant may not depend very sensitively on changes to the copolymer composition for this system. The methylmethacrylate and styrene monomers both produce polymer chains with comparable mechanical properties. This is the reason why homopolymers produced by each of these monomers have almost the same glass transition temperature (Table 2.2). From equation 3.19 we know that the attenuation constant depends on the bulk loss modulus. If this property does not change significantly with composition for a particular pair of monomers, it might be expected that the attenuation constant is not affected by changes in composition.

5.3 Results for the Styrene-Butadiene System

Attenuation measurements on the styrene-butadiene system produced a measurement space which varied greatly from sample to sample. Samples at 1/4 dilution or about 13 mass percent solids were measured by the rigorous method and samples at 1/2 dilution and 1/4 dilution were measured by the shortcut method. Good agreement between the rigorous and shortcut methods was observed for the 1/4 diluted samples (Appendix 1B

vs Appendix 4 and Table A5.2 vs Table A5.3). Because the shortcut method can measure larger attenuation constants, the summarized slopes and intercepts in Appendix 5 should have a higher accuracy for the shortcut method than for the rigorous method.

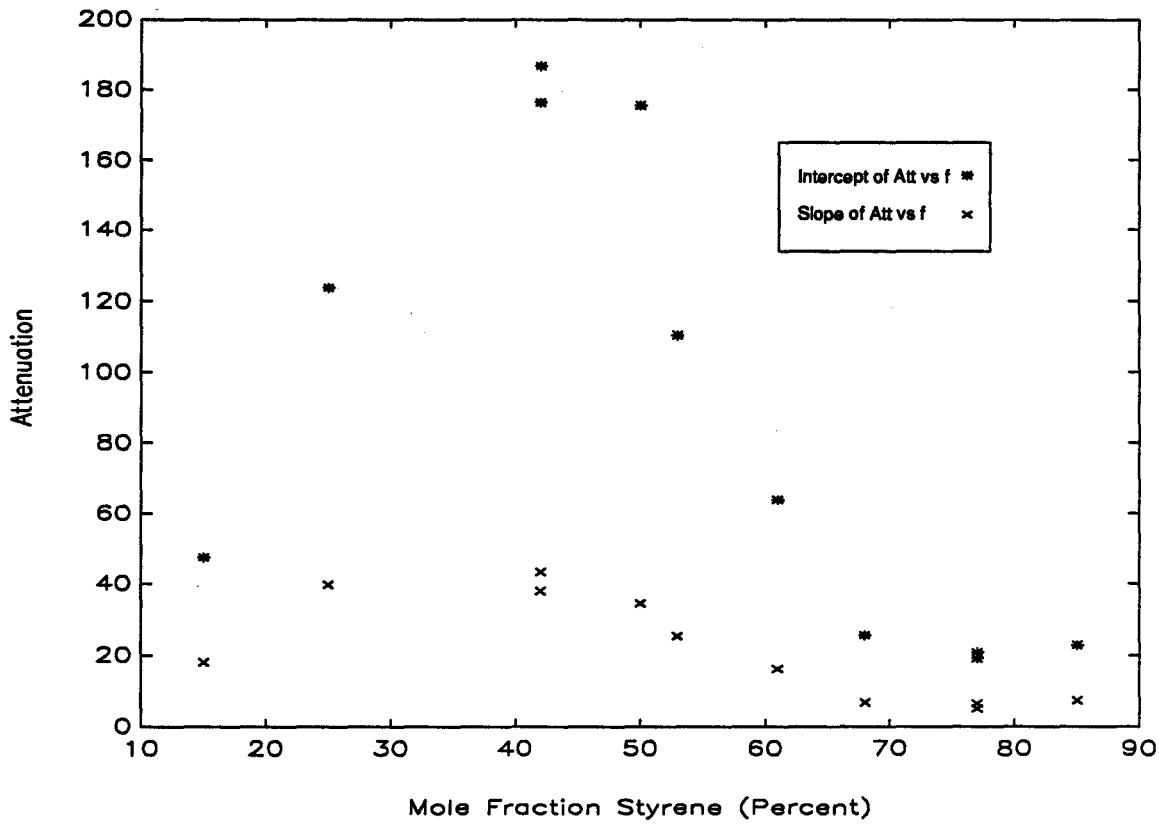

Figure 5.1. The summarized attenuation behavior of styrene butadiene latices at about 13 percent solids vs composition.

The intercept and slope ($\alpha|_{f=5MHz}$ and $\Delta\alpha/\Delta f$) of each of the measurements have been plotted against composition for the 1/4 diluted samples in Figure 5.1 and the 1/2 diluted samples in Figure 5.2. Mole percent of styrene is used to indicate composition. Three observations can be made from these plots. The first is that dilution by a common factor does not drastically change the position of a sample's attenuation constant relative to other samples. The second observation is that the slopes and intercepts in Appendix 5 are highly

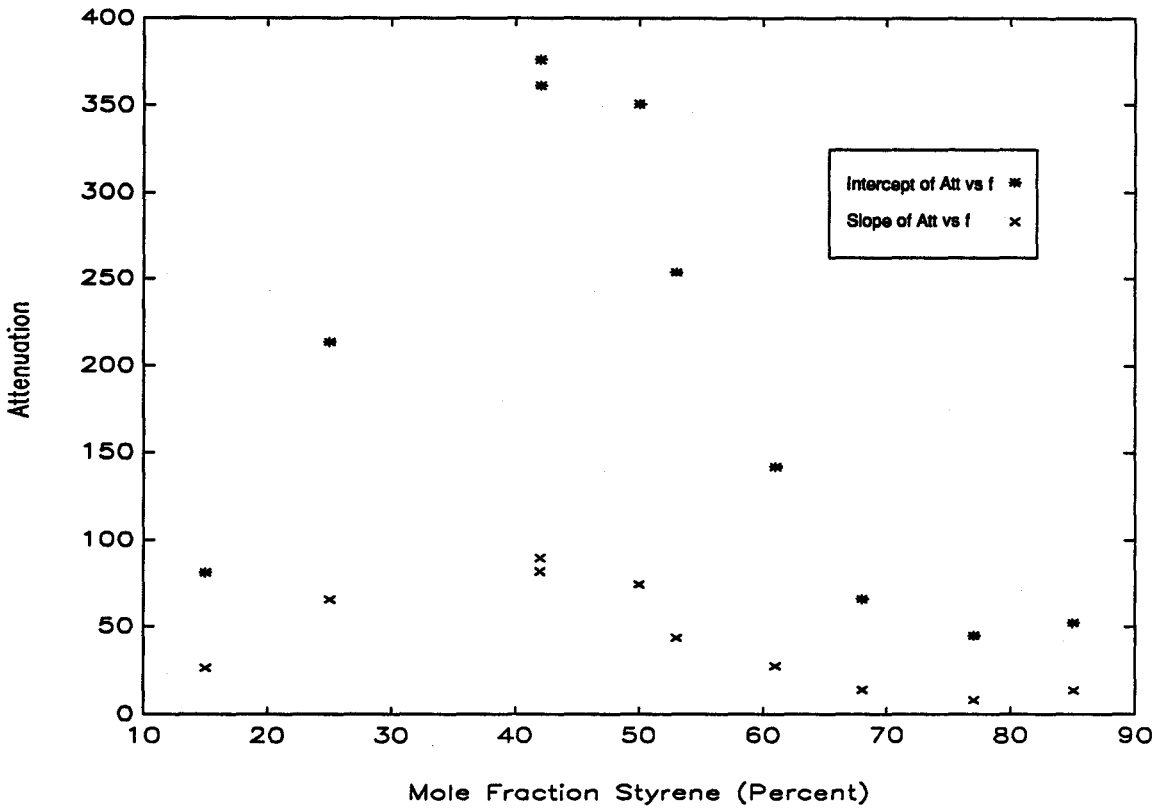

Figure 5.2. The summarized attenuation behavior of styrene butadiene latices at about 26 percent solids vs composition.

correlated with each other (correlation coefficients for $\alpha|_{f=5\text{MHz}}$ and $\Delta\alpha/\Delta f$ in Tables A5.1 through A5.3 are .901, .958 and .978 respectively). This was despite the fact that the intercept was chosen near the centroid of the attenuation spectra (5MHz) so as to be as uncorrelated with the slope as possible. The third observation is that the relationship between the summarized attenuation data and composition is severely non-linear. This would present a problem for any linear regression algorithm. Moreover, the form of this non-linearity is troubling because it tells us that there are two possible copolymer compositions that correspond to one set of attenuation data. This presents a difficulty when trying to develop a predictive relationship to infer variables such as composition from the attenuation behavior.

The form of these plots creates two problems that will be discussed in the remainder of this section. The first problem is to determine whether there is any theoretical explanation for the non-linear behavior. The second problem is to evaluate whether it is possible to build a predictive model with a data set containing such a non-linear relationship.

5.3.1 An Explanation of the Non-linear Dependence of Attenuation on Composition

A plot of the glass transition temperature vs composition for this system is shown as Figure 5.3. The relationship between T_g and composition is approximately linear. The relationship would be even more linear than Figure 5.3 except that T_g also depends on crosslinking which is varied independently of composition in this data set (Figure 2.2). It has been established in the literature that the T_g determined by DSC with 10°C/min heating corresponds to a structural relaxation with a time constant of 10^3 seconds (Johari (1991)). This means that an SBR copolymer with 15 mole percent styrene has a structural relaxation time constant τ_c of 10^3 seconds at -62°C and a copolymer with 85 mole percent styrene has a structural relaxation time constant of 10^3 seconds at approximately 47°C. If we assume that the relaxation time constant decreases with increasing temperature (this is true if the relaxation is endothermic), then we know that for some constant temperature the relaxation time constant will increase as the fraction of styrene in the copolymer increases. Because $\tau_c = 1/2\pi f_c$, the characteristic frequency of the relaxation f_c will decrease with increasing styrene composition.

The equation that is used to describe attenuation in terms of empirically fitted terms for the characteristic relaxation frequency and classical and excess absorption (f_c, B, A) is equation 3.18. As the composition of styrene increases, we would expect the classical absorption (B) which contains a viscous loss term to decrease. This would reflect the fact that sound waves travel more efficiently through glasses than viscous or viscoelastic rubbers. Therefore we would expect that f_c and B in equation 3.18 should both decrease with increasing percent styrene. The next step is to see whether the slope of the attenuation spectra calculated from equation 3.18 could go through a maximum as f_c is varied. This will help us to assess

whether the experimental results shown in Figures 5.1 and 5.2 make any sense. Three simulations were performed using equation 3.18 and different values for A, B and f_c. These will now be discussed.

In the first simulation, f_c was increased and A and B were kept constant. This simulation corresponds to the situation where the classical and excess absorption values are not a function of copolymer composition. This is an unrealistic situation since copolymer composition does affect many of the properties of equation 3.19. In this case the attenuation spectra is always increasing: when $f \ll f_c$ then $\alpha \approx (A + B)f^2$ and when $f \gg f_c$ then $\alpha \approx Bf^2$. The slope or intercept of the attenuation spectra does not go through a maximum for this situation.

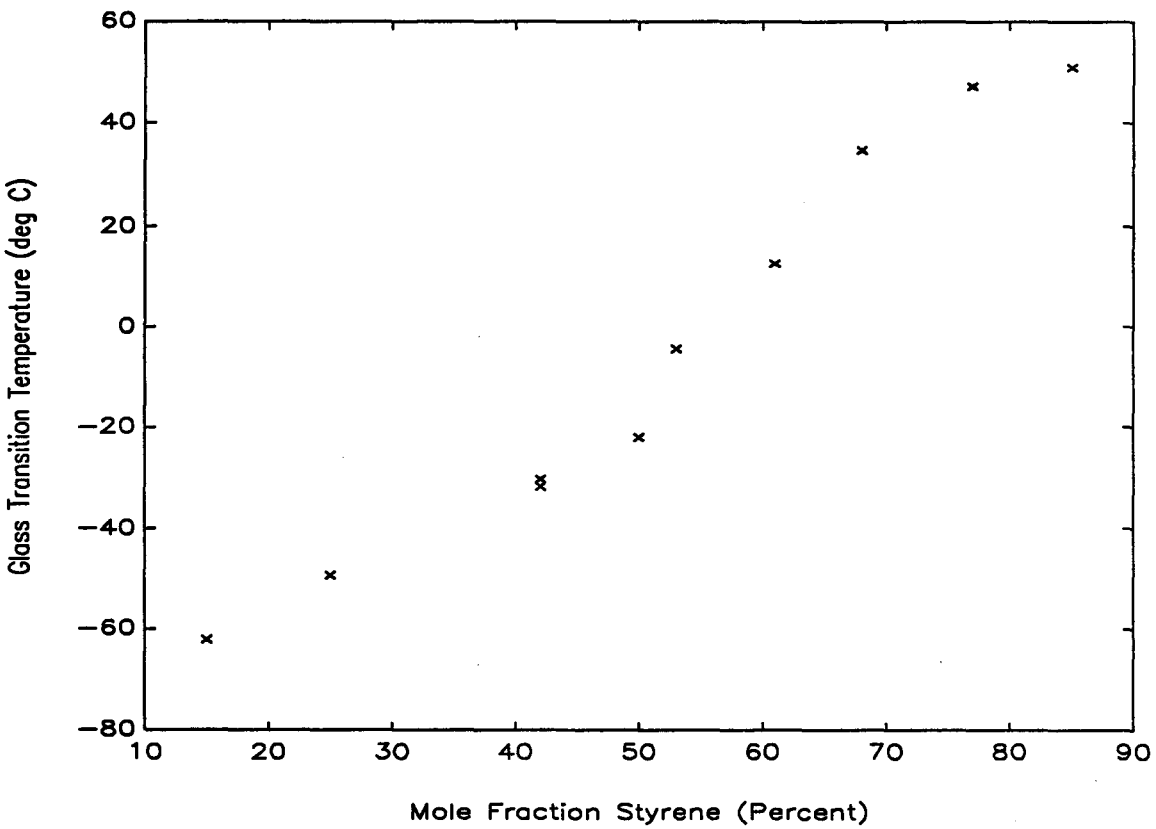

Figure 5.3. The dependence of the glass transition temperature on composition for the SBR system.

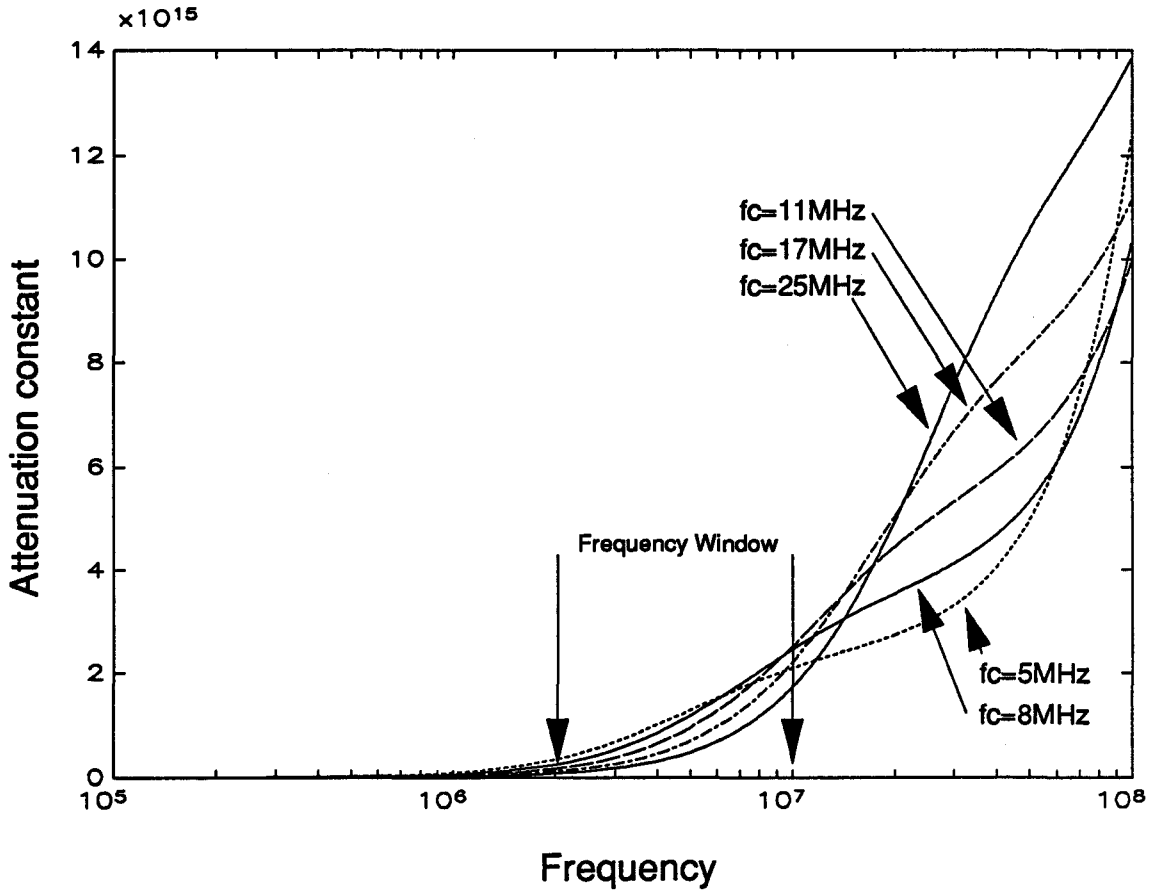

Figure 5.4. Attenuation spectra for simulation 2: the situation when A and B decrease by a common factor as f_c increases by the same factor. The slopes of the spectra within the frequency window go through a maximum as f_c increases.

In the second simulation, A and B decreased by a common factor of 1.5 as f_c increased by the same factor. This simulation corresponds to the situation where the classical and excess absorption both decrease with increasing percent butadiene. This is also not a very realistic situation because we expect that increasing butadiene in the polymer chain would increase the classical absorption. The values of A, B, and f_c that are used in equation 3.18 are shown in Table 5.1. The simulated attenuation spectra are shown in Figure 5.4. Although these curves are quadratic functions, they are approximated by straight lines in the "frequency window" where measurements are made (2 to 10 MHz). The intercepts and

slopes for each of these curves ($\alpha|_{f=5MHz}$ and $\Delta\alpha/\Delta f$) are also given in Table 5.1. In Figure 5.5 the slopes of these curves are plotted against f_c. From Figure 5.3, we know that each composition is related to a unique f_c at some common temperature and that f_c decreases with increasing percent styrene. This means that this plot should have the same form as $\Delta\alpha/\Delta f$ vs composition.

Table 5.1. The values of each of the constants used in the second simulation and the slopes and intercepts from a first order regression inside the frequency window.

f_c	A	B	$\alpha|_{f=5MHz}$	$\Delta\alpha/\Delta f$
$5X10^6$	100	1	$11.0X10^8$	$2.19X10^8$
$5X10^6X1.5$	100/1.5	1/1.5	$-2.98X10^4$	$2.88X10^8$
$5X10^6X1.5^2$	$100/1.5^2$	$1/1/5^2$	$-5.52X10^{14}$	$3.07X10^8$
$5X10^6X1.5^3$	$100/1.5^3$	$1/1.5^3$	$-5.92X10^{14}$	$2.71X10^8$
$5X10^6X1.5^4$	$100/1.5^4$	$1/1.5^4$	$-5.00X10^{14}$	$2.09X10^8$

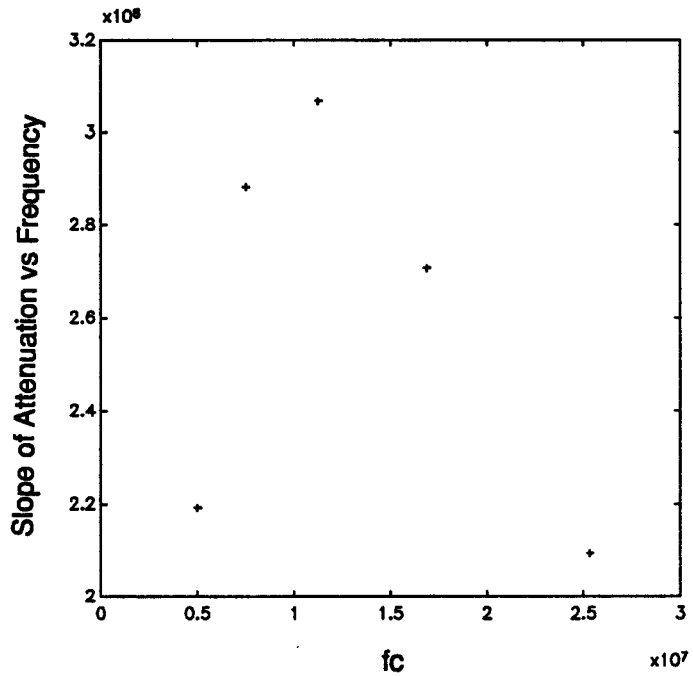

Figure 5.5. The calculated slopes ($\Delta\alpha/\Delta f$) from Table 5.1 are plotted against the characteristic frequency f_c for simulation 2 to show the maximum as f_c is varied.

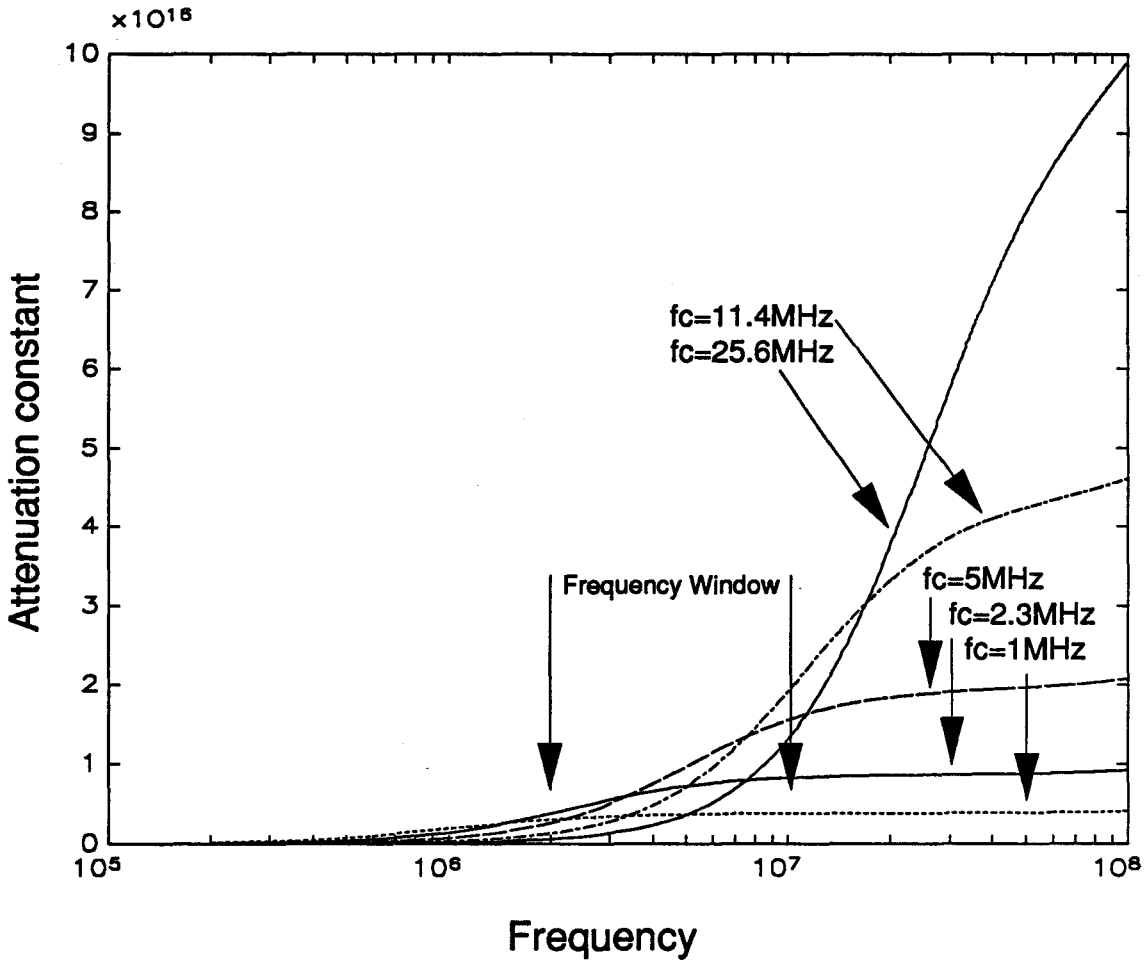

Figure 5.6. Attenuation spectra for simulation 3: the situation when A decreases as B and f_c increase by the same factor. The slopes of the spectra within the frequency window go through a maximum as f_c increases.

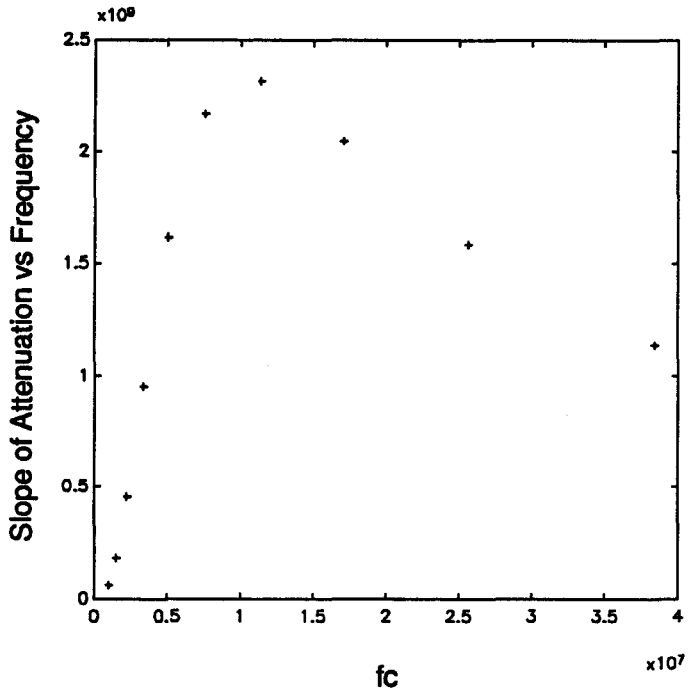

Figure 5.7. The calculated slopes ($\Delta\alpha/\Delta f$) from Table 5.2 are plotted against the characteristic frequency f_c for simulation 3 to show the maximum as f_c is varied.

In the third simulation, B and f_c were increased by a common factor of 1.5 as A was decreased by the same factor. This simulation corresponds to the situation where the classical absorption increases and the excess absorption decreases with increasing percent butadiene. The values of A, B, and f_c that are used in equation 3.18 are shown in Table 5.2. The simulated attenuation spectra are shown in Figure 5.6. In Figure 5.7, the slopes of the attenuation spectra inside the frequency window are plotted against f_c. From the data for simulations 2 and 3 it can be seen that it is possible to get a maximum in $\Delta\alpha/\Delta f$ vs f_c when f_c increases if we assume that the classical and excess absorption both decrease or that the classical absorption increases and the excess absorption decreases.

Table 5.2. The values of each of the constants used in the third simulation and the slopes and intercepts from a first order regression inside the frequency window.

f_c	A	B	$\alpha\|_{f=5MHz}$ ($X10^9$)	$\Delta\alpha/\Delta f$
$1X10^6$	$100X1.5^9$	$1/1.5^9$	.0639	$3.28X10^{15}$
$1X10^6X1.5$	$100X1.5^8$	$1/1.5^8$	.182	$4.13X10^{15}$
$1X10^6X1.5^2$	$100X1.5^7$	$1/1/5^7$	.456	$4.38X10^{15}$
$1X10^6X1.5^3$	$100X1.5^6$	$1/1.5^6$	.954	$3.33X10^{15}$
$1X10^6X1.5^4$	$100X1.5^5$	$1/1.5^5$	1.62	$.801X10^{15}$
$1X10^6X1.5^5$	$100X1.5^4$	$1/1.5^4$	2.17	$-2.22X10^{15}$
$1X10^6X1.5^6$	$100X1.5^3$	$1/1.5^3$	2.32	$-4.18X10^{15}$
$1X10^6X1.5^7$	$100X1.5^2$	$1/1.5^2$	2.05	$-4.48X10^{15}$
$1X10^6X1.5^8$	100X1.5	1/1.5	1.59	$-3.77X10^{15}$
$1X10^6X1.5^9$	100	1	1.14	$-2.81X10^{15}$

Thus we can see how changes in composition will effect the attenuation behavior in a copolymer system where composition is related to the relaxation time constant of a structural relaxation. We can also see that even if the relaxation time constant is increasing or decreasing monotonically with the composition of one monomer, that the slope or intercept of the attenuation spectra over a narrow range might not also increase or decrease monotonically. This scenario can be described mathematically by equations 5.2 and 5.3

$$f_c = g(\%\text{sty}) \tag{5.2}$$

$$\Delta\alpha/\Delta f(2 \rightarrow 10\text{MHz}) = f(f_c) = f(g(\%\text{sty})) \tag{5.3}$$

Even though the function in equation 5.2 might well be a monotonically increasing function as suggested by Figure 5.3, the second function in equation 5.3 makes the overall relationship between attenuation and composition severely non-linear.

5.3.2 Building a Predictive Relationship Between Polymer Properties of the Latex and Attenuation Spectra

Initially the whole SBR data set was included in a PLS calibration; however the attenuation data in the measurement space X is strongly dependent on composition compared with the other properties. This means that the severe non-linearity seen in Figures 5.1 and 5.2 would tend to disguise lesser effects that are due to other polymer properties. PLS is a linear method and is unable to accommodate such a strongly non-linear relationship. The objects P1163 and P1123 (high butadiene) and P9999 (high styrene) were far off the first PLS inner relation for this calibration meaning that these objects were not well correlated with the largest variations in the polymer property space and the attenuation spectra for the remaining data set.

It was decided to break up the data set into a region where the relationship between attenuation and composition was approximately linear. The purpose for this was to have a composition range over which attenuation and composition are related by a linear relationship. Then PLS can be used to determine which other polymer properties have an effect on the attenuation spectra. The range over which the attenuation was approximately linear with composition was 30 to 80 mole percent styrene. Because the attenuation spectra at two different dilution ratios both seemed to contain the same information (Figures 5.1 and 5.2), all calibrations were made at a single dilution ratio.

5.3.2.1 Assessing PLS Models and Data Sets

There are two tests that are used to assess the ability of a PLS latent variable to model a multivariate data set. The first test is to determine whether the nth latent variable

can improve the predictive ability of the model where n is the total number of latent variables in the model. The method used to test this is cross validation (Wold (1978)). This indicates whether a latent variable has any predictive ability for finding remaining relationships hidden in the residual matrices after n-1 latent variables have been extracted. Cross validation is used in the SIMCA algorithm by removing a certain fraction of the data set and calculating a PLS model with the remaining data. The values for **X** of the removed fraction are then put into the model derived from the rest of the data to generate predicted values. This is repeated until all of the objects in a data set have been predicted once. The sum of the squares of the difference between the predicted results and the observed results (PRESS) is then calculated. This is calculated for each additional latent variable. The square root of the PRESS for the nth latent variable divided by the sum of the squares from the residual matrix of **Y** after n-1 latent variables have been removed is called "CSV/SD" in the SIMCA output. The calculation used in the SIMCA package is shown in equation 5.4. The current latent variable has predictive power for a particular property when CSV/SD is less than unity. The square root of the total sum of every PRESS divided by the total sum of the squares of the residuals for **Y** is also included. This is called "CSV/SD overall" in the SIMCA output and is calculated by equation 5.5. The predictive power of the model can also be evaluated by the "percent cross validated sum of squares explained in **Y**". This statistic is obtained by subtracting the sum of every PRESS from the total sum of squares of the residual matrix of **Y** after n-1 latent variables and dividing by the sum of squares of **Y** before any latent variables have been removed. The equation for this statistic is given in equation 5.6.

$$CSV/SD\,(property\,j) \;=\; \sqrt{\frac{PRESS_j(n)}{\sum_i y_{ij}^2(n-1)}} \tag{5.4}$$

$$CSV/SD\,(overall) \;=\; \sqrt{\frac{\sum_j PRESS_j(n)}{\sum_j \sum_i y_{ij}^2(n-1)}} \tag{5.5}$$

$$\%\ \text{Sum of Squares Exp in Y} \;=\; \frac{\sum_j \sum_i y_{ij}^2(n-1) \;-\; \sum_j PRESS_j(n)}{\sum_j \sum_i y_{ij}^2(0)} \tag{5.6}$$

The nth latent variable will have predictive power for the data set when the overall CSV/SD

is less than unity or the percent sum of squares explained in **Y** is greater than zero.

The second test measures how much of the variation in the data has been fitted by the overall PLS model. This test calculates the ratio of the sum of the squares of the residuals after each latent variable is given as a fraction of the original sum of squares for **X** and **Y**. This statistic is called the "percent sum of squares explained" and is included in the second half of the SIMCA output for each latent variable. The overall model is used to fit the data in this case. This test does not evaluate the predictive power of the model but can be used to see how much variation in **X** accounts for how much variation in **Y**.

Both of these tests can be used together to decide when to stop adding latent variables to a PLS model. The predictive test is important for determining whether a given model would be useful for predicting a new **Y** from a new **X** with objects that were not included in the model calibration. The fitting test explains how much of the variation in **X** and **Y** have been fitted by the PLS algorithm for each latent variable.

5.3.2.2 Case One

For the first calibration a six column property space **Y** was regressed onto a two column measurement space **X**. This is an example of PLS2: **Y** with more than one column is regressed onto **X**. The property space included T_g, percent styrene, percent acrylic acid, percent gels, inverse swells, and particle size. The measurement space contained $\Delta\alpha/\Delta f$ and $\alpha|_{f=5MHz}$. Some initial work indicated that all of the information in the attenuation spectra could be summarized by these two variables without any effect on the PLS regression. There were eight objects in this calibration; P1017, P1376, P1377, P1380, P1382, P1406, P1006, and P1764. The SIMCA output for this case is included in Table A6.1 of Appendix 6. **X** and **Y** were autoscaled to unit variance and mean centered.

In Table 5.3 the percent sum of squares explained of **Y** is shown for each individual property. In Table 5.4 the cross validated sum of squares explained in **Y** is also shown for each property. From the cross validation section of the SIMCA output, it is apparent that the first PLS latent variable is useful for predicting changes in the first, second and possibly

third variables in the property space (T_g, %sty, %acr). By subtracting this latent variable out of the data set, 99.6% of the variation in the X block is explained and this accounts for about 43% of the variation in the Y block. This means that almost all of the information in the measurement space can be pulled out with the first latent variable. The second latent variable improves the prediction of the percent acrylic acid and the third latent variable improves the prediction of the particle size. Because the calibration set only consists of eight objects with seven measurements of particle size, it is likely that the correlation between particle size and the residuals of the X matrix after two latent variables is the result of chance rather than an underlying causal relationship. The inner relationships for the first and third latent variables are shown in Figures 5.8A and 5.8B. The scores for the third latent variable (t_3, u_3) which are the least squares projections onto the third latent variable from X and Y after two latent variables have been removed are about sixteen to seventeen orders of magnitude smaller than the scores for the first latent variable. From this we can conclude that at the very best, only a small amount of information in X can be used for predicting particle size.

An example of overfitting latent variables to a PLS model can be seen in Figures 5.8A through 5.8.F. In these plots the fitted values of polymer properties are plotted as functions of their observed values. The predictions were calculated using a PLS model with one latent variable ("+" signs) or three latent variables ("x" signs).

Table 5.3. Percent Sum of Squares Explained in Y by column for Case One

Property	First L.V	Second L.V	Third L.V
T_g	97.51	0.03	0.87
%sty	93.63	0.88	1.23
%acr	19.96	17.44	9.36
%gels	13.40	8.64	40.46
inv swells	12.98	0.08	14.03
part size	16.66	12.48	37.25
Overall	42.98	6.45	16.71

Table 5.4. Cross Validated Percent Sum of Squares Explained in Y by column for Case One

Property	First L.V	Second L.V	Third L.V
T_g	97.23	-0.42	0.42
%sty	93.41	-0.20	-0.10
%acr	7.71	10.85	-3.74
%gels	-15.36	-2.61	19.37
inv swells	-21.17	-1.48	6.61
part size	-13.74	11.09	25.42
Total	25.61	2.67	7.57

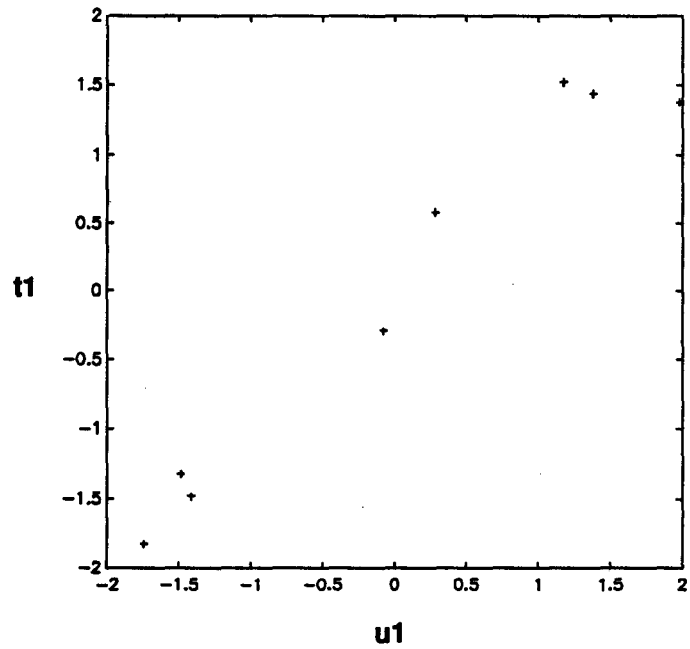

Figure 5.8A. The inner relation for the first PLS latent variable in Case One.

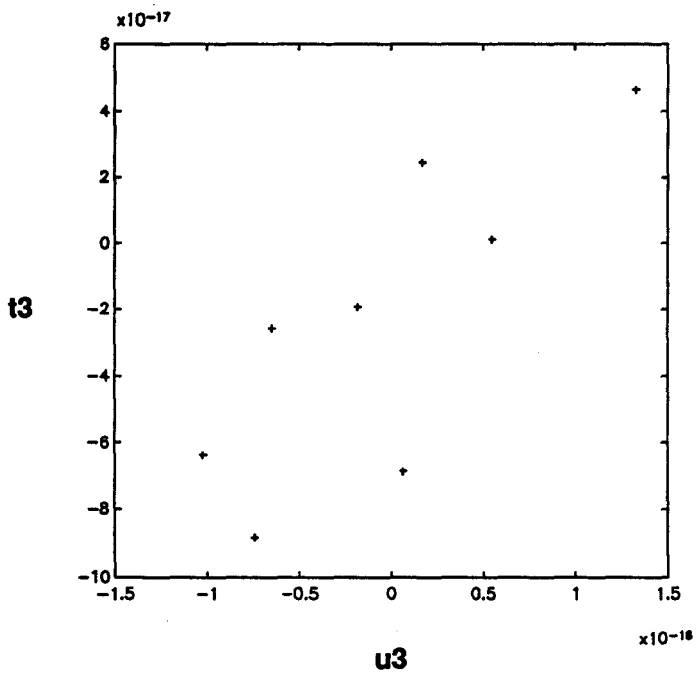

Figure 5.8B. The inner relation for the third PLS latent variable in Case One.

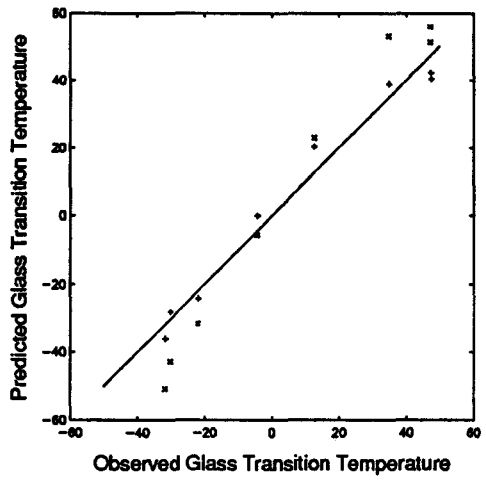

Figure 5.9A. Fitted T_g vs Observed T_g for PLS Case 1: '+' uses a model with one latent variable, 'x' uses a model with three latent variables.

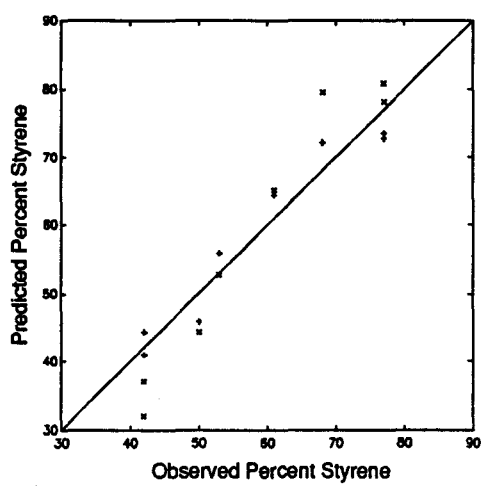

Figure 5.9B. Fitted %sty vs Observed %sty for PLS Case 1: '+' uses a model with one latent variable, 'x' uses model with three latent variables.

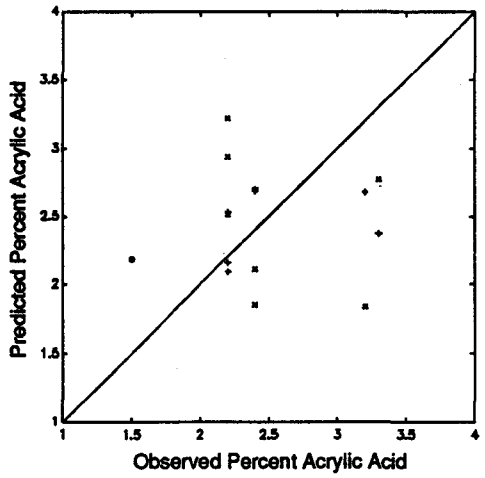

Figure 5.9C. Fitted %acr vs Observed %acr for PLS Case 1: '+' uses a model with one latent variable, 'x' uses a model with three latent variables.

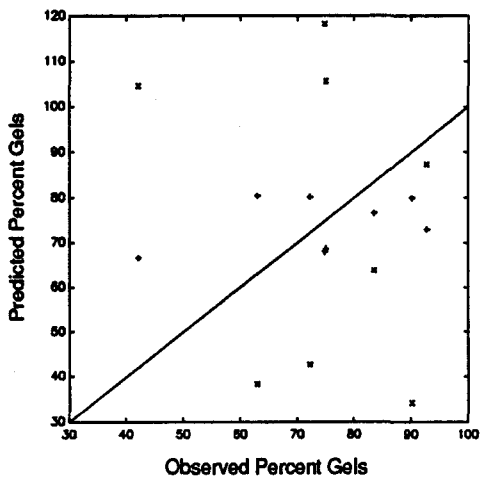

Figure 5.9D. Fitted %gels vs Observed %gels for PLS Case 1: '+' uses a model with one latent variable, 'x' uses a model with three latent variables.

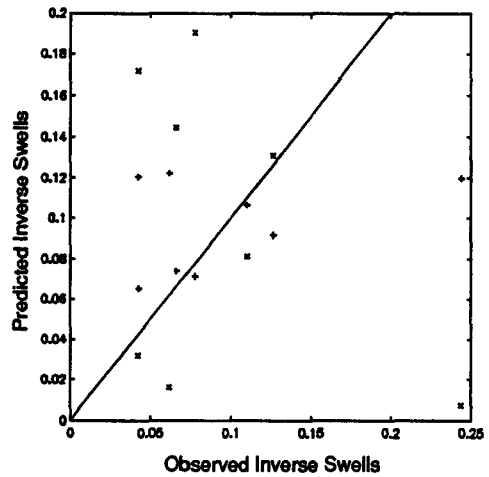

Figure 5.9E. Fitted Invsw vs Observed Invsw for PLS Case 1: '+' uses a model with one latent variable, 'x' uses a model with three latent variables.

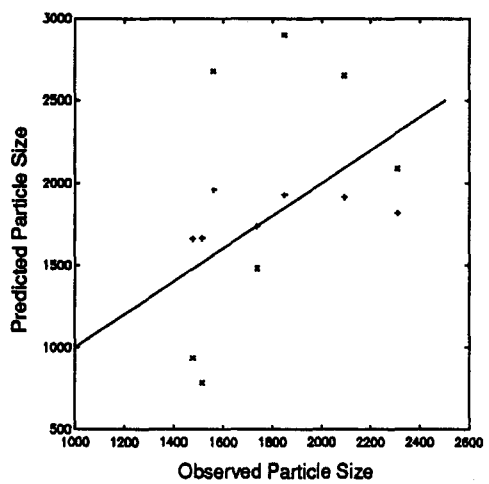

Figure 5.9F. Fitted P.S vs Observed P.S for PLS Case 1: '+' uses a model with one latent variable, 'x' uses a model with three latent variables.

5.3.2.3 Case Two

In this case properties 3 and 4 were dropped from the property space so that **Y** contains columns for T_g, %sty, %acr and particle size. The SIMCA output for this case is given in Table A6.2 and the sum of squares fitted and cross validated for each property are given in Tables 5.5 and 5.6. As expected, the variation in **X** accounted for a greater fraction of the variation in **Y** (58% vs 43%) for the first latent variable. This is expected because we have removed two properties that were not correlated with the first latent variable. For this analysis, the "cross validated sum of squares explained for **Y**" begins to decrease after the second latent variable. Once again, the first latent variable accounts for almost all of the change in **X** and has predictive ability for the first three properties which are all related to composition (T_g, %sty, %acr). The fact that **X** can almost be summarized as one latent variable confirms the earlier observation that $\alpha|_{f=5MHz}$ and $\Delta\alpha/\Delta f$ are highly correlated. The second latent variable improves the prediction of the percent acrylic acid as in the Case One analysis. Interestingly, the prediction of particle size from the residual matrix of **X** after two latent variables does not improve when gels and inverse swells have not been included in the property space. This reinforces the idea that there is no underlying relationship between the measurement space and the particle size. The fitted vs observed properties for each property in the Case Two analysis are shown in Figures 5.9A through 5.9D to show how the fitted model deteriorates after the first latent variable.

Table 5.5. Percent Sum of Squares Explained in **Y** by column for Case Two

Property	First L.V	Second L.V	Third L.V
T_g	97.51	0.03	0.00
%sty	93.63	0.88	0.00
%acr	19.97	17.43	0.03
part size	16.66	12.48	5.53
Total	58.43	7.53	1.24

Table 5.6. Cross Validated Percent Sum of Squares Explained in Y by column for Case Two

Property	First L.V	Second L.V	Third L.V
T_g	97.20	-0.42	-0.70
%sty	93.38	-0.10	-1.35
%acr	7.66	13.04	-8.47
part size	-13.93	10.43	-21.65
Overall	25.61	5.56	-7.54

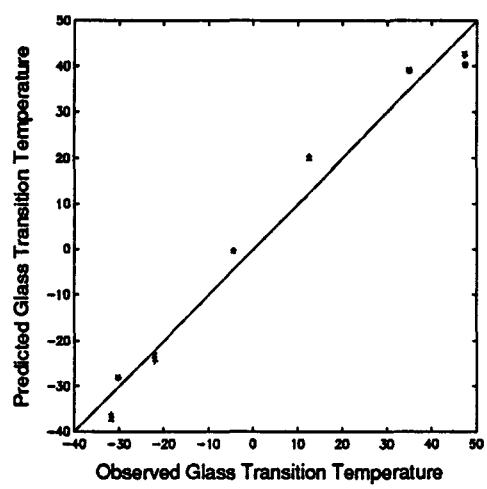

Figure 5.10A. Fitted T_g vs Observed T_g for PLS Case 2: '+' uses a model with one latent variable, 'x' uses two latent variables.

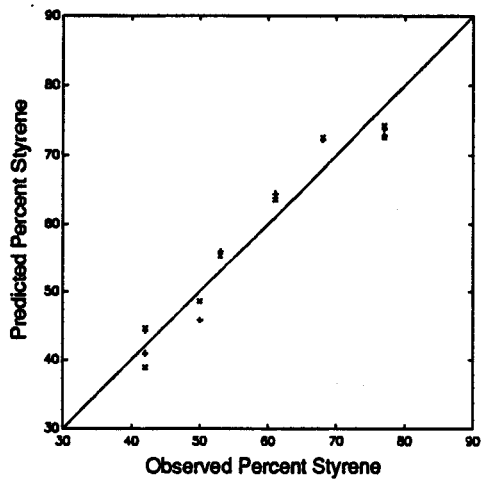

Figure 5.10B. Fitted %sty vs Observed %sty for PLS Case 2: '+' uses a model with one latent variable, 'x' uses a model with two latent variables.

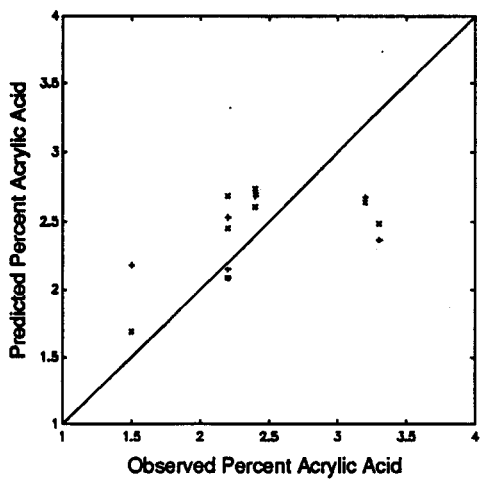

Figure 5.10C. Fitted %acr vs Observed %acr for PLS Case 2: '+' uses a model with one latent variable, 'x' uses a model with two latent variables.

5.3.3 Summary of the Results for the Styrene-butadiene system

The attenuation spectra between 2 and 10 MHz for the styrene-butadiene latices are very strongly dependent on composition. Over the range from 15 to 85 mole percent

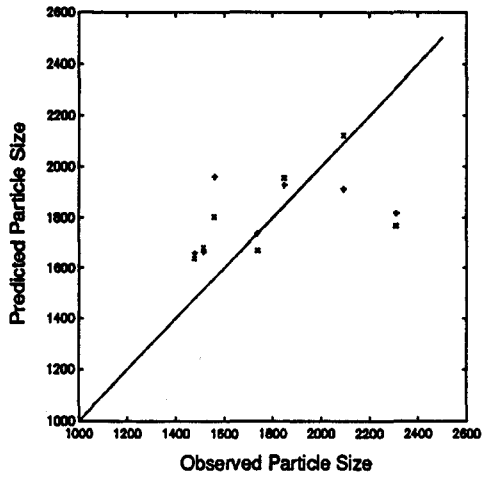

Figure 5.10D. Fitted P.S vs Observed P.S for PLS Case 2: '+' uses a model with one latent variable, 'x' uses a model with two latent variables.

styrene the relationship is severely non-linear. Between 30 and 80 mole percent styrene the relationship between composition of styrene (or butadiene) and attenuation is approximately linear.

In this range a PLS calibration was performed which revealed that the attenuation spectra was able to predict composition properties of the latex with two latent variables. The first latent variable predicted changes in the composition of the two primary constituents (styrene and butadiene) and acrylic acid to a lesser extent while the second latent variable improved the prediction of acrylic acid. No other definite relationships between polymer properties and attenuation were discovered.

CHAPTER SIX

CONCLUSIONS

The purpose of this chapter is to draw together some of the main conclusions of this study. The tractability of ultrasonic sensors for measuring changes in the properties of a polymer latex system will be discussed. Some conclusions regarding the two specific cases examined in this thesis will also be discussed.

6.1 The Sensor Problem for Latex Systems

There is a great need for sensors that can infer polymer properties. This is especially true for latex polymers produced by emulsion polymerization where polymer particles are partitioned in water rather than being in solution. Measuring ultrasonic wave transmission properties through a latex and relating these to the polymer properties is one potential technique for measuring the polymer properties of a latex without separating the particles from the water. Most traditional sensors rely on univariate relationships between a sensor output and measurand. Many of the important physical properties in a polymer system are inter-related to some extent so that a multivariate approach should be considered for selecting and calibrating sensors.

6.2 Ultrasonic Wave Travel in Polymer Latices

Ultrasonic longitudinal waves can be characterized by three travel parameters: the velocity, the attenuation and the frequency. The velocity is dependent on bulk properties of the system such as the longitudinal storage modulus and density while the attenuation

can be attributed to a number of different modes. A major contribution to the attenuation is from the absorption which is a function of the molecular properties of the system (excess absorption) and the physical properties (classical absorption). The excess absorption is associated with a structural relaxation. To avoid measuring other modes of attenuation that are independent of the system's material properties the attenuation must be measured within a "frequency window" for systems of particles suspended in liquids. This avoids spurious attenuation results due to diffraction at the low end of the frequency region and scattering at the high end of the frequency region.

The velocity of sound through polymer latices is not significantly different from the velocity through pure water. The attenuation of ultrasonic waves through polymer latices however is much greater than the attenuation through pure water so that the attenuation as a function of frequency could possibly hold important information about the polymer properties of the latex.

6.3 The Measurement Problem

Measuring sound waves in liquids is achieved by directly coupling the transducer to the liquid sample by immersion. Ceramic transducers or unbacked crystal transducers are able to measure the attenuation and velocity over frequency ranges. Ceramic transducers are broadband and can send/receive signals over a range while crystal transducers have a narrow passband but can send/receive signals at odd harmonics of the fundamental frequency. If some information is known or can be assumed about the attenuation loss that is due to reflection at the liquid/ transducer interface, then attenuation measurements can be taken directly from a pulse echo measurement system. Flow through cells can be used to extract process samples. The diameter of the transducer and the inside diameter of the measurement cell can be designed to minimize the contribution of diffraction to attenuation.

6.4 Ultrasonic Attenuation Measurement in a Polymer System

In a copolymer system, the frequency associated with a structural relaxation will be related to the composition. Depending on the mechanical behavior of each monomer

unit in the chain, the relaxation frequency will either be a weak or strong function of composition. If the mechanical properties imparted by each of the monomers are not very similar, the relaxation frequency will be a strong function of composition. Over a narrow range of frequency this can cause the attenuation to pass through a maximum as composition increases or decreases monotonically. In this case some other information is needed to be able to infer composition from attenuation.

Copolymer latices produced from styrene and methyl-methacrylate were examined first. Each of the monomers had similar mechanical properties. This was shown by the fact that both monomers produced homopolymers with similar T_g's. In addition, the changes in composition between objects were relatively slight. The attenuation measurements were all too similar to distinguish between changes in the property space.

In the second case, copolymers of styrene and butadiene with small amounts of acrylic acid were examined. Each of the two primary monomers imparted different mechanical properties to the copolymer and each sample had varying amounts of crosslinking. In the region where composition and attenuation were related linearly (30 to 80 mole percent styrene) a PLS analysis was performed. All of the information in the attenuation spectra of these latices could be collapsed into one or two PLS latent variables that related directly to copolymer composition. Only polymer properties relating to composition (T_g, %sty and possibly %acr) could be predicted from the attenuation using a PLS model in this range. The attenuation seemed unable to predict crosslinking properties (inverse swell or percent gel) or the particle size. One possible problem is that there is no assurance that quality variables such as percent gel and inverse swell are actually well correlated with the crosslink density over the entire composition range. Another problem is that the objects in the non-linear region of Figures 5.1 and 5.2 were not utilized in the calibration because a linear regression method was used. Future work therefore should focus on better techniques for characterizing the polymer properties and the use of a non-linear multivariate regression method so that all of the data can be used in a calibration.

6.5 Ultrasound as an On-line Sensor For Emulsion Polymerization

Probably the most important property that could be measured on-line would be crosslink density or molecular weight. From a theoretical standpoint, it is expected that the attenuation should respond to changes in these properties since they would effect the relaxation time of the polymer. For the copolymer systems examined in this study however no statistically significant correlation between these properties and the travel parameters of ultrasonic waves was observed. The velocity did not change significantly from object to object and although the attenuation spectra was many times larger than the attenuation due to water, it only responded to composition changes for the copolymer system examined in this thesis. The possibility of extracting multiple pieces of information in this frequency range is unlikely since it was shown that these spectra can be easily collapsed into one or two latent variables. Moreover, for latex systems, the frequency window cannot be greatly expanded because of diffraction or scattering. For these reasons, work to this date suggests that the measurement of travelling longitudinal waves in polymer latices is most useful for measuring composition changes. In this case, the measurement would have to take place in a composition range where the relationship between attenuation and composition was linear and where both of the monomers had dissimilar mechanical properties. A number of other important properties would also have to be considered for their effect on attenuation such as percent solids and temperature.

REFERENCES

Allegra, J., "Attenuation of Sound in Suspensions and Emulsions", J. Acoust. Soc. Am., Vol. 51, No 5 (Part 2), (1972).

Bass, R., "Diffraction Effects in the Ultrasonic Field of a Piston Source", J. Acoust. Soc. Am., Vol 30, No 7, pg 602, (1958).

Callis, J., Illman, D., and Kowalski, B., "Process Analytical Chemistry", Analytical Chemistry, Vol 59, No 9, pp 624A-637A, May, (1987).

Chow, J., "Attenuation of Acoustic Waves in Dilute Emulsions and Suspensions", J. Acoust. Soc. Am., Vol 36, No 12, pg 2395, (1964).

Chien, D. and Penlidis, A., "On-Line Sensors For Polymerization Reactors", Marcel Dekker, Rev. Macromol. Chem. Phys., C30(1), pg 1, (1990).

Croucher, M., "Introduction to Polymers" in Formulating Chemical Products Short Course, McMaster University, Hamilton, On, (1991).

Duck, E., "Emulsion Polymerization", in Encyclopedia of Polymer Science and Technology, Mark, H., and Gaylord, G., (Ed), John Wiley, N.Y, (1966).

Dunn, J., "Carboxylated Rubber", in Handbook of Elastomers, Bhowmick and Stephens, (Ed), Marcel Dekker, (1988).

Draper, N., and Smith, H., Applied Regression Analysis, Wiley Intersciences, N.Y, (1981).

Epstein, P., and Carhart, R., "The Absorption of Sound In Suspensions and Emulsions", J. Acoust. Soc. Am., Vol 25, No 3, pg 553, (1953).

Ferry, J., Viscoelastic Properties of Polymers. John Wiley, N.Y, (1980).

Gagnon, L., and MacGregor, J., "State Estimation for Continuous Emulsion Polymerization", Can. J. Chem. Eng., Vol 69, June, (1991).

Geladi, P. and Kowalski, B., "Partial Least Squares Regression: A Tutorial", Analytica Chimica Acta, Elsevier Science Publishers, Amsterdam, 185, pp 1-17, (1986).

Greenspan, M., Tschiegg, C., "Speed of Sound in Water by a Direct Method", J. of Research of the National Bureau of Standards, Vol 59, No 4, pg 249, Oct, (1957).

Hamielec, A., and MacGregor, J., "Latex Reactor Principles: Design, Operation and Control", in Emulsion Polymerization, Piirma, I., (Ed), Academic Press, N.Y, (1982).

Hawley, S., Ultrasonic Absorption in Aqueous Suspensions of Small Elastic Particles, Ph.D Thesis, University of Illinois (1967).

Herzfeld, K., "Propagation of Sound in Suspensions", LXIX, Phil. Mag., S.7, Vol 9 No 59, Suppl, p 741, May (1930a).

Herzfeld, K., "Propagation of Sound in Suspensions", LXX, Phil. Mag., S.7, Vol 9 No 59, Suppl, p 753, May (1930b).

Herzfeld, K. and Litovitz, A., Absorption and Dispersion of Ultrasonic Waves. Academic Press, N.Y, (1959).

Hiemenz, P., Polymer Chemistry. Marcel Dekker, N.Y, (1984).

Jaffe, B., Piezoelectric Ceramics. Academic Press, N.Y, (1971).

Johari, , Dept of Materials Engineering, McMaster University, Hamilton, On, Private Communication, (1991).

Kirillov,V. and Ray, W., "The Mathematical Modelling of Continuous Emulsion Polymerization Reactors", Chem. Eng. Sci., Vol 33, pg 1499 (1978).

Kline, R., "Measurement of Attenuation and Dispersion using an Ultrasonic Spectroscopy Technique", J. Acoust. Soc. Am., Vol 76, No 2, pg 498, (1984).

Kowalski,B., Chemometrics: Mathematics and Statistics in Chemistry, D. Reidel Publishing Co., Dordrecht, Proceedings of the NATO Advanced Study Institute on Chemometrics, Cosenza, Italy, Sept 12-23 (1983).

Kresta, J. ,Marlin, T., and MacGregor, J., Multivariate Statistical Monitoring of Process Operating Performance, Can. J. Chem. Eng., Vol. 69, pg 35, Feb (1991).

Lamb, J., and Pinkerton, J., "The Absorption and Dispersion of Ultrasonic Waves in Acetic Acid", Proc. Royal Soc. A199, pg 114, (1949).

Liptak, B., Instrument Engineer's Handbook, Volume One (Process Measurements). Chilton, London, (1967).

Litovitz, A., and Davis, C., "Structural and Shear Relaxation in Liquids" in Physical Acoustics, Vol 2A. Mason, W., (Ed), Academic Press, N.Y, (1965).

Lynnworth, L., "Industrial Applications of Ultrasound", IEEE Trans on Sonics and Ultrasonics, Vol SU-22, No 2, March (1975).

Martens, M., and Naes, T., Multivariate Calibration, John Wiley and Sons, N.Y, (1989).

Mason, W., Baker,W., "Mechanical Properties of Long Chain Molecule Liquids at Ultrasonic Frequencies", Physical Review, Vol 73, No 9, pg 1074, (1948).

Mason, W., Piezoelectric Crystals and their Application to Ultrasonics. Van Nostrand, N.Y (1950).

Matec Application Note AN-102, Matec Instruments, Hopkinton, Massachusetts

McAuley, K. and MacGregor, J., "On-Line Inference of Polymer Properties in an Industrial Polyethylene Reactor", A.I.Ch.E.J., Vol 37, No 6, pg 825, June,(1991).

McSkimin, H., "Measurement of Ultrasonic Wave Velocities and Elastic Moduli for Small Solid Specimens at High Temperature", J. Acoust. Soc. Am, Vol 31, No 3 (1959).

McSkimin, H., "Ultrasonic Methods for Measurement" in Physical Acoustics, Vol 1A. W. Mason (Ed), Academic Press, N.Y, (1964).

Meeker, T., and Meitzler, A., "Guided Wave Propagation in Elongated Cylinders and Plates" in Physical Acoustics, Vol 1A. W. Mason (Ed), Academic Press, N.Y, (1964).

Meyer and Neumann, Physical and Applied Acoustics: An Introduction. Meyer and Neumann, Academic Press, N.Y, (1972).

Monkr, M., Nusonics Inc, Tulsa OK, Private Communication, (1990).

Morse, P., and Ingard, K., Theoretical Acoustics, McGraw Hill, N.Y, (1968).

Ottewill, R., "The Stability and Instability of Polymer Latices", in Emulsion Polymerization, Piirma, I., (Ed), Academic Press, N.Y, (1982).

Papadakis, E., "Ultrasonic Velocity and Attenuation: Measurement Methods with Scientific and Industrial Applications" in Physical Acoustics, Vol 12. W. Mason (Ed), Academic Press, N.Y, (1976).

Patel, N., Dept of Materials Engineering, McMaster University, Hamilton, On, Private Communication, (1990).

Pellam and Galt, "Ultrasonic Propagation in Liquids: Application of Pulse Techniques to Velocity and Absorption Measurements at 15 MHz", J. Chem. Phys., Oct, (1946).

Petersen, MATEC Instruments Acoustic Attenuation and Velocity Measurements Using the Phase Sensitive Adjustment Technique. MATEC Instr. Inc., Hopkinton, MA, (1989).

Pethrick, R., "Ultrasonic Studies of Macromolecules", Progress in Polymer Science, Vol 9, pg 197, (1983).

Philippoff, W., "Relaxations in Polymer Solutions, Liquids and Gels" in Physical Acoustics, Vol 2B. W. Mason (Ed), Academic Press, N.Y, (1965).

Pinkerton, J., "Pulse Method for the Measurement of Ultrasonic Absorption in Liquids: Results for Water", Pinkerton, Nature, July (1947).

Pinkerton, J., "On the Pulse Method of Measuring Ultrasonic Absorption in Liquids", Proc.Physical Soc., B62, (1949).

Popiel, W., Introduction to Colloid Science, Exposition Press, Hicksville, N.Y, (1978).

Ratzlaff, K., Introduction to Computer-Assisted Instrumentation. John Wiley and Sons, Toronto, (1987).

Redwood, M., "Dispersion Effects in Ultrasonic Waveguides and their Importance in the Measurement of Attenuation", Proc. Physical Society, B70, pg 721, (1957).

Roffel, J., "Modelling and Control of the Ziegler Natta Polymerization of Butadiene", M.Eng Thesis, McMaster University, Hamilton, On, (1990).

Seki, H., Granato, A., and Truell, R., "Diffraction Effects in the Ultrasonic Field of a Piston Source and their Importance in the Accurate Measurement of Attenuation", J. Acoust. Soc. Am., Vol 28, No. 2, pg 230, (1956).

Serway, R., Physics For Scientists and Engineers. Saunders College Publishing, N.Y, (1982).

Taylor, P., Real-Time Computer Interfacing (Lecture Notes for ENG 6Y3), McMaster University, (1989).

Truell, R., Elbaum, C., and Chick, B., Ultrasonic Methods in Solid State Physics. Academic Press, N.Y, (1969).

Urick, R., "A Sound Velocity Method for Determining the Compressibility of Finely Divided Substances", J. Applied Physics, Vol 18, pp 983-987, Nov (1947).

Urick, R., and Ament, W., "The Propagation of Sound in Composite Media", J. Acoust. Soc. Am., Vol 21, No 2, pp 115-119, Mar (1949).

Van Randeraat, J., (Ed), Piezoelectric Ceramics. Philips Application Book, (1968).

Wada, Y., "Attenuation of Ultrasonic Waves in Suspensions of Viscoelastic Spheres", J. Physical Society Japan, Vol 13, No 11, pg 1390, Nov (1958).

Wold, S., "Cross-Validatory Estimation of the Number of Components in Factor and Principal Components Models", Technometrics, Vol 20, No 4, Nov (1978).

Zacharias, E., "Process Measurements by Sound Velocimetry", Instruments and Control Systems, Sept, pg 112, (1970a).

Zacharias, E., "The Sonic Interface Detector Meets Field Tests In Pipelining", Oil and Gas J., July 6, pg 96, (1970b).

APPENDIX 1

ATTENUATION MEASUREMENTS FROM THE RIGOROUS METHOD

(A) The Styrene methylmethacrylate system

Table A1A.1. SMB52 Attenuation Measurements: 7 MHz trans, 25 °C, Jan3091

f (MHz)	Slope (dB/turn)	SS_{res}	D of F	$\Sigma(x-\bar{x})^2$	$\frac{\text{Conf Int}}{\text{Slope}}$ (±%)	α (nepers/m)
4	.32781	.04999	4	146.83	36.4	**48.3**
5	.20048	.05691	4	146.83	32.0	**29.6**
6	.29970	.25796	4	146.83	29.2	**44.2**
7	.52449	.17893	4	146.83	21.3	**77.4**
8	.61319	.39874	4	146.83	14.6	**90.4**
9	.64458	.51133	4	146.83	11.7	**95.1**
10	.63027	.42671	4	146.83	15.7	**93.0**
11	.70472	.29481	4	146.83	8.8	**103.9**
Ave	.49320	2.1753	32	146.83	8.7	**72.7**

Table A1A.2. SMB53 Attenuation Measurements: 7 MHz trans, 25 °C, Jan2891

f (MHz)	Slope (dB/turn)	SS_{res}	D of F	$\Sigma(x-\bar{x})^2$	Conf Int / Slope (±%)	α (nepers/m)
4	.30104	.51921	4	83.33	36.4	**44.4**
5	.30481	.68249	5	94.86	32.0	**45.0**
6	.40141	.96435	5	94.86	29.2	**59.2**
7	.43426	.59813	5	94.86	21.3	**64.0**
8	.66059	.65317	5	94.86	14.6	**97.4**
9	.72550	.51662	5	94.86	11.7	**107.0**
10	.71277	.88213	5	94.86	15.7	**105.1**
Ave	.46276	4.8161	34	93.57	17.7	**74.6**

Table A1A.3. SMB54 Attenuation Measurements: 7 MHz trans, 25 °C, Feb1b91

f (MHz)	Slope (dB/turn)	SS_{res}	D of F	$\Sigma(x-\bar{x})^2$	$\frac{\text{Conf Int}}{\text{Slope}}$ (±%)	α (nepers/m)
4	.26765	.32299	3	100	39.0	**38.8**
5	.28795	.01899	3	100	8.8	**41.8**
6	.40260	.63789	3	100	36.7	**58.4**
7	.76250	1.3489	3	100	28.1	**110.6**
8	.65215	.38036	3	100	17.5	**94.6**
9	.73680	.50266	3	100	17.8	**106.8**
10	.73375	.38718	3	100	15.7	**106.4**
11	.75815	.22873	3	100	11.7	**109.9**
12	.91160	1.3400	3	100	23.5	**132.2**
Ave	.61257	5.1676	27	100	14.7	**88.8**

Table A1A.4. SMB55 Attenuation Measurements: 7 MHz trans, 25 °C, Feb191

f (MHz)	Slope (dB/turn)	SS_{res}	D of F	$\Sigma(x-\bar{x})^2$	$\frac{\text{Conf Int}}{\text{Slope}}$ (±%)	α (nepers/m)
4	.28096	.24013	3	100	22.3	**41.4**
5	.42761	1.0337	3	100	30.4	**63.0**
6	.41236	1.9245	4	118	43.0	**60.8**
7	.55098	1.0020	4	118	23.2	**81.3**
8	.61635	.95657	4	118	20.3	**90.9**
9	.68115	.30639	4	118	10.4	**100.5**
10	.76469	6.9737	4	118	44.1	**112.8**
11	.77725	.40004	4	118	10.4	**114.6**
Ave	.56392	12.837	32	118	21.2	**83.2**

Table A1A.5. SMB56 Attenuation Measurements: 7 MHz trans, 25 °C, Jan1891

f (MHz)	Slope (dB/turn)	SS_{res}	D of F	$\Sigma(x-\bar{x})^2$	$\frac{\text{Conf Int}}{\text{Slope}}$ (±%)	α (nepers/m)
5	.38373	.51078	6	108	17.9	**56.6**
6	.42235	.14342	6	108	8.6	**62.3**
7	.46181	1.2372	6	108	23.2	**68.1**
8	.58933	.34431	6	108	5.6	**86.9**
9	.68860	.18380	6	108	4.1	**101.6**
10	.79082	.32121	6	108	6.9	**116.6**
Ave	.55611	2.7407	36	108	9.7	**82.0**

Table A1A.6. SMB55 Attenuation Measurements: 3 MHz trans, 25 °C, Mar591

f (MHz)	Slope (dB/turn)	SS_{res}	D of F	$\Sigma(x-\bar{x})^2$	Conf Int / Slope (±%)	α (nepers/m)
2	.13597	.38906	7	155.6	32.0	**19.7**
3	.25930	.39751	7	155.6	16.9	**37.6**
4	.23652	1.6696	7	155.6	38.1	**34.3**

Table A1A.7. SMB56 Attenuation Measurements: 3 MHz trans, 25 °C, Mar491

f (MHz)	Slope (dB/turn)	SS_{res}	D of F	$\Sigma(x-\bar{x})^2$	Conf Int / Slope (±%)	α (nepers/m)
2	.17043	.09514	8	146.4	12.2	**24.7**
3	.24688	.36379	8	146.4	16.4	**35.8**
4	.27322	.96100	8	146.4	24.1	**39.6**

(B) The Styrene Butadiene Rubber system

Table A1B.1. P1017 Attenuation Measurements: 3 & 7 MHz trans, 1/4 dilution,30 °C, May1391

f (MHz)	Slope (dB/turn)	SS_{res}	D of F	$\Sigma(x-\bar{x})^2$	Conf Int / Slope (±%)	α (nepers/m)
2	.57390	.97795	4	73.5	27.9	**84.6**
3	.41252	.32250	4	73.5	22.3	**60.8**
4(l)	.75652	.42454	4	73.5	13.9	**111.6**
4(h)	.70376	.55875	4	73.5	17.2	**103.4**
5	.84976	.71450	4	73.5	16.1	**125.3**
6	1.0347	3.3996	4	73.5	28.8	**152.6**
7	1.1005	1.8889	4	73.5	26.2	**162.3**
Ave	.77589	8.2867	28	73.5	16.5	**114.4**

Table A1B.2. P1163 Attenuation Measurements: 3 & 7 MHz trans, 1/4 dilution,30 °C, May191

f (MHz)	Slope (dB/turn)	SS_{res}	D of F	$\Sigma(x-\bar{x})^2$	$\frac{\text{Conf Int}}{\text{Slope}}$ (±%)	α (nepers/m)
2	.14995	1.5113	6	129.5	72.0	**22.1**
3	.35089	1.2941	6	129.5	28.5	**51.7**
4(l)	.54415	1.0968	6	129.5	16.9	**80.3**
4(h)	.54670	.23293	5	108.9	9.7	**80.6**
5	.74430	2.2380	5	108.9	22.1	**109.8**
6	1.0913	2.2400	5	108.9	15.1	**160.9**
7	1.3949	1.1212	5	108.9	8.4	**205.7**
Ave	.68888	9.7343	38	117.7	13.7	**101.6**

Table A1B.3. P1376 Attenuation Measurements: 3 & 7 MHz trans, 1/4 dilution,30 °C, Apr2691

f (MHz)	Slope (dB/turn)	SS_{res}	D of F	$\Sigma(x-\bar{x})^2$	$\frac{\text{Conf Int}}{\text{Slope}}$ (±%)	α (nepers/m)
2	.03935	2.5728	7	181.6	270	**5.8**
3	.11120	.80026	7	181.6	53.4	**16.4**
4(l)	.16422	.47215	7	181.6	27.8	**24.2**
4(h)	.13859	.71319	7	181.6	40.4	**20.4**
5	.20797	1.6026	7	181.6	40.4	**30.7**
6	.18123	1.2211	7	181.6	40.4	**26.7**
7	.20824	3.6371	7	181.6	60.7	**30.7**
8	.25431	2.4504	7	181.6	40.8	**37.5**
9	.24929	4.7086	7	181.6	57.7	**36.8**
10	.39867	2.1920	7	181.6	24.6	**58.8**
Ave	.17000	20.370	70	181.6	47.1	**28.8**

Table A1B.4. P1377 Attenuation Measurements: 3 & 7 MHz trans, 1/4 dilution,30 °C, May191

f (MHz)	Slope (dB/turn)	SS_{res}	D of F	$\Sigma(x-\bar{x})^2$	$\frac{\text{Conf Int}}{\text{Slope}}$ (±%)	α (nepers/m)
2	.15047	.12322	3	97.2	43.3	**22.2**
3	.16715	.18706	3	97.2	48.2	**24.7**
4(l)	.10276	.11039	3	97.2	18.9	**15.2**
4(h)	.16085	.09798	3	97.2	11.4	**23.7**
5	.25494	.11325	3	97.2	7.7	**37.6**
6	.18467	.60344	4	121.5	53.0	**27.2**
7	.24874	.53354	4	121.5	37.0	**26.7**
8	.38667	.26110	3	97.2	24.6	**57.0**
9	.31235	.92838	3	97.2	57.5	**46.0**
10	.40887	1.0911	3	97.2	47.6	**60.3**
Ave	.26324	4.0486	32	102.1	27.3	**35.1**

Table A1B.5. P1380 Attenuation Measurements: 3 & 7 MHz trans, 1/4 dilution,30 °C, Mar25a91

f (MHz)	Slope (dB/turn)	SS_{res}	D of F	$\Sigma(x-\bar{x})^2$	$\frac{\text{Conf Int}}{\text{Slope}}$ (±%)	α (nepers/m)
2	.16065	.32083	6	124.9	31.5	**23.7**
3	.26019	.12627	4	121.5	17.2	**38.4**
4(l)	.35536	.88573	6	162.0	20.8	**52.4**
4(h)	.31347	.67306	6	162.0	20.5	**46.2**
5	.40859	.38631	4	121.5	19.2	**60.3**
6	.60552	.72476	4	121.5	17.7	**89.3**
7	.69013	.49005	3	97.2	18.9	**101.8**
8	.79174	.81789	3	97.2	21.3	**116.8**
9	.92494	.39104	3	97.2	12.6	**136.4**
10	.98739	2.02832	2	60.8	56.3	**145.6**
Ave	.54980	6.84426	41	116.6	13.9	**81.0**

Table A1B.6. P1382 Attenuation Measurements: 3 & 7 MHz trans, 1/4 dilution,30 °C, May1091

f (MHz)	Slope (dB/turn)	SS_{res}	D of F	$\Sigma(x-\bar{x})^2$	$\frac{\text{Conf Int}}{\text{Slope}}$ (±%)	α (nepers/m)
2	.48481	5.0298	7	124.9	37.0	**71.5**
3	.67008	1.5448	7	124.9	14.8	**98.8**
4(l)	1.0427	8.3581	7	124.9	22.2	**153.8**
4(h)	.96288	1.7523	7	124.9	11.0	**142.0**
5	1.1713	8.0643	6	98.0	24.5	**172.7**
Ave	.86635	24.749	34	119.5	18.2	**127.8**

Table A1B.7. P1406 Attenuation Measurements: 3 & 7 MHz trans, 1/4 dilution,30 °C, May1591

f (MHz)	Slope (dB/turn)	SS_{res}	D of F	$\Sigma(x-\bar{x})^2$	$\frac{\text{Conf Int}}{\text{Slope}}$ (±%)	α (nepers/m)
2	.66940	3.6639	8	132.5	20.3	**98.7**
3	.71695	2.0035	10	142.9	11.6	**105.7**
4(l)	.90190	1.2688	9	138.2	8.0	**133.0**
4(h)	.92109	2.7344	10	142.9	10.6	**135.8**
5	1.2144	3.9216	10	142.9	9.6	**179.1**
6	1.2825	11.068	9	138.2	16.6	**189.1**
Ave	.95103	24.660	56	139.6	11.8	**140.3**

Table A1B.8. P1006 Attenuation Measurements: 3 & 7 MHz trans, 1/4 dilution,30 °C, Apr1691

f (MHz)	Slope (dB/turn)	SS_{res}	D of F	$\Sigma(x-\bar{x})^2$	$\frac{\text{Conf Int}}{\text{Slope}}$ (±%)	α (nepers/m)
2	.62125	.32948	4	96	13.1	**91.6**
3	.80692	.47613	4	96	12.1	**119.0**
4(l)	1.0702	1.9108	4	96	18.3	**157.8**
4(h)	1.0698	1.4500	4	96	16.0	**157.8**
5	1.2822	3.7875	4	96	21.5	**189.1**
6	1.6503	4.2438	3	76.8	26.2	**243.4**
Ave	1.0834	12.208	23	92.8	14.0	**159.8**

APPENDIX 2

VELOCITY MEASURED

Table A2.1. Measured velocity for the styrene methylmethacrylate latex system

f (MHz)	SMB52 Jan30	SMB53 Jan28	SMB54 Feb1b	SMB55 Mar5 Feb1	SMB56 Mar4 Jan18
2				1599.7	1595.4
3				1578.5	1586.2
4	1587.3	1573.1	1579.3	1559.4	1579.3
5	1627.2	1610.6	1566.5	1585.1	1566.5
6	1618.0	1549.1	1591.2	1604.5	1591.2
7	1569.1	1646.9	1618.6	1562.5	1612.8
8	1593.1	1556.5	1591.3	1550.6	1591.3
9	1626.5	1614.5	1580.6	1561.9	1580.6
10	1574.5	1530.9	1643.0	1604.0	1643.0
11	1539.1	1626.8	1671.4	1577.2	1671.4
Ave	**1596.8**	**1587.4**	**1599.6**	**1575.9**	**1599.2**

APPENDIX 3

REFLECTION LOSS MEASURED

Table A3.1. Reflection losses for the styrene methylmethacrylate system in dB

f (MHz)	SMB52 Jan30	SMB53 Jan28	SMB54 Feb1b	SMB55 Mar5 Feb1	SMB56 Mar4 Jan18	Ave
2				4.54	3.30	**3.92**
3				2.03	1.91	**1.97**
4	1.18	1.81	2.74	2.72	2.74	**2.24**
5	4.44	3.75	3.73	1.52	1.08	**2.90**
6	6.04	4.34	3.56	3.92	2.95	**4.16**
7	5.09	5.61	(-1.02)	3.26	4.53	**4.62**
8	3.68	2.77	2.88	3.29	3.11	**3.15**
9	3.92	2.31	1.94	3.06	1.85	**2.62**
10	5.67	3.41	2.87	2.63	1.61	**3.24**
11	6.19	1.61	3.78	3.67		**3.82**
Theoret-ical	**5.48**	**5.49**	**5.48**	**5.49**	**5.49**	**5.49**

Table A3.2. Reflection losses for the styrene butadiene rubber latex system at 1/4 dilution in dB

f (MHz)	P1017 May13	P1163 May1	P1376 Apr26	P1377 May5	P1380 Mar25	P1382 May10	P1406 May15	P1006 Apr16	Ave
2	(-.71)	3.66	3.50	2.10	4.14	2.56	(.10)	(-.27)	**3.19**
3	5.08	1.98	2.17	1.83	3.61	4.08	3.21	1.57	**2.94**
4(l)	1.86	2.45	1.88	3.36	3.45	4.37	5.32	3.65	**3.29**
4(h)	2.27	1.66	1.98	1.91	3.50	4.81	4.10	3.10	**2.92**
5	5.60	4.06	2.84	3.16	5.54	9.89	4.86	4.33	**5.04**
6	6.36	(.81)	3.27	4.23	3.83		(10.36)	(-.36)	**4.43**
7	6.69	3.79	4.42	5.87	6.91				**5.54**
8			4.92	5.07	6.55				**5.51**
9			4.77	6.27	5.71				**5.58**
10			4.27	7.29	7.08				**6.21**

Table A3.3. Reflection losses for the styrene butadiene latex system at 1/8 dilution in dB

f (MHz)	P1017 Mar19	P1380 Apr4	P1380 Apr10	P1382 Apr10	P1406 Apr3	P1006 Mar15	Ave
2	4.38	1.09	4.61	5.75	6.40	2.73	**4.16**
3	(.70)	2.05	1.94	3.29	5.63	(.85)	**3.23**
4(l)	1.04	1.34	2.65	3.33	(8.75)	1.64	**2.00**
4(h)	1.08	2.93	2.51	3.72	(8.75)	(.99)	**2.56**
5	4.16	3.57	1.77	4.53	(10.3)	3.75	**3.56**
6	2.36	(.12)	2.84	2.64		3.84	**2.92**
7	2.61	3.48	5.08	4.07		2.75	**3.60**
8	(.03)	1.82	6.71	5.46		(.68)	**4.66**
9	1.86	(.67)	6.16	4.75		(.93)	**4.26**
10	(-2.70)	1.45	11.19			8.79	**7.14**

Table A3.4. Reflection losses for the styrene butadiene latex system at 1/2 dilution and undiluted in dB

f (MHz)	P1376 May20 undiluted	P1377 May21 undiluted	Average (undiluted)	P1380 Apr18 1/2 dilution
2	3.18	3.20	**3.19**	**3.32**
3	3.97	3.76	**3.86**	**2.26**
4(l)	2.26	1.61	**1.93**	**.76**
4(h)	2.52	1.32	**1.92**	**1.12**
5	3.92	3.55	**3.74**	**5.21**
6	3.32	1.81	**3.32**	**4.71**
7	4.96	(8.76)	**4.96**	
8	5.88		**5.88**	
9	7.17		**7.17**	
10				

APPENDIX 4

ATTENUATION MEASUREMENTS BY THE SHORTCUT METHOD

Table A4.1. Shortcut attenuation constant for the styrene butadiene rubber latex system at 1/4 dilution in neper/m at 30°C: Transceiver mode, May16&May3191

f (MHz)	P1017	P1163	P1376	P1377	P1380	P1382	P1406	P1006
2	22.8	27.4	5.1	8.7	19.3	56.5	76.0	67.3
3	75.2	50.0	16.4	22.7	35.8	106.3	101.7	95.1
4(l)	83.5	79.0	12.5	17.0	60.4	140.5	138.6	127.7
4(h)	86.3	87.8	16.5	16.6	47.5	142.6	139.0	138.8
5	110.8	113.2	10.1	19.1	55.8	183.5	182.8	171.4
6	129.9	166.7	23.2	28.0	71.6	223.6	208.4	224.8
7	166.1	206.0	24.9	32.7	93.9	280.9	244.9	
8	179.0	281.1	47.4	55.3	116.4			
9	218.1	309.7	44.2	50.4	131.4			
10			60.2	63.4	145.5			

Table A4.2. Shortcut attenuation constant for some new styrene butadiene rubber latex samples at 1/4 and 1/2 dilution in neper/m at 30°C: Transceiver mode, Aug28&Sept191

f (MHz)	P1123 1/4 dil	P1764 1/4 dil	P9999 1/4 dil	P1123 1/2 dil	P9999 1/2 dil
2	12.4	10.7	8.7	11.2	22.1
3	18.4	12.3	11.5	27.9	23.4
4(l)	24.8	8.0	9.1	52.8	37.9
4(h)	23.4	16.7	14.7	44.8	37.9
5	28.4	14.9	16.3		43.3
6	51.7	13.4	25.0	101.5	59.5
7	84.0	32.0	39.0	140.5	75.3
8	107.7	38.2	50.1	167.1	101.1
9	123.2	37.7	50.8	184.4	98.6
10	146.4	47.7	62.3		129.9

Table A4.3. Shortcut attenuation constant for the styrene butadiene rubber latex system at 1/2 dilution in neper/m at 30°C: Sender/Receiver mode, May28&May3091

f (MHz)	P1017	P1163	P1376	P1377	P1380	P1382	P1406	P1006
2	117	45	26	32	55	127	129	132
3	152	79	20	30	80	191	194	187
4(l)	207	137	38	51	106	278	282	281
4(h)	209	153	43	59	125	289	260	279
5	247	191	34	58		346	313	337
6	316	258	69	94	176	473	429	460
7	379	350	65	97	216	575	529	529
8	397	423	71	110	224	620	568	
9	431	463	72	113	234			
10	428	561	82	134	279			

APPENDIX FIVE

SUMMARIZED ATTENUATION INFORMATION

Table A5.1. Summarized attenuation spectra for styrene-methylmethacrylate system.

Object	Slope	Intercept ($\alpha\|_{f=5MHz}$)	SS_{res}	D. of F.
SMB52	9.38	48.14	1105	9-2
SMB53	13.45	48.70	474	9-2
SMB54	11.36	56.24	1675	9-2
SMB55	10.46	54.87	396	12-2
SMB56	11.10	54.83	181	9-2

Table A5.2. Summarized Attenuation Spectra for SBR system at 1/4 dilution: Rigorous method

Object	Slope	Intercept ($\alpha\|_{f=5MHz}$)	SS_{res}	D. of F.
P1017	19.42	125.53	1068	7-2
P1163	36.58	122.50	420	7-2
P1376	4.97	24.82	250	10-2
P1377	5.07	31.01	478	10-2
P1380	16.07	68.23	169	10-2
P1382	35.86	178	220	5-2
P1406	25.42	165.68	425	6-2
P1006	37.36	197.15	206	6-2

Table A5.3. Summarized Attenuation Spectra for SBR system at 1/4 dilution: Shortcut method

Object	Slope	Intercept ($\alpha\|_{f=5MHz}$)	SS_{res}	D. of F.
P1017	25.58	110.53	530	9-2
P1163	39.71	123.80	1488	9-2
P1376	6.41	20.91	413	10-2
P1377	6.75	25.71	297	10-2
P1380	16.17	63.89	367	10-2
P1382	43.37	186.75	156	7-2
P1406	34.58	175.66	104	6-2
P1006	37.97	176.41	391	6-2
P1123	18.07	47.59	1151	10-2
P1764	4.95	19.20		10-2
P9999	7.31	22.90	224	10-2

Table A5.4. Summarized Attenuation Spectra for SBR system at 1/2 dilution: Shortcut method

Object	Slope	Intercept ($\alpha\|_{f=5MHz}$)	SS_{res}	D. of F.
P1017	43.32	253.54	4183	10-2
P1163	65.61	213.51	2644	10-2
P1376	8.17	44.79	567	9-2
P1377	13.84	65.97	470	9-2
P1380	27.49	141.81	936	10-2
P1380 (rig)	29.15	145.0	336	6-2
P1382	89.55	376.07	1851	8-2
P1406	74.30	350.66	1211	8-2
P1006	81.84	361.19	1289	7-2
P1123	26.45	81.36	319	8-2
P9999	13.60	52.02	477	10-2

APPENDIX 6

SIMCA OUTPUT FOR CALIBRATION OF SBR DATA SET

Table A6.1 PLS Regression of T_g, Sty, Acr, Gel, Inv Swells and P.S onto Summarized Attenuation Spectra from 1/4 Dilution

PLS dimension # 1 after 5 iterations
X-validation
CSV/SD for each Y-variable
Y(1) = 0.1665 Y(2) = 0.2567 Y(3) = 0.9606
Y(4) = 1.074 Y(5) = 1.1008 Y(6) = 1.0665
CSV/SD overall = 0.8624
% X-validated SS-exp (Y) = 25.617
% cumulative X-validated (Y) = 25.617
Cumulative SS in X = 99.636
Cumulative SS in Y = 42.984
%SS explained in X = 99.636
%SS explained in Y = 42.984
Inner relation = 0.997
PLS dimension # 2 after 2 iterations
X-validation
CSV/SD for each Y-variable
Y(1) = 1.0804 Y(2) = 1.0158 Y(3) = 0.9297
Y(4) = 1.015 Y(5) = 1.0084 Y(6) = 0.931
CSV/SD overall = 0.9762

% X-validated SS-exp (Y) = 2.6714
% cumulative X-validated SS-exp (Y) = 28.288
Cumulative SS explained in X = 100
Cumulative SS explained in Y = 49.431
%SS explained in X = 0.3643
%SS explained in Y = 6.4474
Inner relation = 0.987
PLS dimension # 3 after 4 iterations
X-validation
CSV/SD for each Y-variable
Y(1) = 0.9093 Y(2) = 1.009 Y(3) = 1.0295
Y(4) = 0.8669 Y(5) = 0.9611 Y(6) = 0.8008
CSV/SD overall = 0.9221
% X-validated SS-exp (Y) = 7.5721
% cumulative X-validated SS-exp (Y) = 35.86
Cumulative SS explained in X = 100
Cumulative SS explained in Y = 66.143
%SS and variance explained in X = 0
%SS and variance explained in Y = 16.712
Inner relation = 1.045

Table A6.2 PLS Regression of T_g, Sty, Acr, and P.S onto Summarized Attenuation Spectra from 1/4 Dilution

PLS dimension # 1 after 4 iterations
X-validation
CSV/SD for each Y-variable
Y(1) = 0.1673 Y(2) = 0.2572 Y(3) = 0.9608
Y(4) = 1.0674 CSV/SD overall = 0.7189
% X-validated SS-exp (Y) = 48.308
% cumulative X-validated SS-exp (Y) = 48.308
Cumulative SS explained in X = 99.636
Cumulative SS explained in Y = 58.435

%SS explained in X = 99.636
%SS explained in Y = 58.435
Inner relation = 1.001
PLS dimension # 2 after 2 iterations
X-validation
CSV/SD for each Y-variable
Y(1) = 1.0805 Y(2) = 1.0082 Y(3) = 0.9149
Y(4) = 0.9352 CSV/SD overall = 0.9306
% X-validated SS-exp (Y) = 5.5641
% cumulative X-validated SS-exp (Y) = 53.872
Cumulative SS explained in X = 100
Cumulative SS explained in Y = 65.963
%SS explained in X = 0.3643
%SS explained in Y = 7.5285
Inner relation = 1.019
PLS dimension # 3
X-validation
CSV/SD for each Y-variable
Y(1) = 1.1334 Y(2) = 1.1163 Y(3) = 1.0656
Y(4) = 1.1426 CSV/SD overall = 1.1052
% X-validated SS-exp (Y) = -7.5403
% cumulative X-validated SS-exp (Y) = 46.332
Cumulative SS explained in X = 100
Cumulative SS explained in Y = 67.2
%SS explained in X = 0
%SS explained in Y = 1.2365